2015

Modification of Nanoparticles for Designed Interfaces

Tony Lee Neely, Jr.
University of South Carolina

Modification of Nanoparticles for Designed Interfaces

by

Tony Lee Neely, Jr.

Bachelor of Science
Furman University 2006

Master of Science
Furman University 2008

Submitted in Partial Fulfillment of the Requirements

for the Degree of Doctor of Philosophy in

Chemistry

College of Arts and Sciences

University of South Carolina

2015

Accepted by:

Brian Benicewicz, Major Professor

Chuanbing Tang, Committee Chair

Thomas Vogt, Committee Member

Harry Ploehn, Committee Member

Lacy Ford, Senior Vice Provost and Dean of Graduate Studies

Acknowledgments

I would like to thank Dr. Brian Benicewicz for his guidance and mentorship throughout my Ph.D. work, whether it pertained to chemistry or otherwise. His expertise and support was invaluable in the completion of this research. I would also like to thank my doctoral committee members - Prof. Chuanbing Tang, Prof. Tom Vogt, and Prof. Harry Ploehn for their encouragement and assistance during graduate school.

I would like to thank my collaborators Prof. Linda Schadler (Rensselaer Polytechnic Institute) and her graduate students Bharath Natarajan and Ying Li for their invaluable contributions towards this work as well as Prof. Sanat Kumar of Columbia University.

I am extremely thankful for the support and work environment provided by current and former Benicewicz group members. Even through difficulties in lab, work never became a chore mostly due to them. Special thanks to Atri Rungta for being a great mentor.

Finally I would like to thank my entire family, especially my wife Lauren, for their continued support during these years. I would also like to dedicate this work to my grandmother Jewel Stackley and my grandfather George Neely. Although they were always some of my loudest supporters, they weren't able to see me through this journey and they are missed.

Abstract

The work contained herein, is focused on the design, synthesis, and characterization of polymer nanocomposite interfaces and the property enhancement afforded from said interface design. Through the use of reversible addition fragmentation chain transfer (RAFT) polymerization for the grafting of polymer chains to silica nanoparticles, the surface of silica nanoparticles can be manipulated to tune the properties of the nanocomposite as a whole.

In the first part of this work, heterogeneity is introduced onto the surface of silica nanoparticles via a sequential RAFT polymerization to afford a bimodal brush system. A densely grafted, short brush population is polymerized from the surface in order to provide screening for the enthalpic core-core attraction of the nanoparticles that can lead to agglomeration. Afterwards a second sparsely grafted, long brush population is polymerized to enable the nanoparticle to entangle with the polymer matrix overcoming the entropic preference of the grafted chains dewetting from the matrix chains. These two populations and all their respective molecular variables (graft density, chemistry, end-group chemistry, polydispersity, etc) can be controlled with this approach. With this control in place, the molecular variables were used to produce both bimodal and monomodal samples for comparison of their resulting properties when dispersed in a polymer matrix. It was found that not only do the bimodal samples improve dispersion when compared to monomodal brushes, but that the thermomechanical properties are enhanced as well. Tuning of the long chain graft density determined that very low graft densities were better for improving entanglement. The first bimodal kinetic study was performed to prove that control over the

polymerization can still be obtained using RAFT even when a dense brush is already in place.

Secondly, following the information gained from our first bimodal samples, it was ascertained that with our bimodal system the enthalpic attraction of the particles and the entropic dewetting of the grafted chains were decoupled. This allowed us to pursue the synthesis of mixed bimodal samples. In a mixed bimodal sample the chemistries of the brush populations are distinct. If the long chains are the only population entangling with the matrix, then it can remain matrix compatible while the short brush can be varied to improve other desired properties of the nanocomposite. In order to test whether monomer/polymer incompatibility would allow for the diffusion of a monomer past a short but dense brush of polymer it phase separates with to the surface, a simple poly(methyl)methacrylate/polystyrene mixed bimodal brush was made. With both variations of either chemistries short or long, bimodal samples were possible with control of all previously mentioned molecular variables. In order to push that testing further, bimodal samples of poly(1H,1H-heptafluorobutyl methacrylate) short brushes and polystyrene long brushes were made. A film of these nanoparticles were drop cast onto various substrates showing increased water contact angle measurements when compared with untreated samples. The drop casting of this film onto a sheet of polystyrene followed by annealing shows that the long polystyrene chains of the mixed bimodal brush can still entangle with the polystyrene of the substrate.

For the third section, further work was performed to develop new approaches to the synthesis of bimodal brushes. Taking cues from our testing that showed lower graft densities improved entanglement, it was decided to pursue a one-pot bimodal brush synthesis using a grafting-to approach. While grafting-to is incapable of producing high graft density brushes, this was not needed for our improvement in dispersion and entanglement. Since RAFT polymerization allows for control of the polymer chain

end chemistry, the efficiency of post-polymerization modification was compared to using a modified/activated RAFT agent. The activated RAFT agent showed higher graft densities while still allowing the use of a thermally initiated, bulk polymerization without decomposing at the higher temperatures required for it. This allows for decreased solvent use and therefore easier scale-up. Both long and short chains were attached in a one-pot approach. While not having the control of the sequential RAFT polymerization process, it is much simpler, more efficient, and more modular than the multi-stepped procedure. In addition to overcome issues with characterization of bimodal brushes produced via a one-pot procedure, a new anthracene-containing initiator was created and used to end-label one population of chains via a radical cross coupling mechanism. This allows for characterization of each chain population independently using a combination of UV-Vis and TGA.

Finally, new synthetic strategies towards the modification of the silica nanoparticle surface via different ligands while also focusing on improving efficiency. Previous approaches used a linear aminosilane for the coupling of the RAFT agent to the surface. While successful, the reactions take hours to complete. In a new approach, an amine-containing cyclic azosilane was used for the modification of the silica surface in under five minutes. This new ligand has the same ability as our previous method to be varied in loading in order to vary the graft density. RAFT polymerizations of poly(methyl)methacrylate and polystyrene were performed at various graft densities to show that the attached RAFT agent retained its viability after attachment.

Table of Contents

List of Tables

List of Figures

Chapter 1

Introduction

1.1 Nanocomposites

It is now well known that the incorporation of nanoparticles (NPs) into a polymer matrix can appreciably improve the optical, electrical, and thermomechanical properties of the resulting polymer nanocomposites, (PNCs)[1–14] even over what is obtainable with micrometer sized fillers.[3] Even though this idea has been established, specific dispersion states of the NPs within the PNC can affect the desired property. Therefore, the study of the factors that affect NP distribution within the matrix, along with how this distribution affects the resulting properties, is central to the development of future materials and imperative to the field.[15] These elements continue to be a hurdle to the more universal use of these materials.

It has been shown on micrometer particles that with a high graft density of chains, the particles are miscible within a polymer matrix of the same chemistry so long as the polymer chains of the matrix have a lower molecular weight than those of the brush.[16] However, when the polymer chains of the matrix are of a higher molecular weight than those of the brush, they become immiscible. This immiscibility is attributable to brush autophobicity and is entropic in nature due to the shared chemical composition.[4,17–21] By developing these ideas to incorporate nanoparticles (diameter<100nm) one can control NP polymer matrix miscibility and therefore NP dispersion.[16,22–40] A more recent development is that using these same techniques one can create alternative distributions and structures within the polymer matrix such

as sheets, clusters, strings, etc. while improving a host of properties.[41–46] These new structures are formed when low graft density NPs are incorporated into a polymer matrix, acting like microphase-separated block copolymers and can assemble into an array of differing morphologies.[21,42,46–53]

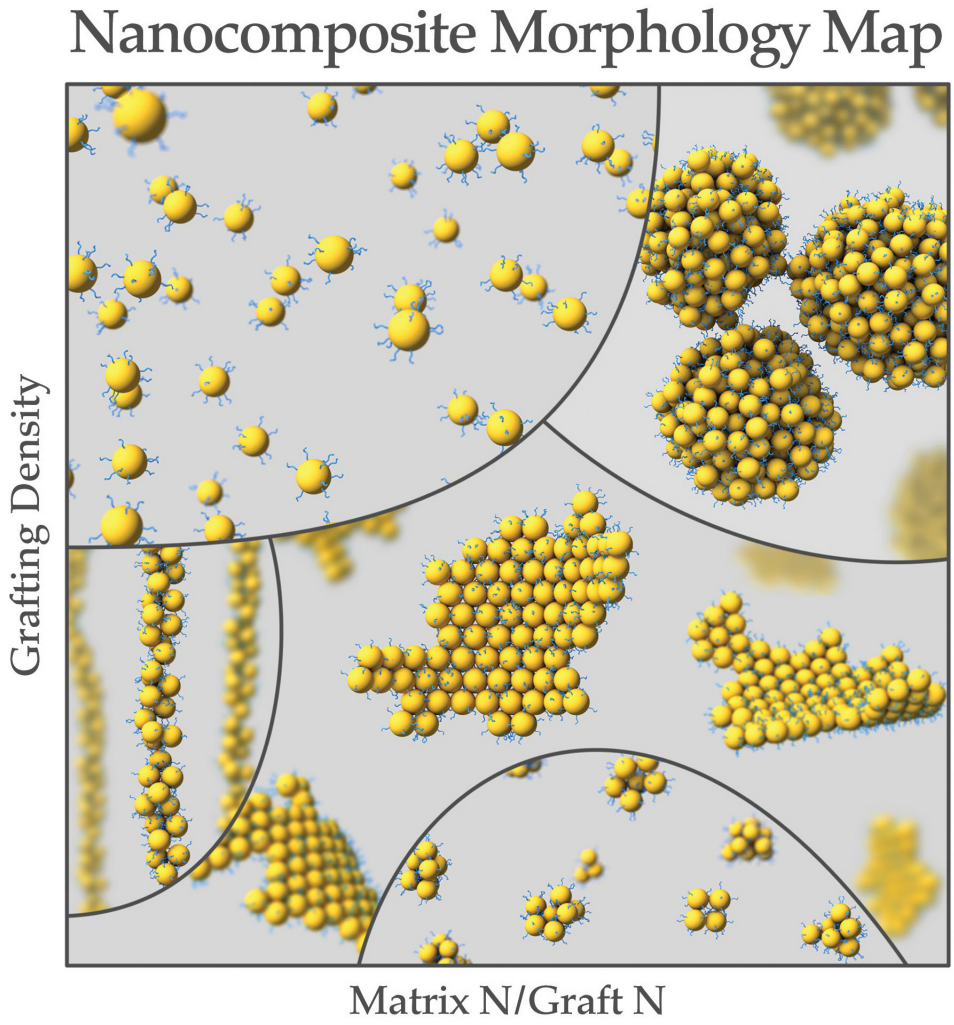

Figure 1.1 Nanocomposite morphology map showing the different nanoparticle dispersion states possible with a variation in graft density (y-axis) and ratio of matrix chain length to grafted chain length (x-axis). N is defined as the number of repeat units in the polymer chain.

While the study of the previously stated factors affecting distributions, morphologies, and the resulting properties is imperative to a more ubiquitous incorporation of these materials; the ability to do so is enabled by synthetic strategies and methodolo-

gies of polymer and organic chemistry. The ability of the polymer chemist to control multiple facets of the PNCs (whether it is NP graft density, polymer composition, polydispersity, molecular weight, and/or architecture) allows for the study of these effects. More comprehensive reviews can be found in literature.[54–56]

These organic and polymer methods allow for the fine-tuning of the substrate surface. Because of this focus on the substrate surface/interface, this introduction is organized with such a focus. First, grafting methods will be discussed, followed by a more detailed view of differing surface chemistries and their resulting attachment/modification chemistries. Then a brief discussion is included of surface polymerization methods with an emphasis on reversible addition fragmentation chain transfer (RAFT) polymerization. This discussion culminates in the properties and applications this tunability allows and an outline for the remainder of this dissertation.

1.2 Grafting Methods

Two broad synthetic strategies exist for the creation of polymer-grafted nanoparticles. These are grafting-to and grafting-from. The grafting-to method involves the attachment of a preformed and end-functionalized polymer chain. The attachment occurs through either physisorption, where the forces involved are intermolecular between the chain and the substrate surface, or chemisorption where a covalent bond is formed between the chain end moiety and the surface. Grafting-to offers the chemist a simple and modular method for the creation of polymer-grafted nanoparticles. Monomers that traditionally cannot be polymerized via a surface initiated (SI) or controlled radical polymerization (CRP) technique can be premade via the required method and then attached. However, this approach restricts the ability to create brushes with high graft density.[57] The diffusion of a polymer chain to a functionalized surface suffers from steric repulsion between the diffusing chain and those chains already at-

tached. This effect can become even more pronounced with higher molecular weight polymer chains.

With a grafting-from strategy, the surface is functionalized with the appropriate initiator or chain transfer agent. The polymer chain is then grown from the surface in a surface initiated polymerization. Small molecules, such as an initiator or monomer, do not suffer from the same steric repulsion as a diffusing polymer chain. This allows for a much higher graft density. However, not all polymer chemistries can be made via a grafting-from strategy. Ultimately the application will determine the appropriate synthetic strategy as factors such as scale, monomer choice, polymerization method, and required graft density will influence the needed method. The variation in graft density can result in a difference in polymer brush height due to the steric interaction between grafted chains. These various methods and their effect on chain density can be seen in Figure 1.2[55]

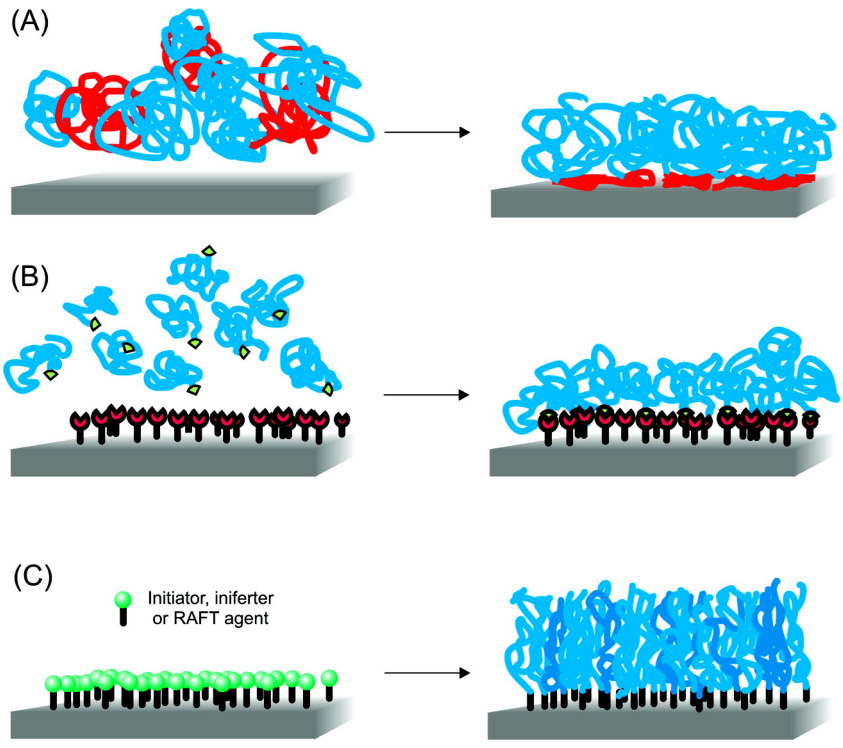

Figure 1.2 Grafting methods: (a) physisoprtion (b) grafting-to (c) grafting-from.

A wide variety of substrates have been modified to graft polymer chains by grafting-to or grafting-from techniques. The functional groups on substrates can be initiator or chain transfer agent (CTA) that allow surface-initiated atom transfer polymerization (ATRP), nitroxide-mediated polymerization (NMP), reversible-addition fragmentation chain transfer (RAFT); or other groups required to couple with free polymer chain end groups in a grafting-to method. This section will discuss the different surface and attachment chemistries among silica, metal oxides, gold, carbon, and polymer nanomaterials.

Silica

Silica substrates, such as nanoparticles, silica gel, glass, and quartz have been widely used for grafting of polymer chains. A general strategy to functionalize silica substrates is using an organosilane to incorporate functional groups onto surfaces, including amino, carboxylic acid, and halogen groups. Further post-functionalization can introduce initiator or CTAs to mediate SI CRP. In this method, a condensation reaction between silanol groups (Si-OH) on silica substrates and alkoxysilane or halogensilane molecules occurs resulting in the formation of a Si-O-Si bond.[46,58–61] A series of mono- and tri-functional silanes have been widely employed, such as $RSi(Me_2)OEt$, $RSi(OMe)_3$, and $RSi(OEt)_3$.

Trifunctional organosilanes have been reported to polymerize with unreacted functional silane moieties in water, restricting the formation of a monolayer of surface functionalized groups.[60] As a different approach, silane-containing initiators or CTAs was employed to directly modify silica surfaces. Benicewicz et al. developed a silane-containing RAFT agent by a multistep synthesis to react with silanol groups on the surface of silica nanoparticles.[58] However, this silane-containing RAFT agent suffered

from issues of low yield due to the silane's affinity for silica gel during column chromatography purification. In order to counteract this, the role of silane coupling and RAFT agent attachment were separated using an aminosilane for modification of the silica surface and an activated RAFT agent for CTA attachment.[59] This has allowed for a range of graft densitites from 0.01 - 0.7 chains/nm^2. Other attachment methods have been employed towards increasing graft density. During a condensation reaction with an alkoxysilane, the alcohol byproduct could also condense onto the surface effectively decreasing the available graft density. Brittain et al. employed the use of an allyl silane whose byproduct would be volatile enough to escape the reaction flask without attaching to the surface.[62] Even though an increase in graft density was seen in some substrates, it was not seen in colloidal silica.

Metal Oxides

Nanocomposites with metal oxide (MO) nanomaterials impart properties unique to the specfic type of metal oxide, such as transpareny, high refractive-index, fracture toughness, etc. Ideally, the property required can be enhanced even at very low loading of the metal oxide. Typically, the majority of metal oxides used in nanocomposites include iron, indium tin, aluminum, and titanium oxides. For these substrates, the most common functional groups used include silanes, carboxylic acids, and phosphonic acids. Carboxylic acids are routinely used to stabilize metal oxide nanoparticles upon their synthesis, with oleic acid being the most commonly used ligand. The oleic acid prevents surface oxidation of the metal oxide and due to its long alkyl chain, improves the solubility of the nanoparticles in nonpolar solvents. However, carboxylic acids are not strong binders, and many procedures use ligand exchange reactions to replace oleic acids with silanes or phosphonic acids. Larsen and coworkers synthesized iron oxide nanoparticles with oleic acid groups, and subsequently modified them through ligand exchange with modified PEG for bioapplications.[63] Similarly, White

et al. have used a similar method to strip oleic acid from iron oxide nanoparticles to attach phosphate functional ATRP initiators on the surface.[64] In this case, the ATRP initiator can polymerize from the surface, as opposed to prefunctionalized polymer as exemplified in the silane modified PEG.

Other carboxylic acids are also used to functionalize metal oxides, for example Hojjati et al. have attached carboxylic acid functionalized RAFT agents to titania nanoparticles.[65,66] Subsequently, polymers including poly(methyl methacrylate) (PMMA) and poly(acrylic acid) (PAA) were demonstrated to have grafted from the surface to obtain dispersed titania nanocomposites. Herein, the carboxylic acid employs multiple types of binding modes to coordinate with the titania surface, including monodentate, chelated, or bridging bidentate architectures.

Small molecule silanes are also important in improving the dispersions of metal oxide nanoparticles in polymer matrices. Truong et al. has demonstrated the effect of octyl triethoxysilane on Al_2O_3 nanoparticles where silane modificed particles displayed superior dispersion quality in polypropylene.[67] Additionally, functional silanes can facilitate reactions with matrix polymers for improved dispersions in polymer films. Gupta and coworkers functionalized Al_2O_3 nanoparticles with aminopropylsilane and crosslinked the nanoparticles with epoxy resins for encapsulant materials.[68] Similarly, functional silanes can also be used to attach initiators on the surface for polymerizations such as ATRP,[69,70] NMP,[71] and RAFT[72] to grow polymers from the surface for MO nanocomposites.

Recently, the trend in functionalizing MOs has shifted towards the use of phosphonic acids. This is mainly attributed to the enhanced hydrolytic stability of the P-O-C and M-O-P bonds as well as the lack of homocondensation between P-OH groups, leading to a robust linkage with the metal oxide.[73–75] Functional phosphonic acids/phosphates with azide functionalities have been anchored to TiO_2 nanoparticles, followed by click reactions with alkyne-terminated polymers to pro-

duce nanocomposites with excellent dispersions.[76–78] Alternatively, phosphate functionalized PDMS has been used to graft polymers to TiO_2, where the dispersion of the nanocomposite can be tailored with fine-tuning the enthalpic and entropic factors through bimodal populations of the PDMS brush.[79] Controlled radical polymerizations have also been facilitated from metal oxide surfaces through the use of phosphonic acid functional initiators via RAFT,[80] NMP, and ATRP.[81]

Gold

The general strategy to functionalize gold nanoparticles is forming an Au-S bond on the surface. The first strategy is preparing gold nanoparticles in situ under the stabilization of polymers containing thiol end groups. Lowe and coworkers reduced several RAFT end group-containing polymers and a gold precursor complex simultaneously in water resulting in a variety of polymer stabilized gold nanoparticles.[82] The second strategy is preparing initiator or RAFT agent coated gold nanoparticles followed by SI-CRP. Fukuda et al. reduced $HAuCl_4$-$4H_2O$ and ATRP initiator containing disulfide simultaneously to prepare ATRP initiator functionalized gold nanoparticles followed by SI-ATRP.[83] Dithioesters or trithiocarbonates have been reported to directly attach to gold substrates.[84] This straightforward strategy provides a simple tool to prepare polymer grafted gold nanoparticles by SI-RAFT.

Carbon

Generally, there is no functional group on carbon nanotubes or nanoparticles. Thus the modification of the carbon nanomaterial needs an oxidative activation with HNO_3 or H_2SO_4 to introduce carboxylic acid moieties on the surface. The further conversion of carboxylic acids with initiator-containing groups via an esterification reaction resulted in ATRP initiator modified nanotubes[85] or nanoparticles[86]. Alternatively, while carbon surfaces can be treated as a site for polymer chain growth or chain-end

attachment, fullerene can be modified and then attached to repeat units in a polymer chain, increasing loading of C_{60}.[87]

Polymer Surfaces

The surface functionalization of polymer nanomaterials varies depending on the nature of the substrates. Generally, there are two categories of the substrate polymer surfaces, namely functional group containing and inert polymer nanomaterials. The strategy to modify functional group containing polymer substrates is either converting these groups into initiators followed by SI-CRP or coupling with other free functional group containing polymers. Naturally occurring cellulose with hydroxyl groups, for example, can be coupled with ATRP initiators by condensation reactions.[88] Halogen and epoxide containing polymer substrates can be treated with sodium N,N-diethyldithiocarbonate and carboxylic acid containing ATRP initiators respectively to incorporate initiators and/or RAFT agents onto surfaces.[89]

The inert polymer substrates need to be prepared to incorporate functional groups on the surface followed by above-mentioned strategies or directly used as a platform for growing polymers via irradiation or plasma procedures. The pretreatment method varies depending on the polymer substrate. For example, polypropylene, poly(tetrafluoroethylene) (PTFE), and various rubbers were selected and treated with ozone,[90] hydrogen plasma/ozone,[89] and $NaOH/KMnO_4$[91] respectively. The newly generated -OH groups on the polymer substrates can be postfunctionalized with initiators or RAFT agents followed by SI-CRP. An alternative strategy to grow polymers on inert polymer substrates is employing irradiation or plasma techniques. UV, γ-radiation, and plasma have been widely used to generate radicals on poly(vinylidene fluoride), polyethylene, and PTFE surfaces followed by SI-RAFT or SI-ATRP to grow polymer chains.[92–94]

Controlled or "living" polymerization techniques allow for control of the polymer composition, molecular weight, architecture, and polydispersity. However, controlled **radical** polymerizations (CRP) offer certain advantages over other methods such as anionic, cationic, and ring-opening polymerizations. Radical polymerizations are generally less restrictive in terms of reaction media and compatible functional groups while still allowing for control of the previously mentioned molecular variables. The principle CRP methods are nitroxide-mediated polymerization (NMP), atom transfer radical polymerization (ATRP), and reversible-addition fragmentation chain transfer (RAFT).

NMP

Nitroxide mediated polymerization elicits control via a reversible activation mechanism of the polymer chain. This is based on a nitroxide radical that "end-caps" the polymer chain, allowing for a persistent radical effect without the need for a separate initiator or catalyst.[95,96] Husseman et al. performed the first work with surfaces using this technique.[97] Polystyrene brushes were grown using 2,2,6,6-tetramethylpiperidinyloxy (TEMPO) functionalized silicon wafers. More recently Chevigny and coworkers have used NMP to produce polystyrene on silica nanoparticles.[98] First, an aminosilane reagent was condensed onto the surface and then a modified ester was reacted with the available amino groups. While the ability to control the polymerization without added reagents such as initiator, chain transfer agent (CTA), or catalyst is advantageous, NMP is not without its drawbacks. The nitroxide must be meticulously chosen to ensure proper control as most NMP reactions show best results with styrenic monomers. Also, while the addition of other reagents is unnecessary, control is best seen with sacrificial nitroxide added in solution. This, however, allows

for the formation of polymer chains in solution which can be difficult to remove and separate from modified substrates. Finally, the required high temperatures for the formation of nitroxide radicals can eliminate the use of monomers with thermally sensitive functional groups.

ATRP

The most popular method for the synthesis of polymer brushes is ATRP. First described in 1995, ATRP also controls the polymerization through an equilibrium of active and dormant species.[99,100] The mechanism of control is through the reversible redox activation of a dormant alkyl halide/polymer species. This is done via homolytic transfer of the halide to a transition metal/ligand complex, allowing for the propagation of the radically active polymer species and then quickly reversed to revert the polymer chain back to its dormant state, once again end-capped with the halide. A much more flexible method than NMP due to its ability to polymerize a wider range of monomers under a wider range of reaction conditions, ATRP also has the flexibility of its own variations. Due to the ability in variation of transition metals, their oxidation states, the attached ligands, the halide initiator, etc., there has been an expansion of ATRP techniques. These include, but aren't limited to, reverse ATRP, activators generated by electron transfer (AGET), initiators for continuous activator regeneration, and activators regenerated by electron transfer (ARGET); but their discussion is outside the scope of this review.[101] The first surface initiated ATRP was performed by Huang and Wirth.[102]. Using silica particles that were functionalized with benzyl chloride, brushes of poly(acrylamide) were grown from the surface. Since then, ATRP has become increasingly popular for the synthesis of polymer brushes, including the use of reverse ATRP[103] and ARGET ATRP.[104] However, the variability of ATRP can prove to be an impediment. When a complex system contains an alkyl halide initiator, monomer, solvent, and metal/ligand complex designed to work

together, there are many variables to coincide correctly for the successful design of a synthetic system. Also, removal of the catalyst in the final product can eliminate its use from certain biomedical or electronic applications.

RAFT

The versatility of choice in monomer functionality, lack of catalyst, and mild reaction conditions of RAFT has made its continued growth of use in the last decade possible. Discovered at CSIRO and first published in 1998, RAFT controls the polymerization through a different mechanism than NMP and ATRP.[105] Instead of a reversible termination, RAFT is based on a reversible chain transfer. With a suitable chain transfer agent (CTA), the growing chains reach equilibrium between active propagating radical species and the CTA as the active radical is shuffled between them. The RAFT agent contains a stabilizing Z group and a reactivating R group that are selected based upon monomer choice.

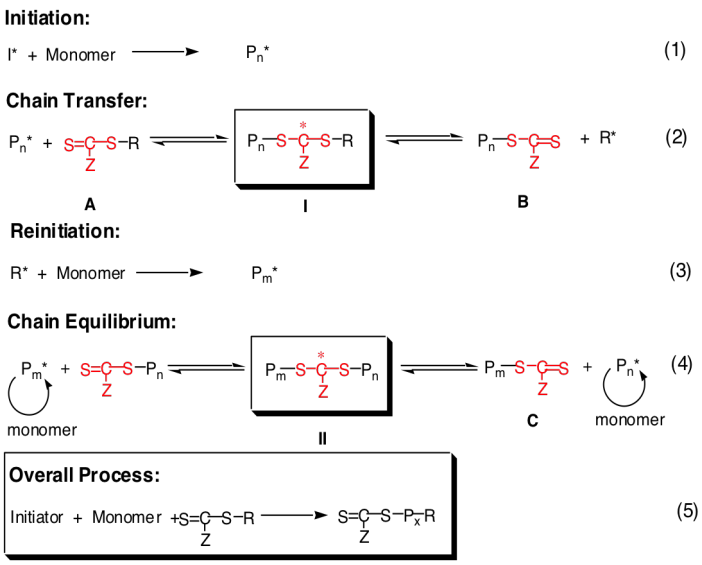

Figure 1.3 Mechanism of RAFT Polymerization

An added benefit of RAFT polymerization is once a suitable RAFT agent is chosen, the remaining process is similar to a conventional free radical polymerization.

The other parameters such as solvent, initiator, and temperature can remain the same. For surface initiated (SI) RAFT polymerizations, there are two attachment methods of the RAFT agent. Both the Z and R group (when modified accordingly) can become the attachment point for the growing polymer chain. Due to the mechanism of RAFT, the R group approach is most popular due to the R group's role as the propagating species. When the Z group is attached to the surface, the propagating chain has to then detach, propagate, and then reattach. This, in effect, is very similar to the grafting-to method and has its limitations on graft density.[106] In early reports of RAFT for grafting polystyrene chains on nanoparticles by Tjujii et al., some shouldering of GPC traces were seen and was attributed to a surface radical migration effect.[107] However, with advances in RAFT and coupling agents, we can now control the graft density from 0.01 to 0.7 chains/nm^2 while growing polymer brushes of molecular weights over 200 kg/mol with a polydispersity index below 1.15.[58,59,108]

1.5 Properties and Applications

Polymer brush grafted nanoparticles have found use in a range of applications, for example switchable response, biosensing, localized heating, drug delivery, metal ion recovery, catalysis, etc. More detailed coverage of these topics can be found elsewhere.[109,110] In nanocomposites, grafted particles act as filler materials. The individual properties of the particle and the matrix polymer determine the application. Based on the properties offered by the particle, enhacements can be made in optical, electrical, and mechanical properties of the composite as a whole.[47,79,111,112] Significant enhancements are usually greatest when the properties of the filler are different than that of the matrix. This, however, leads to incompatibility. The grafting of polymer chains allows for the tuning of the interface and therefore compatibility between the nanoparticle and matrix. This tunability can be used to control the dispersion of

the nanoparticles, interphase characteristics, and properties of the nanocomposite.

The synergistic role of the particle interface on relevant interphase polymer characteristics remains an open problem. This is due in part to the difficulty in probing nanoscale properties. Nanoparticle dispersion, however, is fairly well understood. In homopolymer matrices, monomodal brush grafted nanoparticles are found to display distinctly different dispersion behavior in the high (autophobic) and low (allophobic) graft density regimes.[113] High graft density brushes can screen core-core attractions, however, they can also cause the expulsion of matrix chains from the brush layer leading to mean field entropic surface tension. This can lead to an attractive potential well at intermediate distances[16] and this attraction leads to nanoparticle aggregation.[114] When particle surfaces become exposed with decreasing graft density, there is an increased domination of enthalpic core-core attractions on the dispersion. This low graft density regime has generated the most interest in literature thus far, due to the previously mentioned issues. This balance between enthalpic core-core attractions and entropic excluded volume repulsion results in the formation of a set of dispersion morphologies such as spherical aggregates, sheets, strings, and individually dispersed particles.[46] Morphology plots of these various dispersion states, taking into account graft density versus matrix/brush molecular weight ratios guided this early research. In order to predictably tune dispersion for a wide range of chemistries, however, a different approach was used. Kumar et al. presented simulation studies that employed a mean-field energetic balance between core attractions and brush repulsions to identify phase boundaries between the various morphologies. This approach was then modified by Benicewicz and Schadler to develop phase diagrams that accurately predict dispersion morphologies for a range of filler-matrix chemistries for monomodal and bimodal brush modified particles.[79,115,116]

Mechanical Properties

It has been established that the linear and non-linear elastic/viscoelastic properties are dependent upon dispersion state, loading, and the interfacial binding.[4] This complexity arises out of the co-dependence of dispersion and interphase properties on the linked enthalpic and entropic effects in monomodal brush grafted nanocomposites (lower graft densities favor entanglement but increase particle attraction). This is in addition to findings showing dispersion to play different roles in glassy and liquid states of the composite system.[117]

Glassy State

The glassy/solid state properties of brush grafted composites are normally enhanced by superior dispersion and interfacial binding. While great enhancements in elastic moduli have been demonstrated at very low filler loadings (<5 wt%) of well-dispersed polymer grafted graphene, PVA paper, and nanotube composites,[79,118–121] most investigations have been carried out on spherical silica nanoparticles in homopolymer matrices.[46,47,116,117] This is because of the ease of surface modification of silica, the isotropic interactions of spherical particles, and the absence of a net enthalpic interaction between the chemically identical brush and matrix. In monomodal brush grafted systems, strong matrix brush entanglement favors a uniformly dispersed morphology. Therefore, in situations where the brush is wetted the best enhancements in glassy state mechanical properties are realized.[117] This is due to the strongly bound interphase polymer (better load transfer), whose contribution to bulk properties is further enhanced by superior surface area to volume ratio offered by the well-dispersed particles.[116] McEwan et al. have shown through USAXS measurements that increased brush stretching causes increased interparticle repulsions and therefore a larger glassy state storage modulus.[122] Additionally, Kumar et al. observed the elastic modulus to be best enhanced in a dispersed system using a bubble inflation technique.[117] How-

ever, since wetting requires the brush to be significantly larger than the matrix, it is often a difficult task to obtain dispersed particles while still optimizing particle loading.[46,123]

As a solution to this problem, we have suggested the use of a second densely grafted brush in addition to the first low graft density long chain population.[115,116] The short brush is used to screen core-core attractions while the low density long brush creates favorable excluded volume repulsions by entangling with the matrix. The bimodal particles have shown superior dispersion over corresponding monomodal brush systems. They were also found to cause an enhanced glassy state storage modulus (measured by dynamic mechanical analysis) and elastic modulus (measured by nanoindentation).[116] We note that since the high graft density plays a purely enthalpic role it may be synthesized of a different chemistry. This is an additional parameter that can be varied to preditably tune dispersions as well as to add surface functionalities for other applications. Further discussion of bimodal brushes, their synthesis, and property enhancement is discussed in Chapter 2.

Liquid/Rubbery State

In monomodal brush grafted systems, dewetting that leads to the formation of connected percolating assemblies causes the best mechanical reinforcements in the rubbery regime. Hasegawa et al. were the first to identify this interesting behavior. They found a plateau in the low frequency storage modulus to increase in height with increasing anisotropy in filler dispersion state.[16] Ackora et al. obtained similar results in polystyrene grafted silica/polystyrene matrix systems and corresponding poly(methyl)methacrylate systems.[46,52] This reinforcement was attributed to the formation of particle networks, bridged by interdigitated polymer brushes. These percolating particle-polymer structures channel stress effectively throughout the nanocomposite, causing a higher low-frequency modulus. Unlike the case of bare particle

aggregates, the inferfacial binding, glassy bridges, and deagglomeration participate negligibly in this mechanism.[124–126] These observations were further supported by the findings of Kumar et al. who found start-up overshoots in stress-strain curves in steady shear experiments to increase with increasing percolation.[47] They also observed analogous solid-state mechanical property of yield stress to be best enhanced in a fractally aggregated system.[117]

Optical Properties

There is considerable interest in enhancing the optical properties of industrial polymers by the addition of fillers that display fascinating nanoscale optical behavior. One optical property that has received substantial attention is the refractive index of LED encapsulant materials. An enhanced refractive index is expected to increase the total internal reflection within the encapsulant, thereby leading to enhanced light extraction efficiency from the LED.[127] High refractive index metal oxide fillers, such as titania (∼2.5) and zirconia (∼2.2), have been added to traditional encapsulants such as epoxies and silicones for this purpose.[127,128] These materials, however, suffer from a loss in transparency attributed to scattering from aggregated nanoparticles. Benicewicz and Schadler adopted the bimodal brush idea in conjunction with the modified phase diagram approach to predictably achieve well-dispersed morphologies of high refractive index fillers that show remarkable improvements in refractive index over monomodal brush grafted particle while still retaining the transparency of the neat polymer matrix.

Another often explored application in LED encapsulants is color conversion. Tao et al. used bimodal PDMS grafted quantum dots (CdSe) to obtain transparent photoluminescent silicone based composites.[128] The uniformly dispersed bimodal particles also led to enhanced stability over the poorly dispersed monomodal brush grafted particles. In other applications, epoxy with a matrix compatible PGMA grafted in-

dium tin oxide was found to have homogenous particle dispersions. These composites displayed 90% optical transparency in the visible range and increasing UV absorption with increasing ITO loading.[78]

1.6 Dissertation Outline

This dissertation will focus on the design, synthesis, and characterization of polymer nanocomposite interfaces and the property enhancement afforded from said interface design. Through the use of reversible addition fragmentation chain transfer (RAFT) polymerization for the grafting of polymer chains to silica nanoparticles, the surface of silica nanoparticles can be manipulated to tune the properties of the nanocomposite as a whole.

In Chapter 2, heterogeneity is introduced onto the surface of silica nanoparticles via a sequential RAFT polymerization to afford a bimodal brush system. A densely grafted, short brush population is polymerized from the surface in order to provide screening for the enthalpic core-core attraction of the nanoparticles that can lead to agglomeration. Afterwards a second sparsely grafted, long brush population is polymerized to enable the nanoparticle to entangle with the polymer matrix overcoming the entropic preference of the grafted chains dewetting from the matrix chains. These two populations and all their respective molecular variables (graft density, chemistry, end-group chemistry, polydispersity, etc) can be controlled with this approach. With this control in place, the molecular variables were used to produce both bimodal and monomodal samples for comparison of their dispersion state and resulting properties when mixed in a polymer matrix. The bimodal brush samples had a greater dispersion compared to their monomodal counterparts, even in a matrix that has a higher molecular weight than that of the attached brush. It was found that not only do the bimodal samples improve dispersion when compared to monomodal brushes, but that the thermomechanical properties are enhanced as well. Tuning of the long

chain graft density determined that very low graft densities were better for improving entanglement, while resulting in an increase in modulus and Tg. The first bimodal kinetic study was performed to prove that control over the polymerization can still be obtained using RAFT even when a dense brush is already in place.

In Chapter 3, following the information gained from our first bimodal samples, it was ascertained that with our bimodal system the enthalpic attraction of the particles and the entropic dewetting of the grafted chains were decoupled. This allowed us to pursue the synthesis of mixed bimodal samples. In a mixed bimodal sample the chemistries of the brush populations are distinct. If the long chains are the only population entangling with the matrix, then it can remain matrix compatible while the short brush can be varied to improve other desired properties of the nanocomposite. In order to test whether monomer/polymer incompatibility would allow for the diffusion of an incompatible monomer past a short, dense brush to the surface, a simple poly(methyl)methacrylate/polystyrene mixed bimodal brush was made. While varying the chemistries of both short and long brushes, bimodal samples were created with control of all previously mentioned molecular variables. These mixed bimodal samples were then mixed with both PMMA and PS matrices. We found that as long as the long brush remained matrix compatible, the short brush can be of a different and incompatible chemistry and still remain entangled with the matrix and well dispersed even in a matrix of molecular weight higher than the long brush. In order to push that testing further, bimodal samples of poly(1H,1H-heptafluorobutyl methacrylate) short brushes and polystyrene long brushes were made. A film of these nanoparticles were drop cast onto various substrates showing increased water contact angle measurements when compared with untreated samples. These tests prove the effective decoupling of the roles of short and long brushes: the sole role of the long brush is that of entanglement and the sole role of the short brush is that of screening core-core attractions.

For Chapter 4, further work was performed to develop new approaches to the synthesis of bimodal brushes. Taking cues from our testing that showed lower graft densities improved entanglement, it was decided to pursue a one-pot bimodal brush synthesis using a grafting-to approach. While grafting-to is incapable of producing high graft density brushes, we have shown previously that very high graft densities are not required for dispersion. Since RAFT polymerization allows for control of the polymer chain end chemistry, the efficiency of post-polymerization modification was compared to the use of a modified/activated RAFT agent for attachment to the silica surface. The activated RAFT agent showed higher graft densities while still allowing the use of a thermally initiated, bulk polymerization without decomposition of the CTA at the higher temperatures required. This allows for decreased solvent and monomer use and therefore easier scale-up. Both long and short chains were attached in a one-pot approach. While not having the control of the sequential RAFT polymerization process, it is much simpler, more efficient, and more modular than the multi-stepped procedure. While decreasing the complexity of the process, it increased the difficulty in characterization. If both populations are attached in one step, the analysis of each population's chain density independent from the other becomes difficult. To solve this problem, a new anthracene-containing initiator was created and used to exchange the Z group of the short brush polymer chain end via a radical cross coupling mechanism. Since each population then absorbs in a different region of UV-Vis, the graft densities can be calculated independently.

Finally, in Chapter 5 new synthetic strategies were developed towards the modification of the silica nanoparticle surface via a different ligand while also focusing on improving efficiency. Previous approaches used a linear aminosilane for the coupling of the RAFT agent to the surface. While successful, the reactions take hours to complete. In a new approach, an amine-containing cyclic azasilane was used for the modification of the silica surface in under five minutes. This new ligand has the

same ability as the previous method to be varied in loading in order to vary the graft density. The RAFT polymerization of poly(methyl)methacrylate and polystyrene were performed to show that the attached RAFT agent retained its viability after attachment while still maintaining control of the polymerization.

1.7 References

[1] Zhu, Z. Y.; Thompson, T.; Wang, S. Q.; von Meerwall, E. D.; Halasa, A. *Macromolecules* **2005**, *38*, 8816–8824.

[2] Winey, K. I.; Vaia, R. A. *MRS Bulletin* **2007**, *32*, 314–319.

[3] Vaia, R. A.; Maguire, J. F. *Chemistry of Materials* **2007**, *19*, 2736–2751.

[4] Schadler, L. S.; Kumar, S. K.; Benicewicz, B. C.; Lewis, S. L.; Harton, S. E. *MRS Bulletin* **2007**, *32*, 335–340.

[5] Payne, A. R. *Journal of Applied Polymer Science* **1965**, *9*, 2273–&.

[6] Oberdisse, J. *Soft Matter* **2006**, *2*, 29–36.

[7] Moniruzzaman, M.; Winey, K. I. *Macromolecules* **2006**, *39*, 5194–5205.

[8] Lin, Y.; Boker, A.; He, J. B.; Sill, K.; Xiang, H. Q.; Abetz, C.; Li, X. F.; Wang, J.; Emrick, T.; Long, S.; Wang, Q.; Balazs, A.; Russell, T. P. *Nature* **2005**, *434*, 55–59.

[9] LeBaron, P. C.; Wang, Z.; Pinnavaia, T. J. *Applied Clay Science* **1999**, *15*, 11–29.

[10] Krishnamoorti, R.; Vaia, R. A.; Giannelis, E. P. *Chemistry of Materials* **1996**, *8*, 1728–1734.

[11] Krishnamoorti, R. *MRS Bulletin* **2007**, *32*, 341–347.

[12] Kluppel, M. *Kautschuk Gummi Kunststoffe* **1997**, *50*, 282–291.

[13] Gilman, J. W.; Kashiwagi, T.; Lichtenhan, J. D. *SAMPE Journal* **1997**, *33*, 40–46.

[14] Bockstaller, M. R.; Mickiewicz, R. A.; Thomas, E. L. *Advanced Materials* **2005**, *17*, 1331–1349.

[15] Kumar, S. K.; Jouault, N.; Benicewicz, B.; Neely, T. *Macromolecules* **2013**, *46*, 3199–3214.

[16] Hasegawa, R.; Aoki, Y.; Doi, M. *Macromolecules* **1996**, *29*, 6656–6662.

[17] Zhao, L.; Li, Y. G.; Zhong, C. L. *Journal of Chemical Physics* **2007**, *127*, 154909.

[18] Xu, C.; Ohno, K.; Ladmiral, V.; Composto, R. J. *Polymer* **2008**, *49*, 3568–3577.

[19] Meli, L.; Arceo, A.; Green, P. F. *Soft Matter* **2009**, *5*, 533–537.

[20] Iacovella, C. R.; Horsch, M. A.; Glotzer, S. C. *Journal of Chemical Physics* **2008**, *129*, 044902.

[21] Harton, S. E.; Kumar, S. K. *Journal of Polymer Science Part B-Polymer Physics* **2008**, *46*, 351–358.

[22] Yezek, L.; Schartl, W.; Chen, Y. M.; Gohr, K.; Schmidt, M. *Macromolecules* **2003**, *36*, 4226–4235.

[23] Wang, X. R.; Foltz, V. J.; Rackaitis, M.; Bohm, G. G. A. *Polymer* **2008**, *49*, 5683–5691.

[24] Voudouris, P.; Choi, J.; Gomopoulos, N.; Sainidou, R.; Dong, H. C.; Matyjaszewski, K.; Bockstaller, M. R.; Fytas, G. *ACS Nano* **2011**, *5*, 5746–5754.

[25] Sunday, D.; Ilavsky, J.; Green, D. L. *Macromolecules* **2012**, *45*, 4007–4011.

[26] Sunday, D.; Curras-Medina, S.; Green, D. L. *Macromolecules* **2010**, *43*, 4871–4878.

[27] Shull, K. R. *Macromolecules* **1996**, *29*, 2659–2666.

[28] Reiter, G.; Auroy, P.; Auvray, L. *Macromolecules* **1996**, *29*, 2150–2157.

[29] Ojha, S.; Beppler, B.; Dong, H. C.; Matyjaszewski, K.; Garoff, S.; Bockstaller, M. R. *Langmuir* **2010**, *26*, 13210–13215.

[30] McEwan, M. E.; Egorov, S. A.; Ilavsky, J.; Green, D. L.; Yang, Y. *Soft Matter* **2011**, *7*, 2725–2733.

[31] Lindenblatt, G.; Schartl, W.; Pakula, T.; Schmidt, M. *Macromolecules* **2001**, *34*, 1730–1736.

[32] Lindenblatt, G.; Schartl, W.; Pakula, T.; Schmidt, M. *Macromolecules* **2000**, *33*, 9340–9347.

[33] Jia, X. L.; Listak, J.; Witherspoon, V.; Kalu, E. E.; Yang, X. P.; Bockstaller, M. R. *Langmuir* **2010**, *26*, 12190–12197.

[34] Huang, C. L.; Tassone, T.; Woodberry, K.; Sunday, D.; Green, D. L. *Langmuir* **2009**, *25*, 13351–13360.

[35] Green, D. L.; Mewis, J. *Langmuir* **2006**, *22*, 9546–9553.

[36] Ferreira, P. G.; Ajdari, A.; Leibler, L. *Macromolecules* **1998**, *31*, 3994–4003.

[37] Clarke, C. J.; Jones, R. A. L.; Edwards, J. L.; Shull, K. R.; Penfold, J. *Macromolecules* **1995**, *28*, 2042–2049.

[38] Choi, J.; Hui, C. M.; Pietrasik, J.; Dong, H. C.; Matyjaszewski, K.; Bockstaller, M. R. *Soft Matter* **2012**, *8*, 4072–4082.

[39] Borukhov, I.; Leibler, L. *Macromolecules* **2002**, *35*, 5171–5182.

[40] Borukhov, I.; Leibler, L. *Physical Review E* **2000**, *62*, R41–R44.

[41] Putnam, S. A.; Cahill, D. G.; Ash, B. J.; Schadler, L. S. *Journal of Applied Physics* **2003**, *94*, 6785–6788.

[42] Nie, Z. H.; Fava, D.; Rubinstein, M.; Kumacheva, E. *Journal of the American Chemical Society* **2008**, *130*, 3683–3689.

[43] Nie, Z. H.; Fava, D.; Kumacheva, E.; Zou, S.; Walker, G. C.; Rubinstein, M. *Nature Materials* **2007**, *6*, 609–614.

[44] Nie, Z. H.; Petukhova, A.; Kumacheva, E. *Nature Nanotechnology* **2010**, *5*, 15–25.

[45] Merkel, T. C.; Freeman, B. D.; Spontak, R. J.; He, Z.; Pinnau, I.; Meakin, P.; Hill, A. J. *Science* **2002**, *296*, 519–522.

[46] Akcora, P.; Liu, H.; Kumar, S. K.; Moll, J.; Li, Y.; Benicewicz, B. C.; Schadler, L. S.; Acehan, D.; Panagiotopoulos, A. Z.; Pryamitsyn, V.; Ganesan, V.; Ilavsky, J.; Thiyagarajan, P.; Colby, R. H.; Douglas, J. F. *Nature Materials* **2009**, *8*, 354–U121.

[47] Moll, J. F.; Akcora, P.; Rungta, A.; Gong, S. S.; Colby, R. H.; Benicewicz, B. C.; Kumar, S. K. *Macromolecules* **2011**, *44*, 7473–7477.

[48] Maillard, D.; Kumar, S. K.; Rungta, A.; Benicewicz, B. C.; Prud'homme, R. E. *Nano Letters* **2011**, *11*, 4569–4573.

[49] Liu, K.; Nie, Z. H.; Zhao, N. N.; Li, W.; Rubinstein, M.; Kumacheva, E. *Science* **2010**, *329*, 197–200.

[50] Lin, Y. L.; Chiou, C. S.; Kumar, S. K.; Lin, J. J.; Sheng, Y. J.; Tsao, H. K. *Journal of Physical Chemistry C* **2011**, *115*, 5566–5577.

[51] Fava, D.; Nie, Z.; Winnik, M. A.; Kumacheva, E. *Advanced Materials* **2008**, *20*, 4318–4322.

[52] Akcora, P.; Kumar, S. K.; Sakai, V. G.; Li, Y.; Benicewicz, B. C.; Schadler, L. S. *Macromolecules* **2010**, *43*, 8275–8281.

[53] Akcora, P.; Kumar, S. K.; Moll, J.; Lewis, S.; Schadler, L. S.; Li, Y.; Benicewicz, B. C.; Sandy, A.; Narayanan, S.; Illavsky, J.; Thiyagarajan, P.; Colby, R. H.; Douglas, J. F. *Macromolecules* **2010**, *43*, 1003–1010.

[54] Zhao, B.; Brittain, W. J. *Progress in Polymer Science* **2000**, *25*, 677–710.

[55] Barbey, R.; Lavanant, L.; Paripovic, D.; Schüwer, N.; Sugnaux, C.; Tugulu, S.; Klok, H.-A. *Chemical Reviews* **2009**, *109*, 5437–5527.

[56] Zou, H.; Wu, S.; Shen, J. *Chemical Reviews* **2008**, *108*, 3893–3957.

[57] Ligoure, C.; Leibler, L. *Journal De Physique* **1990**, *51*, 1313–1328.

[58] Li, C. Z.; Benicewicz, B. C. *Macromolecules* **2005**, *38*, 5929–5936.

[59] Li, C.; Han, J.; Ryu, C. Y.; Benicewicz, B. C. *Macromolecules* **2006**, *39*, 3175–3183.

[60] Fadeev, A. Y.; McCarthy, T. J. *Langmuir* **2000**, *16*, 7268–7274.

[61] Cash, B. M.; Wang, L.; Benicewicz, B. C. *Journal of Polymer Science Part A: Polymer Chemistry* **2012**, *50*, 2533–2540.

[62] Wang, Y.; Hu, S.; Brittain, W. J. *Macromolecules* **2006**, *39*, 5675–5678.

[63] Larsen, E. K. U.; Nielsen, T.; Wittenborn, T.; Birkedal, H.; Vorup-Jensen, T.; Jakobsen, M. H.; Ostergaard, L.; Horsman, M. R.; Besenbacher, F.; Howard, K. A.; Kjems, J. *ACS nano* **2009**, *3*, 1947–1951.

[64] White, M. A.; Johnson, J. A.; Koberstein, J. T.; Turro, N. J. *Journal of the American Chemical Society* **2006**, *128*, 11356–7.

[65] Hojjati, B.; Charpentier, P. A. *Journal of Polymer Science Part aPolymer Chemistry* **2008**, *46*, 3926–3937.

[66] Hojjati, B.; Sui, R.; Charpentier, P. A. *Polymer* **2007**, *48*, 5850–5858.

[67] Truong, L. T.; Larsen, Å.; Holme, B.; Diplas, S.; Hansen, F. K.; Roots, J.; Jørgensen, S. *Surface and Interface Analysis* **2010**, *42*, 1046–1049.

[68] Gupta, S.; Ramamurthy, P. C.; Madras, G. *Polymer Chemistry* **2011**, *2*, 221.

[69] Xiong, L.; Liang, H.; Wang, R.; Chen, L. *Journal of Polymer Research* **2010**, *18*, 1017–1021.

[70] Liu, X.; Ye, Q.; Yu, B.; Liang, Y.; Liu, W.; Zhou, F. *Langmuir : The ACS Journal of Surfaces and Colloids* **2010**, *26*, 12377–82.

[71] Robbes, A.-S.; Cousin, F.; Meneau, F.; Chevigny, C.; Gigmes, D.; Fresnais, J.; Schweins, R.; Jestin, J. *Soft Matter* **2012**, *8*, 3407.

[72] Ngo, V. G.; Bressy, C.; Leroux, C.; Margaillan, A. *Polymer* **2009**, *50*, 3095–3102.

[73] Demmer, C. S.; Krogsgaard-Larsen, N.; Bunch, L. *Chemical Reviews* **2011**, *111*, 7981–8006.

[74] Mutin, P. H.; Guerrero, G.; Vioux, A. *Journal of Materials Chemistry* **2005**, *15*, 3761.

[75] Queffélec, C.; Petit, M.; Janvier, P.; Knight, D. A.; Bujoli, B. *Chemical reviews* **2012**, *112*, 3777–807.

[76] Tchoul, M. N.; Fillery, S. P.; Koerner, H.; Drummy, L. F.; Oyerokun, F. T.; Mirau, P. A.; Durstock, M. F.; Vaia, R. A. *Chemistry of Materials* **2010**, *22*, 1749–1759.

[77] Tao, P.; Li, Y.; Rungta, A.; Viswanath, A.; Gao, J. N.; Benicewicz, B. C.; Siegel, R. W.; Schadler, L. S. *Journal of Materials Chemistry* **2011**, *21*, 18623–18629.

[78] Tao, P.; Viswanath, A.; Schadler, L. S.; Benicewicz, B. C.; Siegel, R. W. *ACS Applied Materials & Interfaces* **2011**, *3*, 3638–3645.

[79] Li, Y.; Tao, P.; Viswanath, A.; Benicewicz, B. C.; Schadler, L. S. *Langmuir* **2013**, *29*, 1211–1220.

[80] Boyer, C.; Bulmus, V.; Priyanto, P.; Teoh, W. Y.; Amal, R.; Davis, T. P. *Journal of Materials Chemistry* **2009**, *19*, 111.

[81] Dong, H.; Huang, J.; Koepsel, R. R.; Ye, P.; Russell, A. J.; Matyjaszewski, K. *Biomacromolecules* **2011**, *12*, 1305–11.

[82] Lowe, A. B.; Sumerlin, B. S.; Donovan, M. S.; McCormick, C. L. *Journal of the American Chemical Society* **2002**, *124*, 11562–11563.

[83] Ohno, K.; Koh, K.-m.; Tsujii, Y.; Fukuda, T. *Macromolecules* **2002**, *35*, 8989–8993.

[84] Duwez, A.-S.; Guillet, P.; Colard, C.; Gohy, J.-F.; Fustin, C.-A. *Macromolecules* **2006**, *39*, 2729–2731.

[85] Qin, S.; Qin, D.; Ford, W. T.; Resasco, D. E.; Herrera, J. E. *Journal of the American Chemical Society* **2003**, *126*, 170–176.

[86] Yang, Q.; Wang, L.; Xiang, W.-d.; Zhou, J.-f.; Tan, Q.-h. *Journal of Polymer Science Part A: Polymer Chemistry* **2007**, *45*, 3451–3459.

[87] Li, J.; Benicewicz, B. C. *Journal of Polymer Science Part A: Polymer Chemistry* **2013**, 3572–3582.

[88] Carlmark, A.; Malmström, E. *Journal of the American Chemical Society* **2002**, *124*, 900–901.

[89] Liu, Y.; Klep, V.; Zdyrko, B.; Luzinov, I. *Langmuir* **2005**, *21*, 11806–11813.

[90] Yao, F.; Fu, G.-D.; Zhao, J.; Kang, E.-T.; Neoh, K. G. *Journal of Membrane Science* **2008**, *319*, 149–157.

[91] Coiai, S.; Passaglia, E.; Ciardelli, F. *Macromolecular Chemistry and Physics* **2006**, *207*, 2289–2298.

[92] Yu, W. H.; Kang, E. T.; Neoh, K. G. *Langmuir* **2004**, *21*, 450–456.

[93] Chen, Y.; Deng, Q.; Xiao, J.; Nie, H.; Wu, L.; Zhou, W.; Huang, B. *Polymer* **2007**, *48*, 7604–7613.

[94] Barner, L.; Zwaneveld, N.; Perera, S.; Pham, Y.; Davis, T. P. *Journal of Polymer Science Part A: Polymer Chemistry* **2002**, *40*, 4180–4192.

[95] Rizzardo, E.; Serelis, A.; Solomon, D. *Australian Journal of Chemistry* **1982**, *35*, 2013–2024.

[96] Moad, G.; Rizzardo, E. *Macromolecules* **1995**, *28*, 8722–8728.

[97] Husseman, M.; Malmström, E. E.; McNamara, M.; Mate, M.; Mecerreyes, D.; Benoit, D. G.; Hedrick, J. L.; Mansky, P.; Huang, E.; Russell, T. P.; Hawker, C. J. *Macromolecules* **1999**, *32*, 1424–1431.

[98] Chevigny, C.; Gigmes, D.; Bertin, D.; Jestin, J.; Boue, F. *Soft Matter* **2009**, *5*, 3741–3753.

[99] Wang, J.-S.; Matyjaszewski, K. *Journal of the American Chemical Society* **1995**, *117*, 5614–5615.

[100] Kato, M.; Kamigaito, M.; Sawamoto, M.; Higashimura, T. *Macromolecules* **1995**, *28*, 1721–1723.

[101] Matyjaszewski, K. *Macromolecules* **2012**, *45*, 4015–4039.

[102] Huang, X.; Wirth, M. J. *Analytical Chemistry* **1997**, *69*, 4577–4580.

[103] Wang, Y.-P.; Pei, X.-W.; He, X.-Y.; Yuan, K. *European Polymer Journal* **2005**, *41*, 1326–1332.

[104] Matyjaszewski, K.; Dong, H.; Jakubowski, W.; Pietrasik, J.; Kusumo, A. *Langmuir* **2007**, *23*, 4528–4531.

[105] Chiefari, J.; Chong, Y. K.; Ercole, F.; Krstina, J.; Jeffery, J.; Le, T. P. T.; Mayadunne, R. T. A.; Meijs, G. F.; Moad, C. L.; Moad, G.; Rizzardo, E.; Thang, S. H. *Macromolecules* **1998**, *31*, 5559–5562.

[106] Li, Y.; Schadler, L.; Benicewicz, B. In *Handbook of RAFT Polymerization*; Barner-Kowollik, C., Ed.; Wiley-VCH: Weinheim: Germany, 2008; pp 423–453.

[107] Tsujii, Y.; Ejaz, M.; Sato, K.; Goto, A.; Fukuda, T. *Macromolecules* **2001**, *34*, 8872–8878.

[108] Wang, L.; Benicewicz, B. C. *ACS Macro Letters* **2013**, *2*, 173–176.

[109] Takafuji, M.; Ide, S.; Ihara, H.; Xu, Z. *Chemistry of Materials* **2004**, *16*, 1977–1983.

[110] Stuart, M. A. C.; Huck, W. T. S.; Genzer, J.; Muller, M.; Ober, C.; Stamm, M.; Sukhorukov, G. B.; Szleifer, I.; Tsukruk, V. V.; Urban, M.; Winnik, F.; Zauscher, S.; Luzinov, I.; Minko, S. *Nature Materials* **2010**, *9*, 101–113.

[111] Roy, M.; Nelson, J. K.; MacCrone, R. K.; Schadler, L. S.; Reed, C. W.; Keefe, R. *Dielectrics and Electrical Insulation, IEEE Transactions on* **2005**, *12*, 629–643.

[112] Lu, A.-H.; Salabas, E. L.; Schüth, F. *Angewandte Chemie International Edition* **2007**, *46*, 1222–1244.

[113] Green, P. F.; Oh, H.; Akcora, P.; Kumar, S. K. *Structure and Dynamics of Polymer Nanocomposites Involving Chain-Grafted Spherical Nanoparticles*; Dynamics of Soft Matter: Neutron Applications; 2012.

[114] Green, P. F. *Soft Matter* **2011**, *7*, 7914–7926.

[115] Rungta, A.; Natarajan, B.; Neely, T.; Dukes, D.; Schadler, L. S.; Benicewicz, B. C. *Macromolecules* **2012**, *45*, 9303–9311.

[116] Natarajan, B.; Neely, T.; Rungta, A.; Benicewicz, B. C.; Schadler, L. S. *Macromolecules* **2013**, *46*, 4909–4918.

[117] Maillard, D.; Kumar, S. K.; Fragneaud, B.; Kysar, J. W.; Rungta, A.; Benicewicz, B. C.; Deng, H.; Brinson, L. C.; Douglas, J. F. *Nano Letters* **2012**, *12*, 3909–3914.

[118] Liang, J.; Huang, Y.; Zhang, L.; Wang, Y.; Ma, Y.; Guo, T.; Chen, Y. *Advanced Functional Materials* **2009**, *19*, 2297–2302.

[119] Coleman, J. N.; Khan, U.; Blau, W. J.; Gun'ko, Y. K. *Carbon* **2006**, *44*, 1624–1652.

[120] Coleman, J. N.; Khan, U.; Gun'ko, Y. K. *Advanced Materials* **2006**, *18*, 689–706.

[121] Fang, M.; Wang, K.; Lu, H.; Yang, Y.; Nutt, S. *Journal of Materials Chemistry* **2009**, *19*, 7098–7105.

[122] McEwan, M.; Green, D. *Soft Matter* **2009**, *5*, 1705–1716.

[123] Pryamtisyn, V.; Ganesan, V.; Panagiotopoulos, A. Z.; Liu, H. J.; Kumar, S. K. *Journal of Chemical Physics* **2009**, *131*, 221102.

[124] Sternstein, S. S.; Zhu, A. J. *Macromolecules* **2002**, *35*, 7262–7273.

[125] Jouault, N.; Vallat, P.; Dalmas, F.; Said, S.; Jestin, J.; Boue, F. *Macromolecules* **2009**, *42*, 2031–2040.

[126] Montes, H.; Chaussée, T.; Papon, A.; Lequeux, F.; Guy, L. *The European Physical Journal E* **2010**, *31*, 263–268.

[127] Tao, P.; Viswanath, A.; Li, Y.; Siegel, R. W.; Benicewicz, B. C.; Schadler, L. S. *Polymer* **2013**, *54*, 1639–1646.

[128] Tao, P.; Li, Y.; Siegel, R. W.; Schadler, L. S. *Journal of Applied Polymer Science* **2013**, *130*, 3785–3793.

Chapter 2

Synthesis of Bimodal Brush Grafted Nanoparticles and Thermomechanical Properties of Bimodal Brush Modified Nanoparticle Composites

2.1 Introduction

The control of the interface between a nanoparticle surface and the polymer matrix is accomplished through the previously described surface modifications, grafting methods, and controlled radical polymerization techniques. We have shown this control previously, along with the resulting control over morphology and properties dependent upon this morphology.[1–5] Using these techniques, heterogeneity can also be introduced onto the interface. While adding complexity to the system, it affords the chemist another parameter for the control and tunability of the resulting properties.[6] This heterogeneity is introduced by varying the architecture of the polymer chain and/or the interface directly. In the following chapter, we describe the development of synthetic methods and the resulting properties by introducing heterogeneity via block and bimodal systems.

Block Copolymers on the Surface

Through the use of CRP, block copolymers can be attached to the surface. Because of block copolymers' phase separation behavior, theoretical studies have indicated a

variety of structures can be formed for control of patterning on surfaces and assembly of nanoparticles in solution.[7,8] Variation of chain composition, graft density, total chain length (molecular weight), and interaction energies between the blocks allows for the tuning of the interface. Bin Zhao and William Brittain reported early synthesis of block copolymer brushes.[9] Using a silicate surface, carbocationic polymerization of styrene was completed followed by ATRP for the polymerization of MMA. A different polymerization method was chosen to ensure initiation of the 2^{nd} block occurred and did not initiate a second chain from the surface. Zhao et al. have used a Z-group-attachment RAFT approach for the synthesis of diblock copolymer brushes using a combination of acrylates, methacrylates, and styrene.[10] More recently, Advincula has employed a combination of layer-by-layer deposition of macroinitiators for control of graft density followed by ATRP for the synthesis of an inner block of polystyrene and outer block of poly-2,2,2-trifluoroethyl methacrylate.[11] This combination of blocks allows for a reversible solvent response, dictating surface properties. The reversiblity can be mechanically based as well as chemical. Igor Luzinov and Sergiy Minko have shown a reversible locking mechanism for iron oxide core silica shell nanoparticles.[12] Through the use of a poly(2-vinylpyridine-*b*-ethylene oxide) block copolymer and a magnetic force, the particles lock together even when the magnetic force is removed. This locking can be reversed with a change in pH. While this can be useful for the control of self-assembly, there is a requirement of an external field. Also, while block copolymer brushes have become more commonplace, their use for the modification of nanoparticles in nanocomposites is still uncommon.

The addition of heterogeneity can also improve physical properties. Through the use of a sequential RAFT polymerization technique, Benicewicz and Schadler have been able to create and study silica grafted block copolymers in an epoxy matrix.[13] A rubbery inner block of poly(n-hexyl methacrylate) (PHMA) allowed for the improvement in physical properties while an outer block of poly(glycidyl methacrylate)

(PGMA) allowed the brush to remain matrix compatible. Adding a rubbery copolymer to rigid particles can toughen glassy polymers. Subsequently, they studied the effect of graft density (from 0.07 to 0.7 chains/nm^2) and molecular weight (20 to 80 kg/mol) on the mechanical properties.[13] It was found that the nanoparticles enhanced ductility by up to 60%, fracture toughness by up to 300%, and fatigue crack growth resistance with loading of less than 2% by volume of silica. In addition to block copolymers, heterogeneity can be introduced via bimodal brushes. While more complex, bimodal brushes afford much more control of the surface architecture by decoupling the graft densities of the separate chain populations.

Bimodal Brushes on the Surface

A bimodal/binary polymer brush is defined as a homopolymer brush with two distinct monodisperse chains attached to the surface.[14] If these polymer chains are chemically distinct, it is deemed a mixed brush. The general benefits of a bimodal system when compared to block architecture is increased control over the different chains' independent graft density and a controlled increase in polydispersity of the brush system which has been suggested to control dispersion.[15]

Few methods have been described for the synthesis of a bimodal brush system. Using a grafting-to approach, flat mixed brush systems of poly(tert-butyl acrylate) (PBA) with poly(2-vinylpyridine) (P2VP)[16,17] as well as polystyrene with P2VP[18,19] were reported by Luzinov, Minko, and Stamm. These systems showed a switchable response to changes in pH and solvent allowing for control over the surface properties. However, a grafting-to approach comes with limitations in graft density as discussed earlier.

In a grafting-from approach Zhao created a Y-shaped initiator.[20–23] One arm of the initiator contained a moiety for ATRP polymerization while the other arm contained a moiety for NMP. Using sequential polymerizations, mixed bimodal brushes of

PBA and PS were made and their resulting phase morphology was studied. While an increase in graft density was seen over other techniques, the control over the separate graft densities for the independent chains is lost when the initiators are combined. Ionov and Minko have also studied the preparation of mixed bimodal brushes via grafting-from techniques.[24] Using sequential activators generated by AGET ATRP, PBA and PS brushes were created followed by hydrolysis to create poly(acrylic acid) - polystyrene mixed brushes. The solvent effect and switching properties of these brushes were studied via AFM and contact angle measurements. Via a layer-by-layer technique, Advincula has created a mixed bimodal system of poly(n-isopropylacrylamide) and polystyrene showing control of the surface properties based on temperature and solvent effects.[25] These approaches laid the foundation for the development of a new group of stimuli responsive materials.[26,27] However, few of these methods are performed on particles and even fewer on nanoparticles (diameter<100nm). Also, very few experimental studies have been performed on the effects of bimodal brushes on the ordering of nanoparticles in a polymer matrix.

Previous work has suggested that the assembly of NPs in the sparse brush regime is a competition between enthalpic core-core van der Waals attractions and entropic repulsion due to distortion of the attached brush.[5,28] Also, theoretical work done by Matsen has suggested the use of a bimodal brush could overcome autophobic dewetting between chains of the polymer matrix and those grafted to the nanoparticle surface.[29] Simulation studies done by Jayaraman also support this theory.[6,15,30]

As a new synthetic approach for controlling the nanoparticle surface and hence the aggregation/separation of nanoparticles, we have synthesized bimodal brushes on silica nanoparticles via RAFT. Both a grafting-to and grafting-from approach have been incorporated into its study. Because of the difficulty in using a surface-initiated grafting-from approach for silicones, due to their production through polycondensation, a grafting-to method was developed for the incorporation of TiO_2 NPs into a

silicone matrix.[31] Poly(dimethyl siloxane) (PDMS) was modified with a phosphate moiety on the chain end and then attached to the titania surface. Compared to monomodal systems, the 10kg/mol short and 36kg/mol long bimodal composites showed greater optical clarity even in 100 kg/mol matrix. While the grafting-to approach allows for the flexiblity in polymer and polymerization method choice, the absolute control over all parameters of the surface is not accomplished. For this, a sequential grafting-from method is necessary.

For the controlled study of the contributing entropic and enthalpic factors of NP organization (separately and independently), a sequential RAFT polymerization technique was employed.[32] The short chains can be grown from the surface using a RAFT agent attached to a silica nanoparticle via an aminosilane. The graft density can be controlled by varying the ratio of aminosilane coupling agent to nanoparticles. In order to prevent the formation of block copolymers, the RAFT agent is cleaved from the chain-end via reaction with dilute AIBN. By keeping a relatively intermediary graft density, the core-ore attractions are well screened by the short brush while leaving silica surface area available for secondary attachment. The long chains are produced via an identical procedure, however, at a low graft density to enable entanglement with the polymer matrix. This method allows for the control of each chain's molecular weight, polydispersity, architecture, chemical identity, and graft density independently. The bimodal nanocomposites showed increased dispersity, as well as increased storage and elastic modulus.[33] As shown in 3.1 combining a long, sparse brush with a short, dense brush also allows for the study of the system's enthalpic and entropic factors independently as they are no longer coupled through the use of a monomodal system. The TEM micrographs along with their analysis and the analysis of the composites' thermomechanical properties was performed by collaborators at Rennselaer Polytechnic Institute.

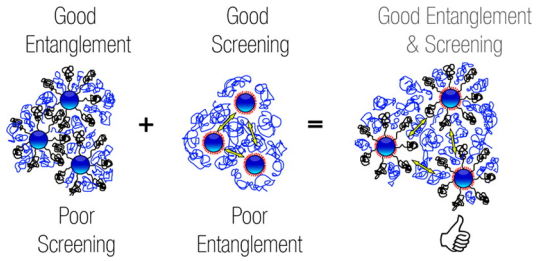

Figure 2.1 Controlling Dispersion and Entanglment via Bimodal Brushes

2.2 Experimental

Materials

Unless otherwise specified, all chemicals were purchased from Fisher Scientific and used as received. Colloidal silica particles (15 nm diameter) were purchased from Nissan Chemical. 2,2'-Azoisobutyronitrile (AIBN) was used after recrystallization in ethanol. Styrene and methyl methacrylate monomers were passed through a basic alumina column to remove the inhibitor before use. Activated 4-cyanopentanoic acid dithiobenzoate (CPDB) was prepared according to a procedure described in literature.[34] 3-Aminopropyldimethylethoxysilane, dimethylmethoxy-n-octylsilane and 3-trimethoxysilylpropyl-2-bromo-2-methylpropionate were purchased from Gelest, Inc. and used as received. Highly Monodisperse Polystyrene (Mw=96000g/mol, PDI: 1.01), was procured from TOSOH Inc.

Instrumentation

NMR spectra were recorded on a Varian 300 spectrometer using $CDCl_3$ as a solvent. Molecular weights and molecular weight distributions were determined using a Waters gel-permeation chromatograph equipped with a 515 HPLC pump, a 2410 refractive index detector, three Styragel columns (HR1, HR3, HR4 in the effective molecular weight range of 100-5000, 500-30000 and 5000-500000, respectively) with THF as eluent at 30 °C and a flow rate of 1.0 mL/min. The GPC system was calibrated with

poly(methyl methacrylate) and polystyrene standards obtained from Polymer Labs.

Synthesis of SiO_2-g-CPDB

A solution (20 mL) of colloidal silica particles (30 wt% in MIBK) was added to a two necked round-bottom flask and diluted with 75 mL of THF. To it was added dimethylmethoxy-n-octylsilane (0.1 mL) and 3-aminopropyldimethylethoxysilane (0.32 mL, 2 mmol) and the mixture was refluxed at 75 °C overnight under nitrogen protection. The reaction was then cooled to room temperature and precipitated in a large amount of hexanes (500 mL). The particles were then recovered by centrifugation and dispersed in THF using sonication and precipitated in hexanes again. The amine functionalized particles were then dispersed in 40 mL of THF for further reaction. A THF solution of the amine functionalized silica nanoparticles (40 mL, 6 g) was added drop wise to a THF solution (30 mL) of activated CPDB (0.67 g, 2.4 mmol) at room temperature. After complete addition, the solution was stirred overnight. The reaction mixture was then precipitated into a large amount of a 4:1 mixture of cyclohexane and ethyl ether (500 mL). The particles were recovered by centrifugation at 3000 rpm for 8 minutes. The particles were then re-dispersed in 30 mL THF and precipitated in 4:1 mixture of cyclohexane and ethyl ether. This dissolution-precipitation procedure was repeated 2 more times until the supernatant layer after centrifugation was colorless. The red CPDB anchored silica nanoparticles were dried at room temperature and analyzed using UV analysis to determine the chain density using a calibration curve constructed from standard solutions of free CPDB.

Graft polymerization of methyl methacrylate from CPDB anchored colloidal silica nanoparticles to make SiO_2-g-PMMA

A solution of methyl methacrylate (17 mL), CPDB anchored silica nanoparticles (1 g, 80 μmol/g), AIBN (1.6 mL of 0.005M THF solution), and THF (17 mL) was prepared in a dried Schlenk tube. The mixture was degassed by three freeze-pump-thaw cycles, back filled with nitrogen, and then placed in an oil bath at 60 °C for 3 h. The polymerization solution was quenched in ice water and poured into hexanes to precipitate polymer grafted silica nanoparticles. The polymer chains were cleaved by treating a small amount of nanoparticles with HF (0.2 mL of a 51% solution in water) and the resulting polymer chains were analyzed by GPC. The polymer cleaved from the SiO_2-g-PMMA particles had a PDI of 1.07 and a molecular weight of 24400 g/mol which is close to the theoretical value of 26037 g/mol expected for this reaction.

Chain end deactivation and cleavage of RAFT agent from SiO_2-g-PMMA

Solid AIBN (130 mg) was added to a solution of SiO_2-g-PMMA1 in THF (1 g by weight of silica in 40 mL THF) and heated at 65 °C under nitrogen for 30 minutes. The resulting solution was poured into 100 mL hexanes and centrifuged at 8000 rpm for 5 minutes to recover SiO_2-g-PMMA nanoparticles. GPC analysis of the cleaved polymer revealed the molecular weight of the polymer was 24200 g/mol and the polydispersity was 1.09.

2.3 Results and Discussion

It is challenging to prepare a bimodal polymer brush with conventional free radical polymerization while maintaining simultaneous control over multiple variables such as

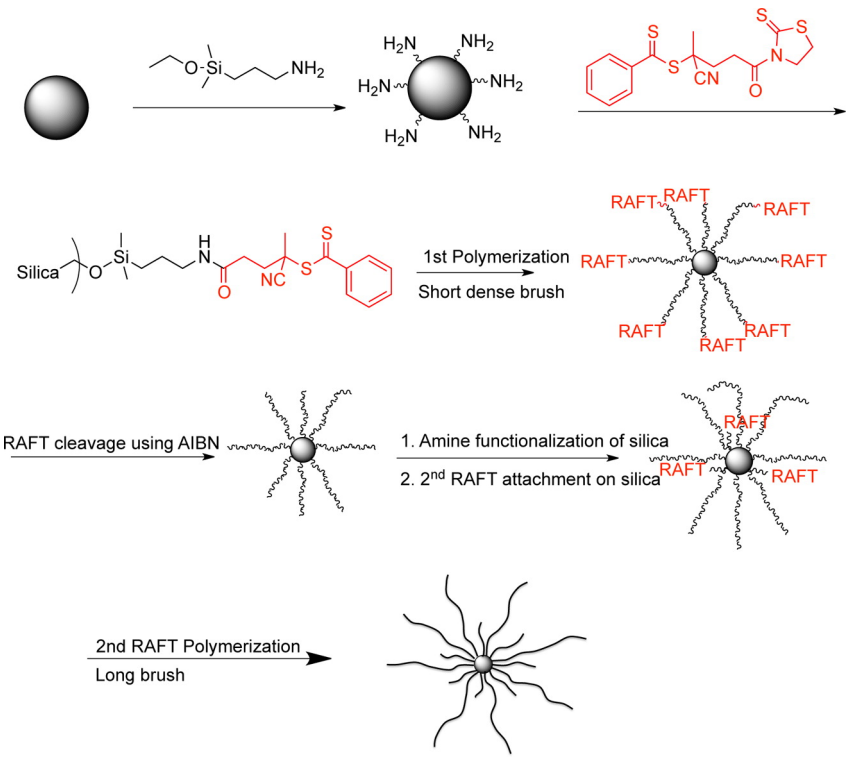

Figure 2.2 Sequential RAFT Polymerization for Synthesis of Bimodal Brushes

Table 2.1 Various Bimodal/Mixed Bimodal Brush-Anchored Silica Nanoparticles Synthesized Using Sequential RAFT Polymerization. All weights reported as g/mol and graft densities as chains/nm^2

Number	1st Monomer	1st MW	1st Density	2nd Monomer	2nd MW	2nd Density
NP-1	styrene	2000	0.26	styrene	40,000	0.30
NP-2	styrene	3200	0.26	styrene	25,000	0.33
NP-3	styrene	1600	0.26	MMA	205,000	0.07
NP-4	MMA	24,400	0.26	MMA	103,000	0.21
NP-5	styrene	7200	0.18	styrene	119,000	0.05
NP-6	NA	NA	NA	styrene	100,000	0.05

grafted chain molecular weight and polydispersity. Using the grafting-from approach and controlled radical polymerization techniques, several groups have previously demonstrated effective methods of synthesizing monodisperse polymer brushes on various surfaces. We have investigated a method of synthesizing bimodal and/or mixed brush grafted silica nanoparticles (4.1) using a step-by-step RAFT polymerization technique from surface anchored chain transfer agents, which we used to synthesize the first population of chains. In this process, a mercaptothiazoline activated-CPDB (4-cyano-4(phenylcarbonylthioylthio)pentanoate) chain transfer agent was condensed

onto the surface of silica nanoparticles functionalized with amine groups. This approach has been used to prepare SiO_2-g-CPDB nanoparticles with grafting densities varying from 0.01 - 0.7 RAFT agents/nm^2. An inherent advantage of this technique, compared to the other grafting-from methods, is the ease and accuracy in measuring the graft density prior to polymerization. The UV absorption at 302 nm of the SiO_2-g-CPDB nanoparticles is compared to a standard absorption curve made from known amounts of free CPDB to determine the concentration of the RAFT agents attached onto the nanoparticles before polymerization. For example to prepare sample NP-4 listed in Table 2.1, surface initiated polymerization of methyl methacrylate was initially conducted from the surface of the CPDB immobilized colloidal silica nanoparticles (SiO_2-g-CPDB) to give poly(methyl methacrylate) brush anchored silica nanoparticles (SiO_2-g-$PMMA_1$). Azobisisobutyronitrile was used as the initiator for the polymerization. A 10:1 [CTA] / [AIBN] ratio was utilized for all polymerizations. The PMMA chains were etched from the SiO_2-g-$PMMA_1$ nanoparticles by dissolving an aliquot (50 mg) of the nanoparticles in 4 mL THF and stirring overnight in 0.2 mL HF. Upon evaporation of the THF and HF, the molecular weight of the etched polymer measured by GPC was 24400 g/mol with a polydispersity of 1.07 which agreed with the theoretical molecular weight and indicated control over the polymerization.

Chain End Deactivation

Prior to attachment of the second chain transfer agent, it was necessary to cleave the first chain transfer agent, which remained as an end group from the first polymer population, as a consequence of the first RAFT polymerization. This was achieved using a process similar to that described earlier in literature.[35] Although these techniques have been successfully applied to cleave chain transfer agents from RAFT synthesized homopolymers and copolymers, the removal of a chain transfer agent from a

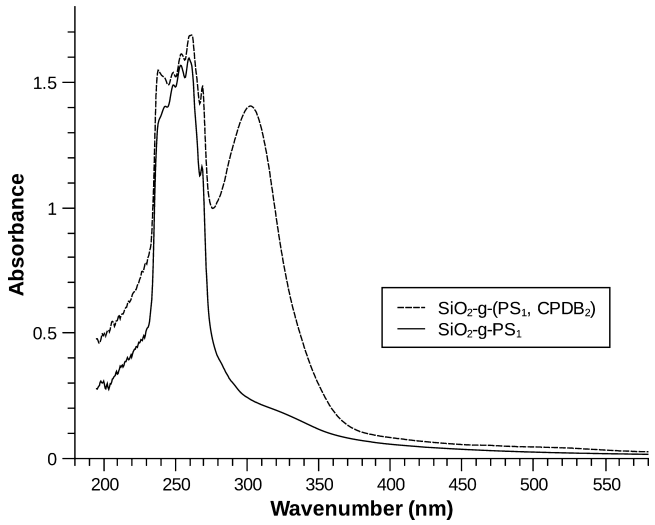

Figure 2.3 UV absorption spectra of (1) SiO_2-*g*-PS_1 with cleaved CPDB (solid line) and (2) SiO_2-*g*-PS_1 with 2nd CPDB immobilized on silica surface (dashed line).

polymer brush has not yet been reported. In this work, chain end deactivation was achieved via a radical cross coupling mechanism using AIBN. However, reducing the AIBN:CTA ratio to 10:1 from 20:1 led to an efficient cleavage reaction and prevented nanoparticle agglomeration. The molecular weight and polydispersity of the polymers before the RAFT cleavage reaction were 24400 g/mol and 1.07 respectively, while after the RAFT cleavage reaction they were 24200 g/mol and 1.09. SiO_2-g-$PMMA_1$ nanoparticles appeared pink in color before the cleavage reaction when the RAFT agent was still attached to the polymer. After the cleavage reaction with AIBN, the pink color disappeared to give white polymer coated nanoparticles, which were easily dispersed in THF. Efficient cleavage of the RAFT chain transfer agent is also evident from the UV traces shown in Figure 2.3.

Attachment of the Second RAFT Agent

Immobilization of the second RAFT agent on the surface of SiO_2-g-$PMMA_1$ nanoparticles was achieved using a similar approach as employed for the first RAFT polymerization. The hydroxyl groups on the surface of the silica nanoparticles that remained

unreacted during the first chain transfer agent immobilization were reacted with 3-aminopropyldimethylethoxysilane. The 3-aminopropyldimethylethoxysilane molecule is small and can diffuse to the surface of the silica particles to react with the hydroxyl groups even in the presence of the grafted polymer chains from the first polymer population. The concentration of the amine functional silane was critical in determining the graft density of the second polymer brush. By controlling the weight ratio of the 3-aminopropyldimethylethoxysilane to the SiO_2-g-POLYMER$_1$ brush nanoparticles, we successfully varied the graft density of the second population of chains from 0.07 - 0.36 ch/nm^2. After functionalization of the SiO_2-g-POLYMER$_1$ nanoparticles with amine silane molecules, activated-CPDB was attached to the silica nanoparticles by means of a condensation reaction between the mercaptothiazoline activated-CPDB and the amine groups on the silica surface. The activated-CPDB was used in slight excess (1.4:1) relative to the amine to ensure complete conversion of the amine groups to RAFT chain transfer agents. These CPDB functionalized nanoparticles were washed several times by precipitation in a 4:1 mixture of hexanes and ether and re-dispersed in THF to remove unreacted CPDB.

RAFT polymerization of second polymer brush population

Following the immobilization of the second CPDB chain transfer agent on the surface of SiO_2-g-PMMA$_1$ nanoparticles to generate SiO_2-g-(PMMA$_1$, CPDB) grafted nanoparticles, the surface initiated RAFT polymerization of methyl methacrylate was conducted to give bimodal brush anchored silica nanoparticles. Methyl methacrylate monomer can easily diffuse to the surface of the silica even in the presence of polymer chains to react with the chain transfer agent after initiation. A monomer to chain transfer ratio in excess of 10000:1 was used to keep the conversion low and avoid gelation, while ensuring the formation of high molecular weight polymer. The molecular weight and polydispersity of the second population of polymer chains, measured

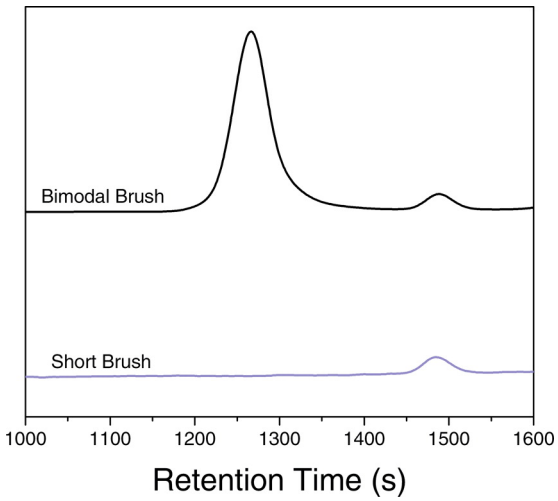

Figure 2.4 GPC trace of short and bimodal PS chains cleaved from silica nanoparticle

by GPC, were 103000 g/mol and 1.13, respectively, indicating excellent control over the second polymerization also. The GPC trace of the cleaved polymer chains from the bimodal nanoparticles is shown in Figure 2.3, and is compared to the GPC trace obtained from the first polymer brush.

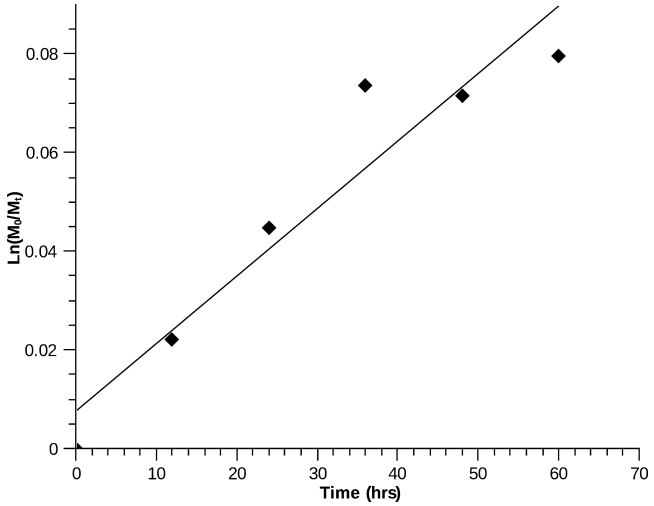

Figure 2.5 Kinetic plot for polymerization of second population of polystyrene at 0.11 chains/nm^2. First population of polystrene graft density of 0.20 chains/nm^2 with molecular weight of 7200 g/mol and PDI of 1.04.

The step-by-step RAFT polymerization approach described above was then used to prepare several different types of binary polymer brush anchored silica nanopar-

ticles as described in Table 2.1. Bimodal polystyrene graft nanoparticles were synthesized where the polymer composition of both the chains remained the same but the molecular weight of the two populations was varied. For polystyrene, a short dense brush was polymerized at 0.2 ch/nm^2 with a molecular weight of 7200 g/mol and PDI of 1.04. Using these particles, a second polystyrene brush population was polymerized at a density of 0.11 ch/nm^2 under controlled radical polymerization conditions with molecular weights up to 83000 g/mol and polydispersities less than 1.3. The kinetic curve for these polymerizations is shown in Figure 3.9. Mixed brush anchored nanoparticles containing polymer brushes of two distinct polymers were also synthesized using this step-by-step RAFT polymerization procedure.

Polymer nanocomposites using bimodal grafted nanoparticles

To study the effect of the bimodal population of grafted polymer chains on the dispersion and properties of nanocomposites, several nanocomposite samples with monomodal and bimodal polystyrene grafted nanoparticles (NP-6 and NP-5 from Table 2.1) were prepared and their thermal and mechanical properties investigated. The details of the free polymer weight fraction and silica content of the various composite samples are described in Table 2.2. Care was taken to ensure that the monomodal brush grafted nanoparticles (NP-6) had a long chain with the same molecular weight and graft density as NP-5, such that based on prior work autophobic dewetting was not a concern for composites system prepared using a 96000 g/mol monodisperse polystyrene matrix.

Table 2.2 Matrix Properties, Silica Content, and Polymer Content of Various Nanocomposite Samples Prepared Using NP-5 and NP-6 Brush Grafted Silica Nanoparticles

Grafted Particle	**Matrix Polymer**	**Silica Loading (wgt %)**	**Matrix Polymer (wgt %)**
NP-5	PS (MW=96,000 g/mol, PDI=1.01)	0	100
		0.1	99.6
		0.5	98.2
		1.0	96.4
		3.0	89.2
		5.0	81.9
		10	63.8
		25	9.55
		31	0
NP-5	PS (MW=190,000 g/mol, PDI=1.01)	0	100
		0.1	99.6
		0.5	98.2
		1.0	96.4
		5.0	81.9
NP-6	PS (MW=96,000 g/mol, PSI=1.01)	0	100
		5.7	90
		11.5	70
		23.1	50
		35.5	25
		39.0	0

Comparison of Dispersions of Bimodal and Monomodal Long Brush Grafted Nanoparticles

The dispersion of grafted silica nanoparticles was examined using Transmisson Electron Microscopy (TEM) as shown in Figure 2.6. Quantitative descriptions of dispersions (Skewness and Nearest Neighbour Index (NNI)), which are often more sensitive than visual examination, were obtained by analyzing the TEM images taken at 100000X, as described in the literature. Skewness measures the asymmetry in the distribution; therefore a higher skewness indicates a poorer dispersion state. The nearest neighbor index is a measure of regularity in distribution: NNI $>$ 1 implies regularity and NNI $<$ 1 indicates clustering. The larger the departure is from unity,

the more significant the regularity or clustering. Figures 2.6a and b show a representative comparison of monomodal and bimodal particle distributions (NP-5 and NP-6) at 5 wt% silica core loading. Figures 2.6c and d are skewness and NNI plots for other silica loadings. It is evident from visual examination of the TEM images and from the plots that the bimodal grafted nanoparticles disperse more randomly than the monomodal brush grafted nanoparticles. The monomodal grafted particles displayed aggregated anisotropic assemblies which is consistent with the morphologies predicted for this graft density and molecular weight ratio. This is also reflected by the larger skewness and lower NNI values for the monomodal brush systems at these loadings. The improved dispersion in bimodal brush composites is attributed to the addition of short chains, which improves the screening of core/core attraction as suggested by theoretical studies introduced earlier. The NP-5 particles can be envisioned to have a hybrid core with a lowered enthalpic gain per contact χ, but with the same excluded volume advantage as the monomodal long brush. By lowering the enthalpy gain from aggregation, the randomly dispersed morphology becomes the minimum free energy morphology in this parameter space. Note that the bimodal brush grafted nanoparticles are well dispersed even in a 190000 g/mol polystyrene matrix (Figure 2.6e).

Initial Comparison of Thermal Properties

The glass transition temperature (Tg) of the bimodal particle filled nanocomposites was measured using Differential Scanning Calorimetry. The temperature was increased at a rate of 10 °C/min from room temperature to 150 °C, held isothermally for 10 minutes, and then cooled at 10 °C/min to 20 °C. This was repeated three times per specimen. Data from the first cycle was not considered in order to eliminate thermal history effects and the Tg was calculated by averaging the Tg values from the second and third cycles. The calculated Tg values are shown in Figure 2.7.

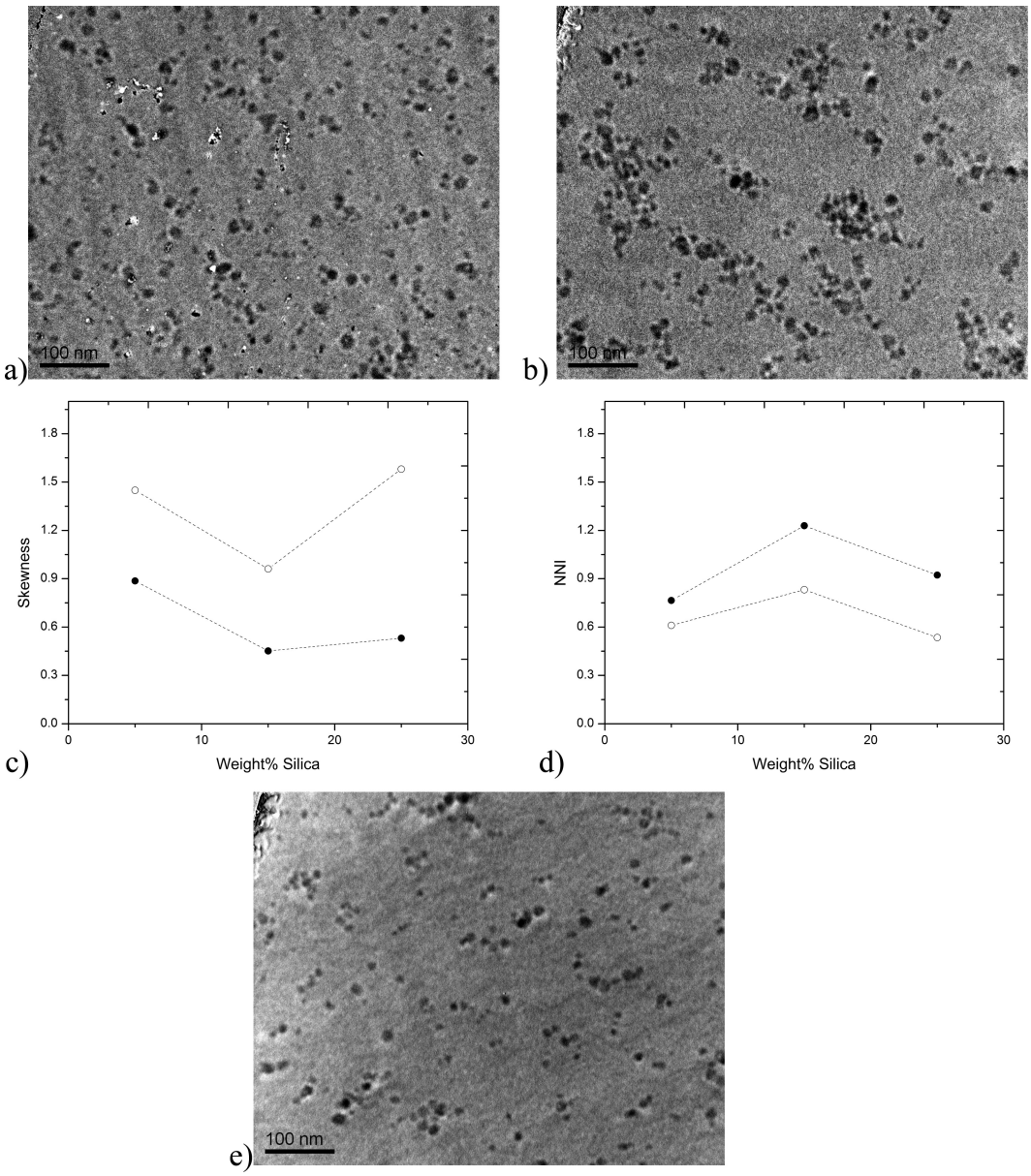

Figure 2.6 TEM micrographs (at 200,000x magnification) of (a) 5% silica loading of NP-5 in 96,000 g/mol matrix and (b) 5% silica loading of NP-6 in 96,000 g/mol matrix. (c) Plots of skewness and (d) nearest neighbor index obtained from TEM micrographs (at 100,000x magnification) for various loading of bimodal (filled circle) and monomodal (unfilled circle) brush grafted silica in the 96,000 g/mol matrix. (e) 5% silica loading of NP-5 in a 190,000 g/mol monodisperse matrix.

Previous work on monomodal nanoparticles composites showed that a matrix of molecular weight larger than that of the grafted brush dewets from the brush resulting in a decrease in Tg due to an excluded volume interaction at the interface. Conversely,

the matrix was found to wet the brush at lower molecular weights. The Tg was found to increase in these systems with wetting matrices due to higher matrix-brush friction. Thus, the current Tg data showed a wet to dry transition when the matrix was changed from 96000 g/mol to 190000 g/mol. The 190000 g/mol matrix did not wet the lower molecular weight brush causing a decrease in glass transition temperatures (even with good dispersion), whereas the 96000 g/mol matrix, which was comparable to the brush molecular weight, showed little or no change in Tg. The shift in Tg at 2.5% volume fraction is -3.1 °C for the 190000 g/mol matrix while the shift is 0.5 °C for the 96000 g/mol matrix. These shifts are representative of the dewetting nature of the larger 190000 g/mol matrix, which was observed without any particle agglomeration as would be expected for monomodal systems. We note that these bimodal particles provide the opportunity to isolate wetting and dispersion effects on glass transition temperature, since particles were well dispersed in all systems.

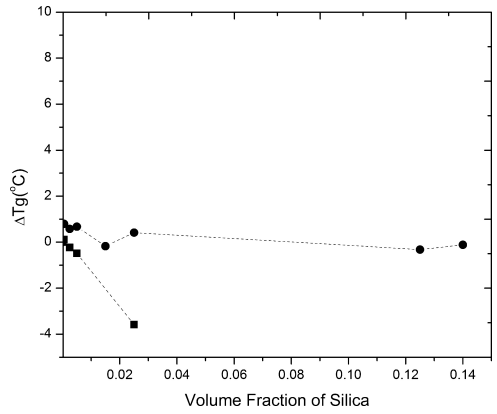

Figure 2.7 Change in glass transition temperature, T_g, for bimodal grafted NP-5 nanocomposites in 96,000 g/mol (filled circle) and 190,000 g/mol (filled square) PS matrices.

Initial Comparison of Mechanical Properties

Composite samples prepared using the 96000 g/mol polystyrene matrix were processed into dog-bone shaped specimens and subjected to frequency sweep studies on

a Rheometric Scientific DMTA V machine. At this matrix molecular weight, it is expected that the matrix wets the brush reasonably well. This is reflected in the Tg data shown in the previous section. Time-Temperature Superposition was performed on the data to obtain master curves of the storage and loss moduli. Comparative plots of the storage modulus of identical loadings of colloidal silica core in bimodal and monomodal systems are shown in Figure 2.8a. The bimodal particles displayed a significant improvement in storage modulus over monomodal particles at 5% loading. The improvement in properties at 5% loading can be explained by the improved dispersion state of the bimodal particles at lower loadings as discussed earlier, as well as the strong entanglement with the matrix. This difference in rheological properties becomes less discernable at high loadings (15%, 25%).

Nano-indentation tests were also conducted on the surface of bimodal and monomodal nanocomposite samples. A 150 nm Berkovich diamond tip indentor (Hysitron Company) was used for the test. Hardness and elastic moduli (Figure 2.8b) of bimodal brush grafted nanoparticle composites measured by nano-indentation show a remarkable improvement with increasing silica loadings. This improvement for bimodal brush grafted nanoparticles was greater than monomodal brush grafted nanoparticle composites, particularly at lower loadings and even superior to the values suggested by the Halpin-Tsai mixing rule. We, again, attribute the enhancement to the excellent dispersion morphology of the nanoparticles and the entanglement with the matrix that causes a physical crosslink. It is also noted that the standard deviation of the hardness and moduli is extremely small in the bimodal systems due to the uniform dispersion of particles. Monomodal nanocomposite samples with agglomerated fillers conversely exhibit large deviations from average values in nanoindentation tests.

Based on the initial testing of the dispersion behavior and thermomechanical properties of these bimodal brush grafted systems, it was decided to perform more complete testing to compare not only the dispersion state and properties of monomodal

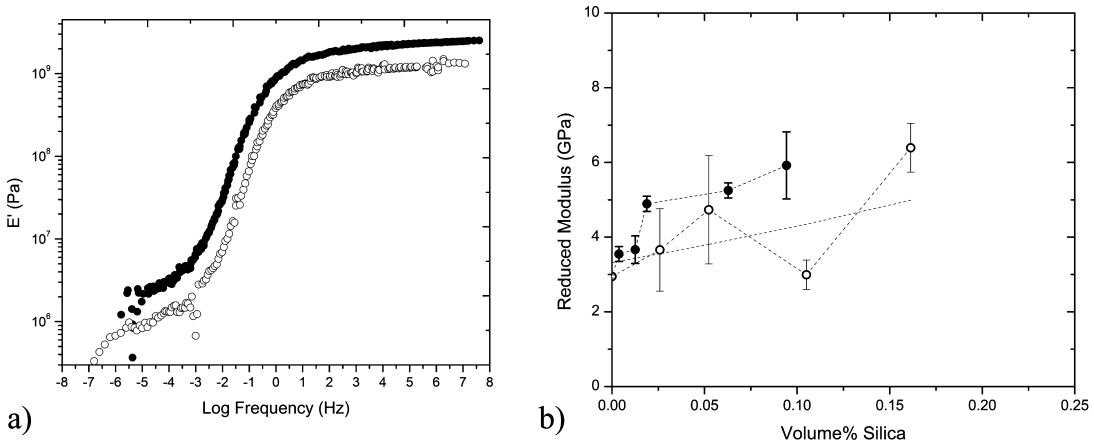

Figure 2.8 (a) Comparative plot of storage modulus (E') vs log frequency (Hz) for 5% core loadings of bimodal (filled circle) and monomodal (unfilled circle) brush grafted silica in the 96,000 g/mol matrix. The plots are shifted to align T_g to obtrain a true comparision of rheological response near the glass transition temperature. (b) Reduced elastic modulus for monomodal (unfilled circle) and bimodal (filled circle) grafted nanoparticle composites measured by indentation, also showing Halpin-Tsai precidtions (–).

long brushes with their bimodal counterparts but to also include monomodal short brush grafted nanoparticles. In the following systems, all brushes and matrices are polystyrene. This ensures that any change in dispersion and/or thermomechanical behavior is due solely to changes in the brush architecture and not driven by chemical incompatibilities. The properties of the various composites prepared for testing are listed in Table 2.3.

Comparison of Dispersion Behavior Between Monomodal Short, Monomodal Long, and Bimodal Brushes

The dispersion testing of all polymer brush systems (monomodal short, monomodal long, and bimodal) demonstrates the advantage of grafting bimodal brushes. (Figure 2.9) The micrographs of the short high density brush grafted monomodal particles (MS-25) dispersed in the 96 kg/mol matrix show that these particles organize into micrometer-sized agglomerates that grow in volume with increased particle loading.

Table 2.3 Brush Properties of Various Composites Prepared and Their Respective Labels

Matrix	Molecular Weight (kg/mol)	PDI	Graft Density (chains/nm^2)	Label
96 kg/mol	7.2	1.04	0.18	BM-05-96
	118	1.19	0.05	
96 kg/mol	100	1.14	0.05	ML-05-96
96 kg/mol	6.7	1.05	0.20	BM-10-96
	99.47	1.13	0.10	
96 kg/mol	99	1.1	0.10	ML-10-96
96 kg/mol	7	1.05	0.25	MS-25-96
190 kg/mol	7.2	1.04	0.18	BM-05-190
	118	1.19	0.05	
190 kg/mol	6.7	1.05	0.20	BM-10-190
	99.47	1.13	0.10	

This agglomeration is attributed to the entropic (conformational) penalty of the matrix mixing with a dense brush of much smaller molecular weight ($P/N \sim 13.5$). The positive surface tension that arises out of this balance leads to a net attraction between brushes, even when the core enthalpies are well screened.[36,37] This observation corroborates well with the dispersions reported for similar values of σ and P/N by Chevigny et al.[38] and in addition, fits into the autophobic dewetting regime of the emperical phase diagram developed by Sunday et al.[39] (dewetting phase begins at $P/N \geq 4.3$ for $\sigma = 0.28$ ch/nm^2).

Note than in order to frame the large clusters within the micrographs, magnifications had to be low (20,000x) for MS-25-96. These micrographs also show the dispersions of the 5 silica wgt % long brush grafted monomodal particles at $\sigma = 0.05$ and 0.1 ch/nm^2 (ML-05-96 and ML-10-96) at 100,000x magnification. The dispersion of long monomodal brush grafted particles was far superior to the dispersion of the short grafted particles. They also display self-assembly into anisotropic agglmoerates that grow laterally with the addition of particles for both graft densities. These microstructures are as suggested by the morphology diagram developed by Akcora et al.[5] and are placed well in the allophobic dewetting regime of Sunday et al.'s phase

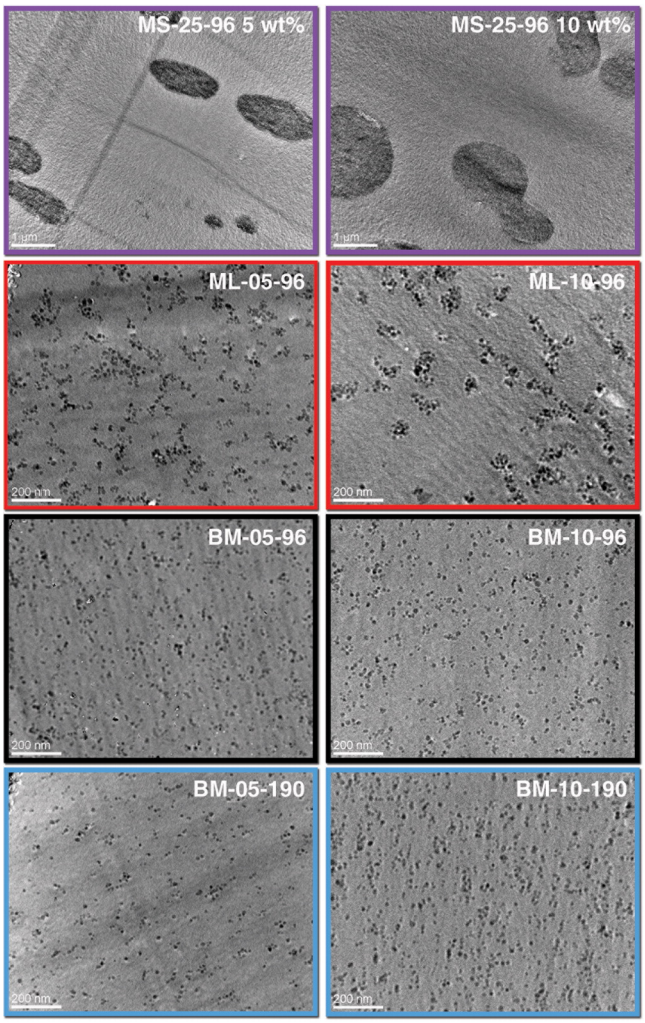

Figure 2.9 TEM micrographs of silica loadings of 5 wt % (except when otherwise noted) of various systems at 100,000x magnification (20,000x for MS-25-95 systems).

diagram.[39] When compared to the bimodal brush grafted particles we see that the combination of long and short brush causes a significant improvement in dispersion, for both $\sigma_l = 0.05$ and 0.1 ch/nm^2, in the 96 kg/mol matrix (BM-05-96, BM-10-96). Remarkably the particles remain well dispersed even in a matrix of much larger molecular weight 190 kg/mol (BM-05-190, BM-10-190), for which there is a stronger entropic drive to agglomerate.

These dispersions are quantified as described earlier to obtain the skewness and Q_{mean} and plotted versus the concentration of silica (wt %). (Figure 2.10). These

plots confirm the qualitative inferences made from the micrographs. At all loadings, the bimodal systems exhibit lower skewness values than the monomodal systems suggesting that they have a superior distribution of particles. Additionally the Q_{mean} for the bimodal systems at every loading is much higher than that of the monomodal systems indicating that there are more indiviudally dispersed particles. These plots reveal that all the bimodal systems are better distributed and more uniformly dispersed than the monomodal particles. The skewness is found to increase with decreasing loading. This is because for the same cell size and quality of dispersion, at lower loadings fewer quadrants register particles. Q_{mean} on the other hand, increases with the loading because more particles are registered for the same number of cells. Since the dispersion in MS-25-96 are manifestly poor, their skewness (>10) and Q_{mean} ($\sim 10^{-4}$) are not plotted.

We attribute improvement in dispersion in the bimodal composites to the addition of a dense short brush to the long brush population (or conversely, the addition of a few long chains to the dense short brush population). Both of these points of view have significant qualitative support in literature. The former is as per finding of Pryamitsyn et al.,[28] which suggest that a lowered enthalpic gain of core aggregation leads to an improved probability of dispersion. The latter is in accordance with simulation results, which suggest that addition of a small number of "wettable" long chains to a dense brush (i.e., the bimodal limit of polydispersity) abates the attractive energy well between particles at transitional distances.[6,29,40] Evidently the combination of the two brushes tenders enough enthalpic screen and entropic excluded volume repulsion to keep these particles well dispersed in both the 96 kg/mol and 190 kg/mol matrices. In order to explain these results quantitatively, a predictive phase diagram incorporating enthalpic and entropic contributions to dispersion was sought. The discussion of the methods, calculations, and simulations that are used to generate this phase diagram is outside the scope of this dissertation. The reader

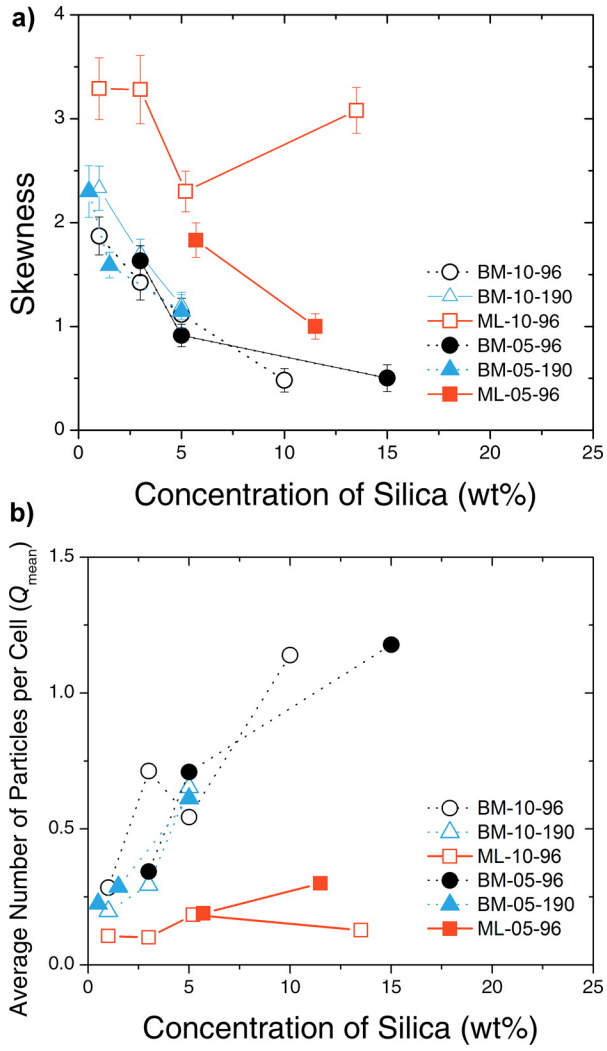

Figure 2.10 (a) Skewness vs silica weight % and (b) average number of particles per cell (Q_{mean}) vs silica wt %, for systems under our purview. Lines are merely as illustration of trends

is encouraged to look in the published literature for a more complete explanation.[33]

The trends in the phase diagrams (Figure 3.3) are quite clear. For a constant particle size, R, and constant chain length, N ($\sim R_g$), the tendency to disperse increases with an increase in the number of chains (n_p). For a constant particle size, R, and constant n_p, the dispersion improves with an increase in the chain length N ($\sim R_g$). Additionally, the agglomeration regime grows with increasing P. The phase boundary is found to shift favorably toward a higher probability of a dispersed phase for the bimodal systems. It is observed that the diagram is able to predict the disper-

sion morphology of both monomodal and bimodal particles. The monomodal brush grafted particles embedded in a 96 kg/mol matrix lie in the connected (C) region of the phase diagram, whereas bimodal brush grafted particles lie in the dispersed region (D) corresponding to their phase boundary. This observation is also true of the 0.1 ch/nm^2 particles and 190 kg/mol matrix bimodal systems.

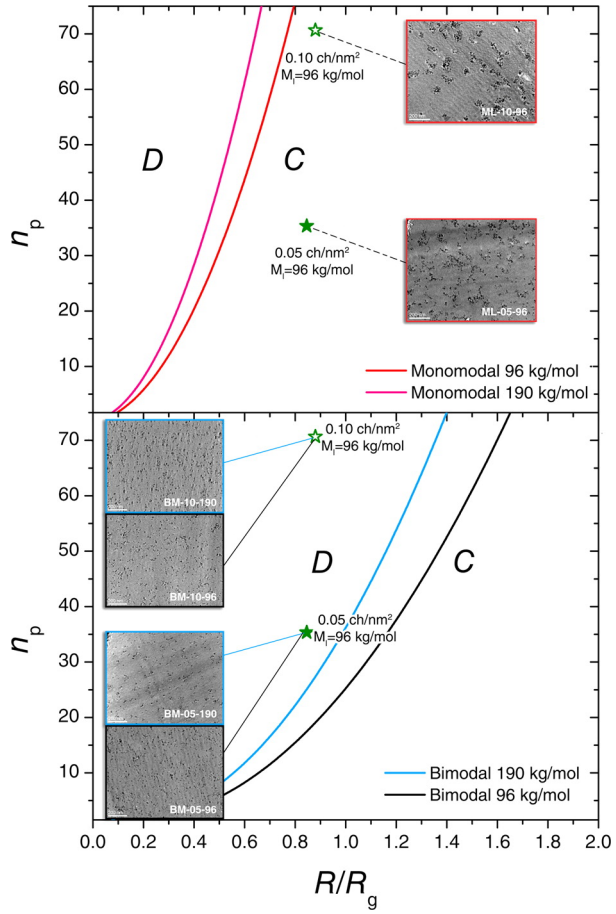

Figure 2.11 Parametric phase diagram of the homopolymer PS-silica: (a) monomodal and (b) bimodal systems under our purview, showing the dispersed and string-like agglomerate regions. The experimental micrographs of 5 wgt % silica loading of the samples are shown to demonstrate the validity of predictions. The open and filled stars correspond to graft densities of 0.10 ch/nm^2 and 0.05 ch/nm^2. The monomodal 190 kg/mol boundary is shown purely to illustrate the shift in phase boundaries with varying matrix molecular weight.

Role of Dispersion on Mechanical Behavior

The mechanical properties of all composite types were investigated at various concentrations of silica. The viscoleastic properties, measured through isothermal frequency sweeps on DMTA, are shown in Figure 2.12 . These plots show the glassy state storage moduli of 5 wgt % silica loadings ML-10, BM-10, ML-05, AND BM-05 in the 96 kg/mol matrix. The neat polymer curve is also plotted for reference. These curves were obtained by frequency shifting of master curves such that the peak loss moduli corresponding to the glass transition coincided. This T_g normalization was performed in order to make a true comparison of glassy properties at identical decades of frequency away from the glass transition temperature. The 4-6 decade regime (0 being T_g) shown corresponds to temperatures 10-15 °C less than T_g. It is evident when comparing glassy state mechanical properties of BM-10-96 and ML-10-96 and of BM-05-96 and ML-05-96, that the enhacnement following the addition of bimodal particles is greater than that presented by the monomodal particles for each of the grafting densitites.

This enhancement is further investigated by static nanoindentation tests at room temperature. The elastic modulus is calculated from the reduced modulus. The results of the indentation experiments are shown in Figure 2.13, as plots of the normalized modulus vs silica weight loadings. The trends observed in the DMTA data in Figure 2.12 are in agreement with those in Figure 2.13. This is found to be true at all intermediate loadings. Additionally, the bimodal results are found to be far superior to the predictions made by the Halpin-Tsai and Guth micromechanical models. We attribute this larger enhancement offered by the bimodal particles to their superior dispersion state, while still maintaining the same entanglement effects ($Skewness_{BM-10-96} < Skewness_{ML-10-96}$, $Skewness_{BM-05-96} < Skewness_{ML-05-96}$) The largest increase in glassy properties such as the elastic modulus was observed in the best dispersed system. This follows from the notion that better dispersed

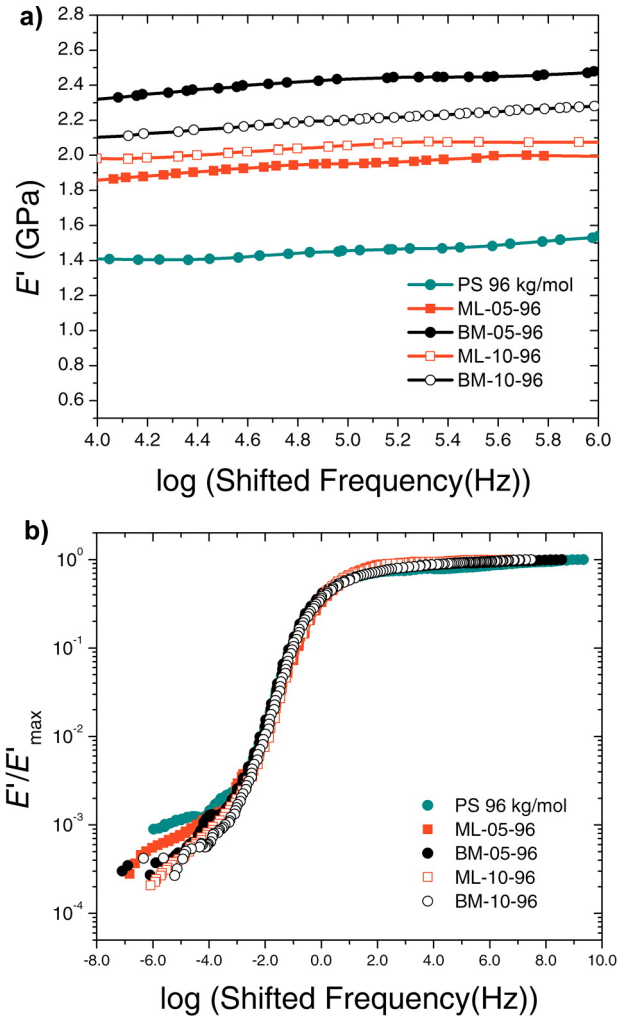

Figure 2.12 (a) Storage modulus E' (GPa) vs log(shifted frequency(Hz)) for 5 wgt % silica loadings of various systems compared with neat 96 kg/mol PS. (b) Normalized storage modulus E'/E'$_{max}$ vs log(shifted freqency(Hz)) for 5 wgt % silica loadings of varous systems compared with neat 96 kg/mol PS.

systems benefit from a larger interfacial surface to volume ratio. We have thus, for the first time, been able to observe the role of dispersion in grafted systems while maintaining the same entanglement properties. Additionally, we observe that there is no significant impact on high temperature mechanical reinforcement in the bimodal and monomodal systems. A representative plot of this observation is shown in Figure 2.12b. Here the frequency shifted moduli, scaled down by the neat polymer modulus, are all found to overlap; that is to say that they all possess the same shape as a

function of frequency. The lack of reinforcement is also seen within all the systems at nearly all loadings of silica. The bimodal systems are well dispersed, with no stress propagating interparticle bridges. In the monomodal systems, the anisotropic aggregates are found not to be extending through the sample and neither are there any glassy bridges (PS and silica have a repulsive interface). The only systems showing reinforcement is ML-05-96 at 35.5% silica by weight. We attribute this observation to the physical constraints imposed on the matrix chains at such high loading.

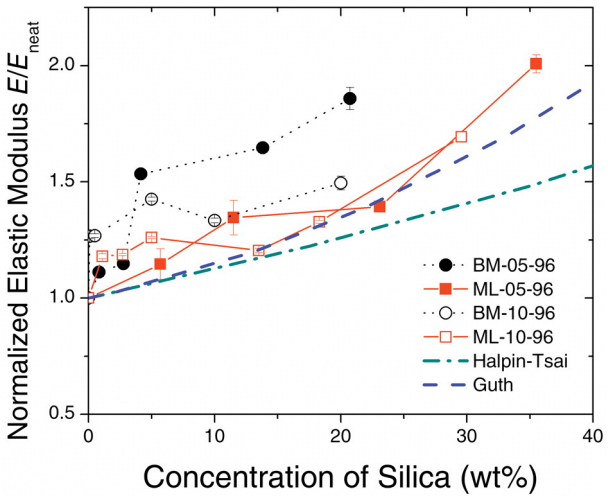

Figure 2.13 The elastic modulus normalized by pure polymer modulus E/E_{neat} vs silica concentration (wt %) for various systems compared with the Halpin-Tsai and Guth predictions for silica in the 96 kg/mol matrix

Role of Brush-Matrix Entanglement on Mechanical Properties

As was shown earlier, the dispersion in all the bimodal systems are qualitatively and quantitatively similar. Therefore, any divergence in the normalized mechanical properties is to be attributed to the differences in the degree of brush-matrix entanglement. Nanoindentation tests (Figure 2.14a) reveal that the bimodal particles offer a larger elastic modulus augmentation in the 96 kg/mol matrix when compared to enhancements in the larger molecular weight 190 kg/mol matrix, which show only a marginal

improvement. We also observe that as the graft density increases, the increase in modulus decreases. These observations suggest that the poorer the entanglement of the matrix chains, the lower the modulus. We test the same by measuring the T_g in these systems, since T_g has been established as being indicative of entanglement behavior in grafted systems.[41] The Tg shifts are shown in Figure 2.14b. We note that shifts in DMTA peaks are well correlated with the T_g as shown by a representative plot for BM-10-96 and BM-10-190 (Figure 2.14c and d).

The T_g drops (~3 degC at 10 wt % silica) following the addition of $\sigma_l = 0.1$ ch/nm^2 bimodal particles to the 96 kg/mol (BM-10-96), are found to be higher than those in the 0.05 ch/nm^2 system, which shows no change in T_g. The T_g drops induced in the 190 kg/mol matrix are much higher than the drops in the 96 kg/mol matrix. While this lowering of T_g in the 190 kg/mol could be due to the plasticizing effect of a lower molecular weight 100 kg/mol chains, we rule this out since the 100 kg/mol and 190 kg/mol have silimar T_gs.

It has been established that the glass transition temperature in the athermal graft polymer-matrix systems can be increased or decreased when the matrix chains entangle favorably or poorly with the brush, respectively.[42] When the matrix chains are partially entangled,[37] they experience a lowered friction leading to faster relaxation times expressed in bulk as lowered T_gs.[43] Ferreira et al. have identified a boundary for such "dewetting" for sparse brushes using self-consistent field analysis.[37] This ratio is calculated for the systems under our purview: BM-05-96 (1.23), BM-10-96 (3.13), BM-05-190 (5.27), and BM-10-190 (12.29). Since this boundary is defined for flat brushes, the condition is expected to be relaxed for spherical brushes in which the volume available increases with the increased distance from the particles.[44] Nevertheless, the value of the ratio is comparable to unity only for the BM-05-96 system, and increases with increasing graft density and matrix molecular weight. We are therefore led to conclude that the 96 kg/mol matrix is reasonably well entangled

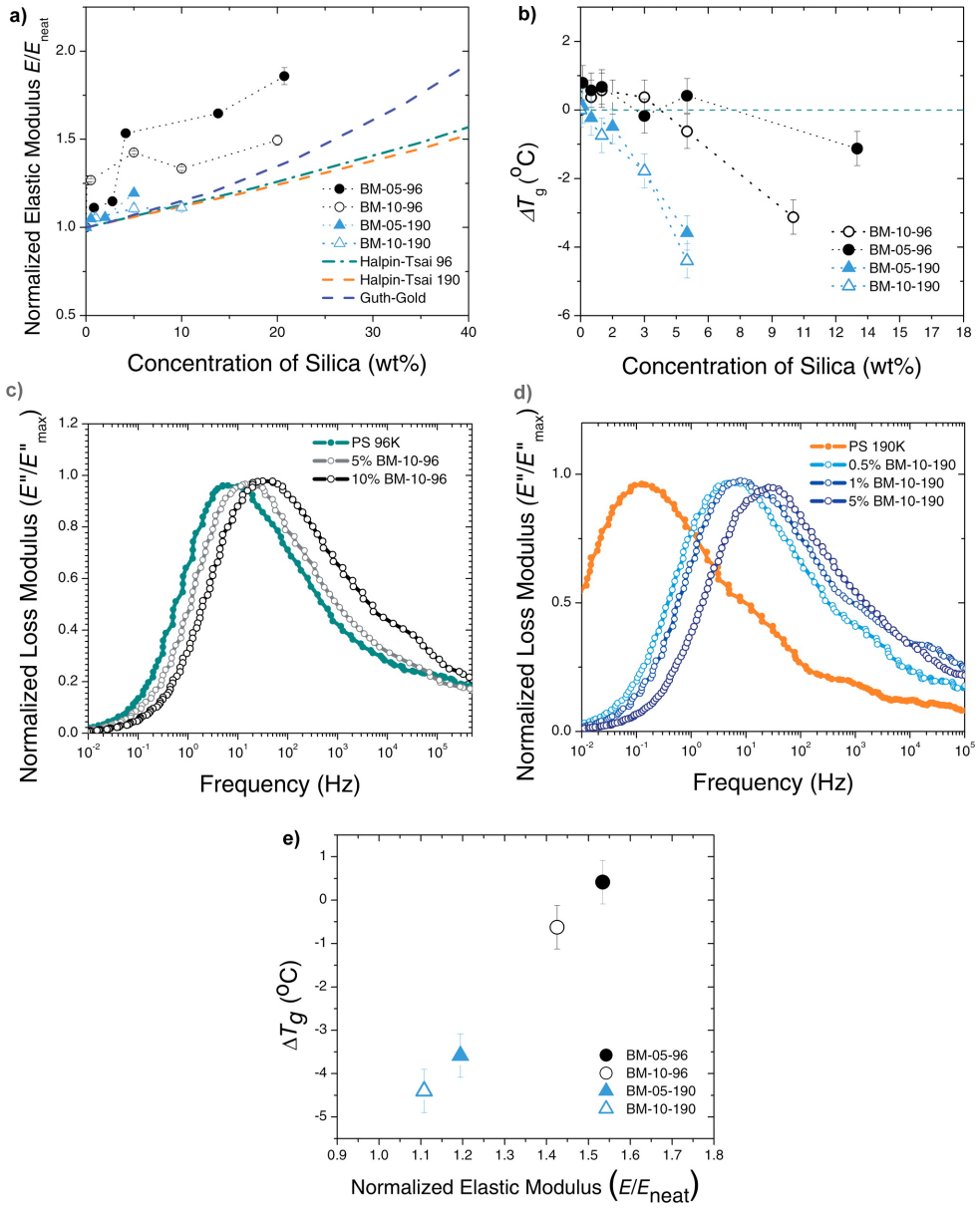

Figure 2.14 (a) Elastic modulus normalized by pure polymer modulus E/E_{neat} vs silica concentration (wgt %) for bimodal systems, compared with the Halpin-Tsai and Guth predictions. (b) $\triangle$Tg (°C) vs silica weight % for bimodal systems. (c and d) Normalized loss modulus curves in BM-10-96 and BM-10-190, respectively, showing a shift in loss modulus peak to higher frequencies with increased loading. A positive frequency shift in glass transition is equivalent to a negative shift in Tg. (e) Plot of normalized elastic modulus vs $\triangle T_g$ at 5 wt % silica loading of the various systems

with the 0.05 ch/nm^2 brush, and less entangled with the 0.10 ch/nm^2 brush. As the matrix molecular weight is increased above the brush molecular weight, the entangle-

ment worsens. With poorer entanglement, the matrix chains enjoy a lower interfacial friction, thereby leading to observed drops in T_g. Furthermore, since the particles that cause "dewetting" act as plasticizers in the matrix, they are found to not induce the same amount of modulus enhancement as particles that show strong interfacial binding. To further support the view that for the same dispersion state, glassy state property enhancements in grafted particle filled composites are strongly dictated by the extent of entanglement we plot the $\triangle T_g$ vs normalized elastic modulus for 5 wt % silica loading. This graph reveals a remarkable correlation that confirms this notion. We have therefore been able to characterize the influence of brush-matrix entanglement on the mechanical properties of grafted particle filled systems, for the first time isolation the effects of dispersion.

2.4 Summary

We have developed and demonstrated a robust technique using RAFT polymerization to synthesize binary polymer brush anchored nanoparticles. A layer of dense brush constituting the first population was initially prepared using surface initiated RAFT polymerization from silica nanoparticles. The active chain transfer agent at the chain ends was cleaved from the first population of polymer chains using a radical cross coupling reaction. A second RAFT agent was attached to the portion of silica surface not covered by the first chains and was followed by polymerization of a second monomer which could be the same or different from the first brush. This versatile route of using step-by-step controlled polymerization techniques enabled the independent control of the individual molecular variables such as composition, molecular weight, molecular weight distribution and graft density of the two chain populations. The presence of the binary brush was confirmed by GPC traces of the cleaved chains which showed two peaks indicating a bimodal system. TEM analysis of the binary brush grafted nanoparticles showed that the particles were well dispersed and free

from agglomerates. Composites prepared with bimodal brush grafted nanoparticles showed improved mechanical and thermal properties when compared to monomodal grafted nanoparticles, due to improved nanoparticle dispersion and matrix entanglement. With monomodal grafted particles the dispersion state and matrix-brush entanglement are linked. Through the use of bimodal brushes we have effectively decoupled the contributions by tuning enthalpic screening with the short brush and entropic entanglment with a long brush. The decoupled enthalpic and entropic control over dispersion in these binary/bimodal brush grafted nanoparticles renders them potentially useful, as functional additives, in a wide range of applications, such as in smart lighting, stimuli responsive materials, etc.

2.5 References

[1] Akcora, P.; Harton, S. E.; Kumar, S. K.; Sakai, V. G.; Li, Y.; Benicewicz, B. C.; Schadler, L. S. *Macromolecules* **2011**, *44*, 416–416.

[2] Moll, J. F.; Akcora, P.; Rungta, A.; Gong, S. S.; Colby, R. H.; Benicewicz, B. C.; Kumar, S. K. *Macromolecules* **2011**, *44*, 7473–7477.

[3] Maillard, D.; Kumar, S. K.; Rungta, A.; Benicewicz, B. C.; Prud'homme, R. E. *Nano Letters* **2011**, *11*, 4569–4573.

[4] Akcora, P.; Kumar, S. K.; Moll, J.; Lewis, S.; Schadler, L. S.; Li, Y.; Benicewicz, B. C.; Sandy, A.; Narayanan, S.; Illavsky, J.; Thiyagarajan, P.; Colby, R. H.; Douglas, J. F. *Macromolecules* **2010**, *43*, 1003–1010.

[5] Akcora, P.; Liu, H.; Kumar, S. K.; Moll, J.; Li, Y.; Benicewicz, B. C.; Schadler, L. S.; Acehan, D.; Panagiotopoulos, A. Z.; Pryamitsyn, V.; Ganesan, V.; Ilavsky, J.; Thiyagarajan, P.; Colby, R. H.; Douglas, J. F. *Nature Materials* **2009**, *8*, 354–U121.

[6] Jayaraman, A. *Journal of Polymer Science Part B: Polymer Physics* **2013**, *51*, 524–534.

[7] Martin, T. B.; McKinney, C.; Jayaraman, A. *Soft Matter* **2013**, *9*, 155–169.

[8] Singh, C.; Balazs, A. C. *Macromolecules* **1996**, *29*, 8904–8911.

[9] Zhao, B.; Brittain, W. J. *Journal of the American Chemical Society* **1999**, *121*, 3557–3558.

[10] Zhao,; Perrier, S. *Macromolecules* **2006**, *39*, 8603–8608.

[11] Estillore, N. C.; Advincula, R. C. *Macromolecular Chemistry and Physics* **2011**, *212*, 1552–1566.

[12] Motornov, M.; Malynych, S. Z.; Pippalla, D. S.; Zdyrko, B.; Royter, H.; Roiter, Y.; Kahabka, M.; Tokarev, A.; Tokarev, I.; Zhulina, E.; Kornev, K. G.; Luzinov, I.; Minko, S. *Nano Letters* **2012**, *12*, 3814–3820.

[13] Gao, J.; Li, J.; Zhao, S.; Benicewicz, B. C.; Hillborg, H.; Schadler, L. S. *Polymer* **2013**, *54*, 3961–3973.

[14] Skvortsov, A. M.; Gorbunov, A. A.; Leermakers, F. A. M.; Fleer, G. J. *Macromolecules* **1999**, *32*, 2004–2015.

[15] Martin, T. B.; Jayaraman, A. *Soft Matter* **2013**,

[16] Ionov, L.; Houbenov, N.; Sidorenko, A.; Stamm, M.; Luzinov, I.; Minko, S. *Langmuir* **2004**, *20*, 9916–9919.

[17] Houbenov, N.; Minko, S.; Stamm, M. *Macromolecules* **2003**, *36*, 5897–5901.

[18] Kumar Vyas, M.; Schneider, K.; Nandan, B.; Stamm, M. *Soft Matter* **2008**, *4*, 1024–1032.

[19] Draper, J.; Luzinov, I.; Minko, S.; Tokarev, I.; Stamm, M. *Langmuir* **2004**, *20*, 4064–4075.

[20] Bao, C.; Tang, S.; Horton, J. M.; Jiang, X.; Tang, P.; Qiu, F.; Zhu, L.; Zhao, B. *Macromolecules* **2012**, *45*, 8027–8036.

[21] Jiang, X.; Zhong, G.; Horton, J. M.; Jin, N.; Zhu, L.; Zhao, B. *Macromolecules* **2010**, *43*, 5387–5395.

[22] Jiang, X.; Zhao, B.; Zhong, G.; Jin, N.; Horton, J. M.; Zhu, L.; Hafner, R. S.; Lodge, T. P. *Macromolecules* **2010**, *43*, 8209–8217.

[23] Zhao, B.; He, T. *Macromolecules* **2003**, *36*, 8599–8602.

[24] Ionov, L.; Minko, S. *ACS Applied Materials & Interfaces* **2012**, *4*, 483–489.

[25] Estillore, N. C.; Advincula, R. C. *Langmuir* **2011**, *27*, 5997–6008.

[26] Zhao, B.; Zhu, L. *Macromolecules* **2009**, *42*, 9369–9383.

[27] Stuart, M. A. C.; Huck, W. T. S.; Genzer, J.; Muller, M.; Ober, C.; Stamm, M.; Sukhorukov, G. B.; Szleifer, I.; Tsukruk, V. V.; Urban, M.; Winnik, F.; Zauscher, S.; Luzinov, I.; Minko, S. *Nature Materials* **2010**, *9*, 101–113.

[28] Pryamtisyn, V.; Ganesan, V.; Panagiotopoulos, A. Z.; Liu, H. J.; Kumar, S. K. *Journal of Chemical Physics* **2009**, *131*, 221102.

[29] Edgecombe, S. R.; Gardiner, J. M.; Matsen, M. W. *Macromolecules* **2002**, *35*, 6475–6477.

[30] Jayaraman, A.; Nair, N. *Molecular Simulation* **2012**, *38*, 751–761.

[31] Li, Y.; Tao, P.; Viswanath, A.; Benicewicz, B. C.; Schadler, L. S. *Langmuir* **2013**, *29*, 1211–1220.

[32] Rungta, A.; Natarajan, B.; Neely, T.; Dukes, D.; Schadler, L. S.; Benicewicz, B. C. *Macromolecules* **2012**, *45*, 9303–9311.

[33] Natarajan, B.; Neely, T.; Rungta, A.; Benicewicz, B. C.; Schadler, L. S. *Macromolecules* **2013**, *46*, 4909–4918.

[34] Li, C.; Han, J.; Ryu, C. Y.; Benicewicz, B. C. *Macromolecules* **2006**, *39*, 3175–3183.

[35] Perrier, S.; Takolpuckdee, P.; Mars, C. A. *Macromolecules* **2005**, *38*, 2033–2036.

[36] Trombly, D. M.; Ganesan, V. *Journal of Chemical Physics* **2010**, *133*.

[37] Ferreira, P. G.; Ajdari, A.; Leibler, L. *Macromolecules* **1998**, *31*, 3994–4003.

[38] Chevigny, C.; Dalmas, F.; Di Cola, E.; Gigmes, D.; Bertin, D.; Boue, F.; Jestin, J. *Macromolecules* **2011**, *44*, 122–133.

[39] Sunday, D.; Ilavsky, J.; Green, D. L. *Macromolecules* **2012**, *45*, 4007–4011.

[40] Dodd, P. M.; Jayaraman, A. *Journal of Polymer Science Part B-Polymer Physics* **2012**, *50*, 694–705.

[41] Bansal, A.; Yang, H. C.; Li, C. Z.; Benicewicz, B. C.; Kumar, S. K.; Schadler, L. S. *Journal of Polymer Science Part B-Polymer Physics* **2006**, *44*, 2944–2950.

[42] Green, P. F.; Oh, H.; Akcora, P.; Kumar, S. K. *Structure and Dynamics of Polymer Nanocomposites Involving Chain-Grafted Spherical Nanoparticles*; Dynamics of Soft Matter: Neutron Applications; 2012.

[43] Oh, H.; Green, P. F. *Nature Materials* **2009**, *8*, 139–143.

[44] Dukes, D.; Li, Y.; Lewis, S.; Benicewicz, B.; Schadler, L.; Kumar, S. K. *Macromolecules* **2010**, *43*, 1564–1570.

Chapter 3

Synthesis of Mixed Bimodal Grafted Nanoparticles

3.1 Introduction

Polymer nanocomposites (PNCs) are two-phase systems consisting of polymer loaded with high-surface-area reinforcing fillers.[1] Nanosized fillers offer improved enhancement over their micron-sized counterparts due to a larger surface area to mass ratio even at low filler loadings.[1–3] Within this category of nanofillers, colloidal silica has gained attraction for a multitude of applications, even replacing carbon black for high-performance applications.[4] In addition, nanocomposites are compatible with conventional polymer processing, avoiding costly processes such as those required for the production of conventional fiber-reinforced composites. Property enhancement depends on the intrinsic properties of the matrix and filler as well as the interactions between matrix and filler.[5] Poor enhancement can be attributed to poor dispersion and poor interfacial load transfer.[6] With a large aggregation of nanofillers, the advantage of a larger surface area to mass ratio has is eliminated. Because of this, filler morphology is extremely important to the enhancement of the composite.[7]

Large aggregates form due to core-core attractions between nanoparticles.[8,9] A common way to screen these van der Waals attractions and make nanoparticles compatible with the matrix is the grafting of polymer chains on the surface.[10] Two major classifications of grafting methods are grafting-to and grafting-from. With a grafting-to method a preformed polymer is diffused to the surface of a modified nanoparticle.

However, with this diffusion comes steric hindrance between the diffusing chain and the polymer chains already attached. Because of this, a low graft density is observed. This can be compounded with high molecular weight chains and in a mixed brush system (where Flory-Huggins parameter > 0). In a low graft density regime, the core-core attraction is not well screened which can lead to the aforementioned agglomeration.[11] The second major classification of grafting methods is grafting-from where an initiator or RAFT agent is attached to the surface and the polymer chain is grown from the surface. There is little steric hindrance in comparison with the diffusion of a small molecule to a modified surface. Also, Flory-Huggins parameters for monomers are close to zero, therefore mixed brush systems are much easier to create with a grafting-from method. Due to this decrease, a much higher graft density brush is affordable which creates much better screening and therefore increased dispersion.

However, even in this high graft density regime with a chemically identical brush and matrix, there still remains an unfavorable entropic autophobic dewetting of the matrix from the brush.[12,13] This dewetting of the matrix can cause agglomeration of the nanoparticle filler as well as decreased entanglement of the matrix and brush chains, both of which lead to a decrease in load transfer and therefore property enhancement. Autophobic dewetting can be alleviated by reducing the graft density of the brush or by increasing the brush to matrix molecular weight ratio.[14] Decreasing graft density exposes the surface and prevents screening of the core-core attractions that lead to agglomeration as previously discussed and changing the brush to matrix molecular weight ratio can either eliminate the use of a mechanically strong matrix (too low matrix molecular weight) or reduces the maximum achievable loading of the nanoparticles (too high brush molecular weight). Therefore both a high graft density brush (to prevent agglomeration) and a low graft density brush (to eliminate autophobic dewetting and encourage entanglement) are required for the property enhancement of a polymer nanocomposite. This can be accomplished through the

use of a bimodal brush (Figure 3.1). A bimodal/binary polymer brush is defined as a homopolymer brush with two distinct monodisperse chains attached to the surface.[15] If these polymer chains are chemically distinct, it is deemed a mixed brush. The general benefits of a bimodal system when compared to block architecture is increased control over the different chains' independent graft density and a controlled increase in polydispersity of the brush system which has been suggested to control dispersion.[16]

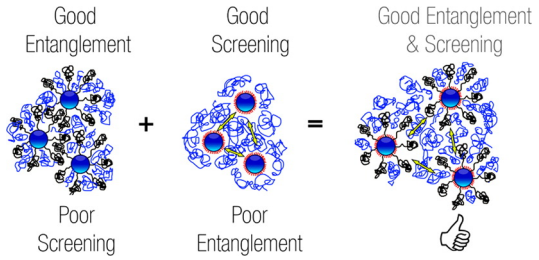

Figure 3.1 Controlling Dispersion and Entanglment via Bimodal Brushes

Few methods have been described for the synthesis of a bimodal brush system. Using a grafting-to approach, flat mixed brush systems of poly(tert-butyl acrylate) (PBA) with poly(2-vinylpyridine) (P2VP)[17,18] as well as polystyrene with P2VP[19,20] were reported by Luzinov, Minko, and Stamm. These systems showed a switchable response to changes in pH and solvent allowing for control over the surface properties. However, a grafting-to approach comes with limitations in graft density as discussed earlier.

In a grafting-from approach Zhao has created a Y-shaped initiator.[21–24] One arm of the initiator contains a moiety for ATRP polymerization while the other arm contain a moiety for NMP. Using sequential polymerizations, mixed bimodal brushes of PBA and PS were made and their resulting phase morphology was studied. While an increase in graft density of polymer chains is seen over other techniques, the control over the separate graft densities for the independent chains is lost when the initiators are combined. Ionov and Minko have also studied the preparation of mixed bimodal brushes via grafting-from techniques.[25] Using sequential activator generated

by AGET ATRP, PBA and PS brushes were created followed by hydrolysis to create poly(acrylic acid) - polystyrene mixed brushes. The solvent effect and switching properties of these brushes were studied via AFM and contact angle measurements. Via a layer-by-layer technique, Advincula has created a mixed bimodal system of poly(n-isopropylacrylamide) and polystyrene showing control of the surface properties based on temperature and solvent effects.[26] These approaches lay the foundation for the development of a new group of stimuli responsive materials.[27,28] However, few of these methods are performed on particles and even fewer on nanoparticles (diameter<100nm). Also, very little experimental studies have been performed on the effects of bimodal brushes on the ordering of nanoparticles in a polymer matrix.

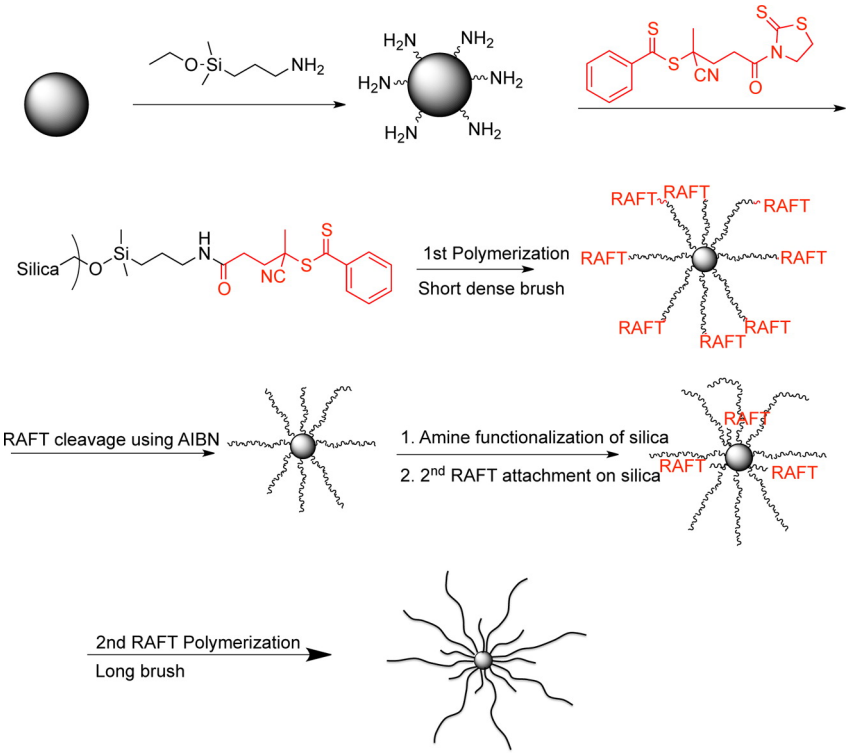

Figure 3.2 Sequential RAFT Polymerization for Synthesis of Bimodal Brushes

As a new synthetic approach for controlling the nanoparticle surface and hence the aggregation/separation of nanoparticles, bimodal brushes have been studied on both silica and titania nanoparticles.[29,30] Both a grafting-to and grafting-from approach

have been incorporated into its study. Because of the difficulty in using a surface-initiated grafting-from approach for silicones, due to their production through polycondensation, a grafting-to method was developed for the incorporation of TiO_2 NPs into a silicone matrix.[30] Poly(dimethyl siloxane) (PDMS) was modified with a phosphate moiety on the chain end and then attached to the titania surface. Compared to monomodal systems, the 10kg/mol short and 36kg/mol long bimodal composites showed greater optical clarity even in 100 kg/mol matrix. While the grafting-to approach allows for the flexiblity in polymer and polymerization method choice, the absolute control over all parameters of the surface is not accomplished. For this, a sequential grafting-from method is necessary.

For the controlled study of the contributing entropic and enthalpic factors of NP organization (separately and independently), a sequential RAFT polymerization technique was employed (Figure 4.1).[29] Through a RAFT agent attached via an aminosilane to a silica nanoparticle, the short chain can be grown from the surface. By varying the ratio of aminosilane coupling agent, the graft density can be controlled. In order to prevent the formation of block copolymers from this first population of chains, the RAFT agent is cleaved from the chain-end via reaction with dilute AIBN. By keeping a relatively intermediary graft density, the core-core attractions are well screened by the short brush while leaving silica surface area available for secondary attachment. The long chains are produced via an identical procedure, however, at a low graft density to enable entanglement with the polymer matrix. This method allows for the control of each chain's molecular weight, polydispersity, architecture, chemical identity, and graft density independently. The bimodal nanocomposites showed increased dispersity, as well as increased storage and elastic modulus.[31] Also, a shift in the nanofiller morphology diagram was created, allowing for the dispersion and entanglement of nanoparticles into a matrix with a molecular weight lower than that of the grafted brush. Combining a long, sparse brush with a short, dense brush

also allows for the study of the system's enthalpic and entropic factors independently as they are no longer coupled through the use of a monomodal system.

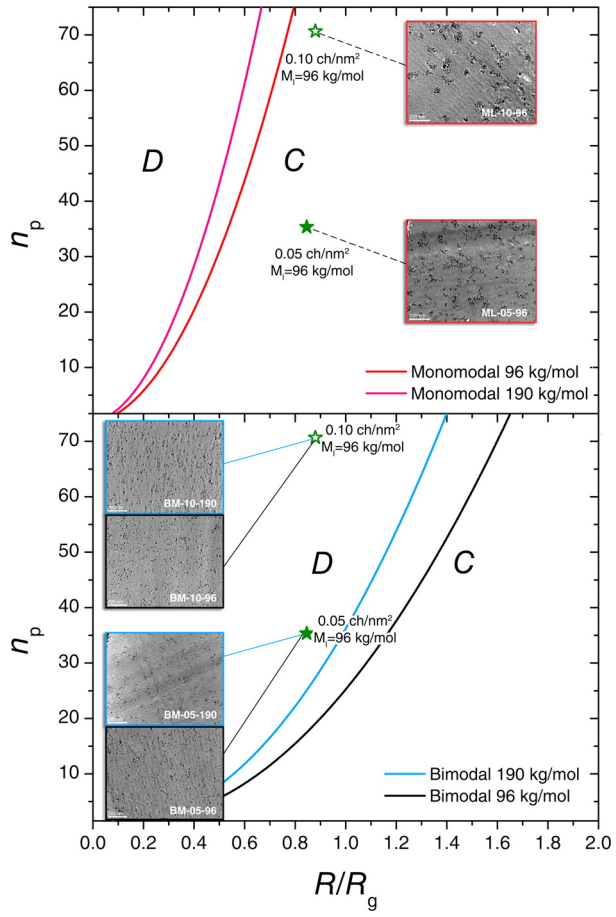

Figure 3.3 Parametric phase diagram of the homopolymer PS-silica: (a) monomodal and (b) bimodal systems under our purview, showing the dispersed and string-like agglomerate regions. The experimental micrographs of 5 wgt % silica loading of the samples are shown to demonstrate the validity of predictions. The open and filled stars correspond to graft densities of 0.10 ch/nm^2 and 0.05 ch/nm^2. The monomodal 190 kg/mol boundary is shown purely to illustrate the shift in phase boundaries with varying matrix molecular weight.

However to bolster the claim of true decoupling of the role of the long and short brushes, the current chapter is focused on the creation of mixed bimodal brushes on nanoparticles along with their dispersion and property enhancement. If the sole role of the long brush is that of matrix entanglement, then the chemistry of the short brush can be changed to that which is incompatible with the long brush and matrix. This

will still allow for the dispersion in a matrix that is compatible with the long brush chemistry. This change in short brush chemistry can also bring about changes to the intrinsic properties of the filler and therefore properties of the composite, similar to that accomplished through the use of block compolymer brushes on nanoparticles however with complete control of the independent graft densities. Both poly(methyl) methacrylate short/polystyrene long and polystyrene short/poly(methyl) methacrylate long mixed bimodal brush nanoparticles were created and then dispersed in both PS and PMMA matrices of different molecular weights. In both systems, the chemistry of the short brush did not affect the morphology of the nanocomposite. Also, the same shift in the morphology phase diagram is present allowing for the dispersion and entanglement of a mixed bimodal system in a matrix with higher molecular weight than that of the long brush. To further push the boundaries of mixed bimodal brush synthesis, properties, and application we have also created a mixed bimodal brush system composed of poly(fluorobutyl) methacrylate short/polystyrene long brushes that are cast as a film atop a sheet of polystyrene. This coated sheet is then annealed to prove the absence of dewetting from the surface, while also showing an increase of the water contact angle. The TEM micrographs along with their analysis and the analysis of the composites' thermomechanical properties was performed by collaborators at Rennselaer Polytechnic Institute.

3.2 Experimental

Materials

Colloidal silica nanoparticles (15 nm diameter) were purchased from Nissan Chemical. 2,2'-Azoisobutyronitrile (AIBN) was used after recrystallization in ethanol. Styrene, methyl methacrylate, and 1H, 1H-heptafluorobutyl methacrylate monomers were passed through a basic alumina column to remove the inhibitor before use.

Activated 4-cyanopentanoic acid dithiobenzoate (CPDB) was prepared according to a procedure described in literature.[32] 3-Aminopropyldimethylethoxysilane was purchased from Gelest, Inc. and used as received. Highly Monodisperse Polystyrene (M_w=9600 g/mol, PDI 1.01), was procured from TOSOH Inc.

Instrumentation

Molecular weights and molecular weight distributions were determined using a Polymer Laboratories PL-GPC 120 with refractive index detector, 3 PLgel 10 μm MIXED-B columns in sequence, each with a molecular weight range of 500 to 10,000,000 g/mol, THF as eluent at 30°C and a flow rate of 1.0 mL/min. The GPC system was calibrated with poly(methyl) methacrylate and polystyrene standards obtained from Polymer Labs.

Synthesis of SiO_2-*g*-CPDB

A solution (20 mL) of colloidal silica (30 wt% in MEK) was added to a two necked round bottom flask and diluted with 75 mL of THF. To it was added 3-aminopropyldimethylethoxysilane (0.32, 2 mmol) and the mixture was heated at 70 °C overnight under nitrogen protection. The reaction was then cooled to room temperature and precipitated in a large amount of hexanes (500 mL). The particles were recovered via centrifugation and then redispersed in THF. This procedure was repeated. The THF solution of amine-functionalized silica nanoparticles (40 mL, 6 g) was added drop wise to a THF solution (30 mL) of activated CPDB (0.67 g, 2.4 mmol) at room temperature. After complete addition, the solution was stirred overnight. The reaction mixture was then precipitated into a large amount of hexanes (500 mL). The particles were recovered via centrifugation. This procedure was repeated until the supernatant was colorless. The red CPDB anchored silica nanoparticles were

dried at room temperature and analyzed using UV-Vis analysis to determine chain density using a calibration curve constructed from solutions of free CPDB.

General procedure for graft polymerization of the first chain population from CPDB anchored silica nanoparticles to make SiO_2-*g*-$Polymer_1$

A solution of $monomer_1$, CPDB anchored silica nanoparticles (1 g 80 μmol/g RAFT), AIBN (0.8 mL of a 10 mM THF solution), and THF (17 mL) was prepared in a dried Schlenk tube. The mixture was degassed by three freeze-pump-thaw cycles, back filled with nitrogen, and then placed in an oil bath for 3-12 hours depending on monomer and desired molecular weight. The polymerization solution was quenched in ice water and poured into hexanes to precipitate polymer grafted nanoparticles and centrifuged to recover the nanoparticles. This process was repeated twice more to ensure removal of small molecules. The polymer chains were cleaved by treated a small amount with HF (0.2 mL of a 51% solution in water) and the resulting polymer chains analyzed by GPC.

General Procedure for chain-end deactivation and cleavage of RAFT agent from SiO_2-*g*-$Polymer_1$

Solid AIBN (10:1 ratio of AIBN:RAFT) was added to a solution of SiO_2-*g*-$Polymer_1$ in THF and heated at 65 °C under nitrogen for 30 minutes. The resulting solution was poured into 100 mL of hexanes and centrifuged for nanoparticle recovery. This process was repeated twice more to ensure removal of excess AIBN.

Functionalization of SiO_2-*g*-$Polymer_1$ by 2nd RAFT agent

The second RAFT agent was attached onto remaining free hydroxy groups of the colloidal silica nanoparticles. The surface was functionalized by amine groups using 0.020 mL of 3-aminopropyldimethylethoxysilane in a process similar to the one described for the first amine functionalization. After the SiO_2-*g*-$Polymer_1$ particles were functionalized by amines, the second population of activated CPDB (30 mg) was condensed onto the surface of the nanoparticles to give SiO_2-*g*-($Polymer_1$, CPDB) nanoparticles.

Calculation of the 2nd Chain Graft Density

There are two methods used for the calcuation of the 2nd chain graft density. One is performed post-polymerzation of the 2nd chain population and has been described in detail previously.[31] In this method, using a combination of first chain graft density measured via UV-Vis, molecular weight of both chain populations via GPC, and percent silica measured via TGA, the chain density of the 2nd chain population can be back calculated. The second method is performed in a similar manner, however, before the 2nd chain is polymerized. UV-Vis analysis is performed on SiO_2-*g*-($Polymer_1$, CPDB) nanoparticles and the absorption compared to a standard calibration curve of free RAFT agent in solution. The concentration of silica is then corrected via percent silica of the sample obtained via TGA.

General Procedure for graft polymerization of $polymer_2$ from SiO_2-*g*-($Polymer_1$, CPDB) to obtain 2nd brush

The 2nd RAFT agent containing SiO_2-*g*-($Polymer_1$, CPDB) particles (1.0 g by weight of silica) were dissolved in roughly 10 mL of THF and added to a dried Schlenk tube along with $monomer_2$ and AIBN (0.19 mL of a 10 mM THF solution). The mixture

was degassed by three freeze-pump-thaw cycles, back filled with nitrogen, and then placed in an oil bath for 12-36 hours depending on monomer and desired molecular weight. The polymerization was quenched in ice water and then poured into hexanes to precipitate bimodal brush grafted nanoparticles and centrifuged to recover SiO_2-*g*-(Polymer$_1$, Polymer$_2$) nanoparticles. The polymer chains were treated with HF and analyzed via GPC similarly to the first chain population.

3.3 Results and Discussion

Table 3.1 Various Mixed Bimodal Brush-Anchored Silica Nanoparticles Synthesized Using Sequential RAFT Polymerization. All weights reported as g/mol and graft densities as chains/nm^2

Number	1st Monomer	1st MW	1st Density	2nd Monomer	2nd MW	2nd Density
NP-1	MMA	20,000	0.24	Styrene	175,000	0.10
NP-2	MMA	6400	0.27	Styrene	75,000	0.10
NP-3	Styrene	1600	0.26	MMA	205,000	0.07
NP-4	HFBMA	4,000	0.24	Styrene	114,000	0.10
NP-5	HFBMA	17,000	0.24	Styrene	150,000	0.09

Previously we have used a sequential RAFT polymerization technique for the production of bimodal brushes on nanoparticles. These brushes allowed for the decoupling of the roles of the short and long brushes. That is, the short brush was tuned for dispersion and the long brush was tuned to allow for entanglement with the matrix. To further illustrate the separation of these roles and show the possibility of further enhancement in filler properties, a series of mixed bimodal samples was made and can be seen in Table 3.2.

Dispersion Behavior

Figure 3.4 shows a representative set of dispersions demonstrating the advantage of grafting bimodal brushes on the surface on nanoparticles. These composite systems were created using NP-3 from Table 3.2. In this system, a mixed bimodal brush was created by first polymerizing a short (1600 kg/mol) polystyrene brush with a graft

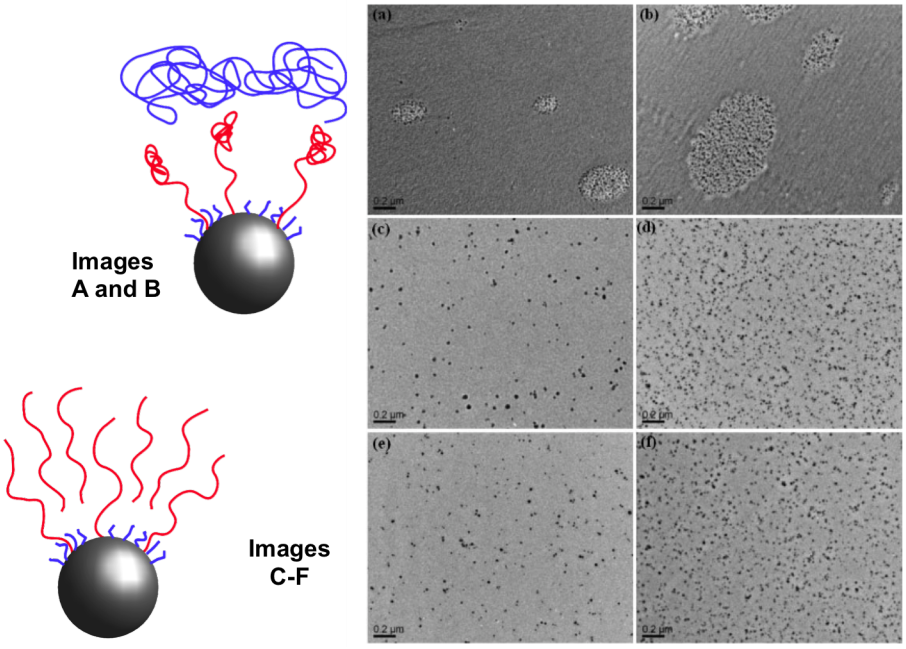

Figure 3.4 TEM micrographs of 1 wt% (left column) and 5 wt% (right column) of NP-3 dispersed in (a-b) 100k PS, (c-d) 100k PMMA, and (e-f) 300k PMMA matrices. Cartoon to left of TEM micrographs used to illustrate chain conformation at nanoparticle/matrix interface in composites. Blue chains are polystyrene and red chains are poly(methyl) methacrylate

.

density of 0.26 chains/nm^2 to encourage dispersion followed by the polymerization of a long (205,000 kg/mol) brush with a graft density of 0.07 chains/nm^2 to encourage entanglement. Following the synthesis of the mixed bimodal brush, nanocomposites were made by dispersing NP-3 in monodisperse matrices of both polystyrene and poly(methyl) methacrylate. The dispersion of the grafted silica nanoparticles was examined using Transmission Electron Microscopy (TEM).

The micrographs of NP-3 dispersed in a 100k PS matrix (Figure 3.4a-b) show complete dewetting of the grafted chains from the matrix. The matrix is chemically identical to the short brush, but immiscible with the long brush. While the PS short brush somewhat shielded the vdW attraction between NP cores in the 100k PS matrix, the PMMA long brush prefers to collapse onto the NP surface to avoid contact with the PS matrix. The tendency for aggregation of the PMMA-covered NPs

to minimize the interfacial area between PMMA and PS cannot be compensated by the screening effect of the PS short brushes and leads to the observed results. Even though there is no entanglement or penetration of the PMMA brush with the PS matrix, the PMMA brush does entangle with the adjacent PMMA brush and phase separates from the matrix.

In Figure 3.4c-d this same system is dispersed in a 100k PMMA matrix. In these micrographs it can be seen that dispersion is greatly enhanced compared to Figure 3.4a-b.. The short PS chains still allow for screening of the core-core attractions, however, the PMMA long chains are now compatible with the PMMA matrix and presumably entangle. This is observed even with 0.26 chains/nm^2 density short brush of incompatible chemistry.

In Figure 3.4e-f NP-3 is dispersed in a matrix of molecular weight larger than the long grafted chains. Within a monomodal system this causes autophobic dewetting, however, within this bimodal brush nanocomposite system it is seen that both dispersion and entanglement is maintained. The shift in the parametric phase diagram of nanoparticle dispersion reported in previous work (Figure 3.3) is still maintained.

In order to further test that all of the previous observations hold true for the inverse case, mixed bimodal brush NP-2 was made. In this system, there is a 6.4k short brush of PMMA and a 75k long brush of PS. This mixed bimodal brush system was then placed into a 100k PMMA matrix as well as 100k PS matrix. The dispersion states of these nanocomposites is shown in Figure 3.5. Similar to the previous example, in Figure 3.5a the grafted long chains completely dewet from the matrix. The chains collapse and entanglement with other PS grafted long chains. This causes phase separation from the matrix.

The dispersion of NP-2 within a 100k PS matrix is shown in Figure 3.5b. In this composite the PS grafted chains promote miscibility with the PS matrix chains. Thus, by using a mixed bimodal brush, nanoparticle dispersion is maintained even in

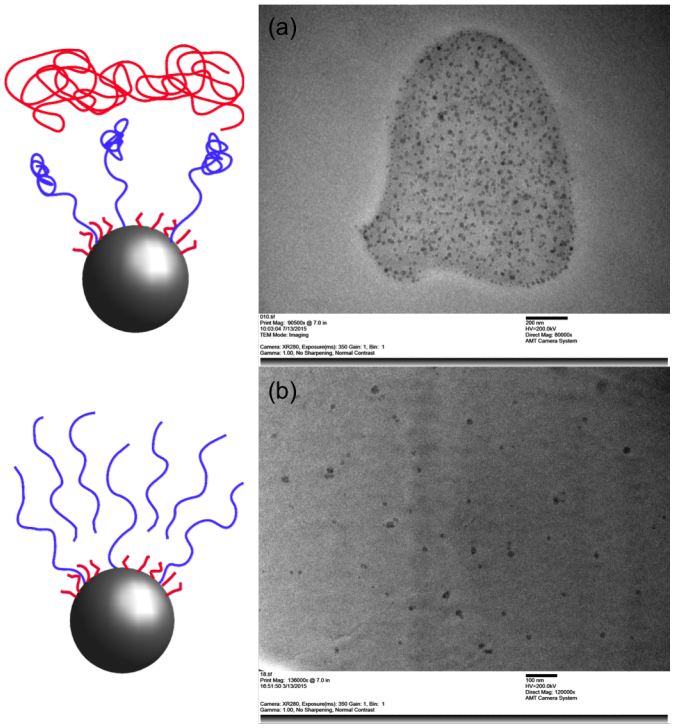

Figure 3.5 TEM micrographs of 1 wt% of NP-2 dispersed in (a) 100k PMMA and (b) 100k PS. Cartoons to the left of TEM micrographs are used to illustrate chain conformation at the nanoparticle/matrix interface in composites. Blue chains are polystyrene and red chains are poly(methyl) methacrylate

.

a matrix with a larger molecular weight than that of the brush. The roles of the short brush and long brush have been truly decoupled. The chemistry of the short brush has no apparent effect on the dispersion of the nanoparticle or its entanglement with the matrix as long as the long brush is matrix compatible. The shift in the parametric phase diagram of nanoparticle dispersion reported in previous work (Figure 3.3) is still maintained.

Mechanical Behavior

In previous work it was reported that the increased dispersion and entanglement of a bimodal brush enhances the mechanical properties of the nanocompoiste.[31] If these factors still exist for mixed bimodal chains, and the roles are truly decoupled

allowing for short and long chains to be of mixed chemsitry, then there should still be an increase in mechanical properties when the long grafted chains entangle with the matrix chains.

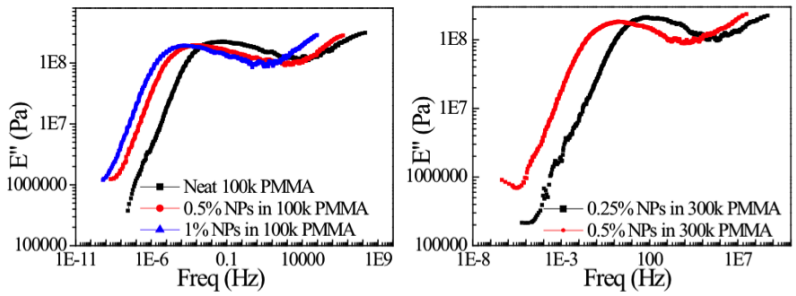

Figure 3.6 Loss Modulus (E") vs. Log Frequency for NP-3/PMMA systems

.

For the testing of the mechanical properties of mixed bimodal grafted nanoparticles, a composite of NP-3 in both 100k and 300k PMMA was created at various levels of silica wt% (Figure 3.6). These systems have a compatible long brush (PMMA), and an incompatible short brush (PS). As observed, there is a shift For NP-3 filled 100k to a lower frequency with increased loading of filler. Entanglement of matrix chains and the grafted long brush leads to decreasing mobility for the chains in the interface, and this decrease influences the properties of the bulk material. This shift to lower frequency is also observed when NP-3 is placed in a 300k PMMA matrix.

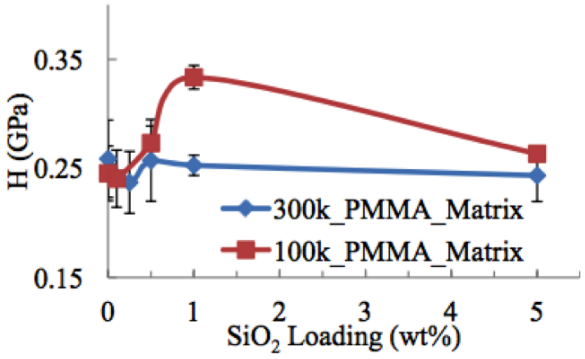

Figure 3.7 Hardness vs silica loading for NP-3/PMMA systems.

The interaction of the brush and matrix also influences hardness measured in

nanoindentation tests (Figure 3.7). Once again a set of nanocomposites with range of silica wt% were prepared using a long brush compatible matrix of 100k and 300k PMMA and their hardness tested. An increase in hardness was observed for 100k PMMA, while no significant change was observed for 300k PMMA due to the weaker interaction of matrix and brush. This observation is in agreement with previous work reported on homopolymer bimodal systems.

Fluorocarbon/Hydrocarbon Mixed Bimodal Brush Synthesis

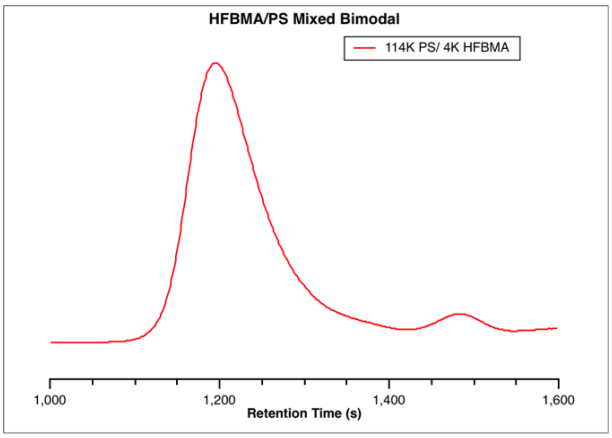

Figure 3.8 GPC trace for mixed bimodal sample NP-4

.

To further test the limits of placing incompatible chains on nanoparticles using the sequential RAFT polymerization technique, mixed bimodal brushes were created with a short, dense brush of heptafluorobutyl methacrylate and a long, sparse brush of polystyrene (NP-4 in Table 3.2). The synthesis of the fluorinated short brush is conducted via attachment of the desired RAFT agent using an aminosilane anchored to the silica NP surface, polymerization, and removal of the chain end's Z group via a radical cross coupling mechanism to prevent the short brush from growing in subsequent polymerizations. An intermediate graft density (controlled via the aminosilane:nanoparticle feed ratio) is chosen to screen the core-core attractions. Once the short brush has been created, the process of aminosilane anchoring, CPDB

attachment, and polymerization is repeated for the polystyrene brush, however, at a lower graft density and higher molecular weight to encourage entanglement. The GPC trace of this mixed bimodal sample is shown in Figure 3.8.

To test the control of heptafluorobutyl methacrylate with our system of RAFT agent modified silica, a kinetic study was performed. As can be seen in Figures 3.9 and 3.10 a short induction time is observed with CPDB as well as linear kinetics with PDIs below 1.2. This is indicative of a well controlled polymerization of the heptafluorobutyl methacrylate brush.

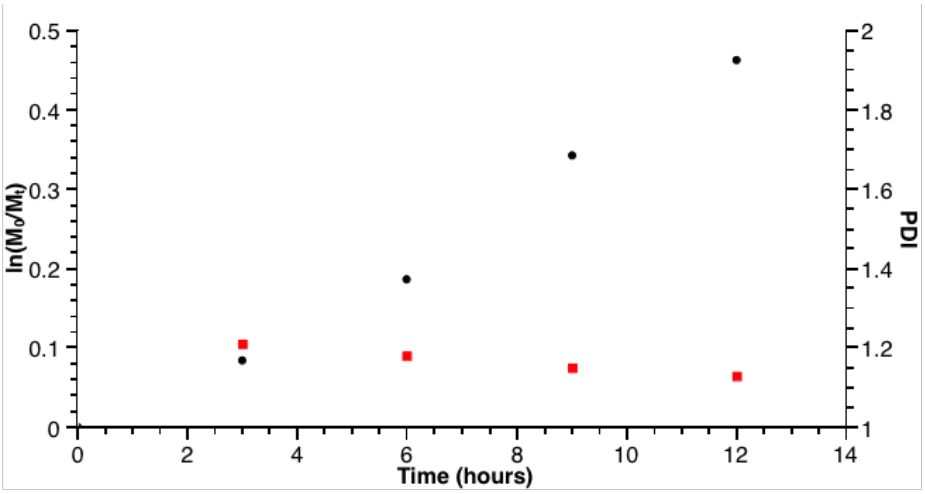

Figure 3.9 Kinetic plot for polymerization of HFBMA from surface of NPs via RAFT.

Property Enhancement of Fluorocarbon/Hydrocarbon Mixed Bimodal Brush

In order to test the compatibility of NP-4 with a hydrocarbon surface, a film of NP-4 in THF was drop cast onto a sheet of polystyrene and allowed to dry. Compatibility of the NP-4 film and the substrate was visually observed, as there was no phase separation. This sample was annealed at 150 °C for 48 hours. After annealing, the sample appeared homogenous with no evidence of phase separation or an incompatible

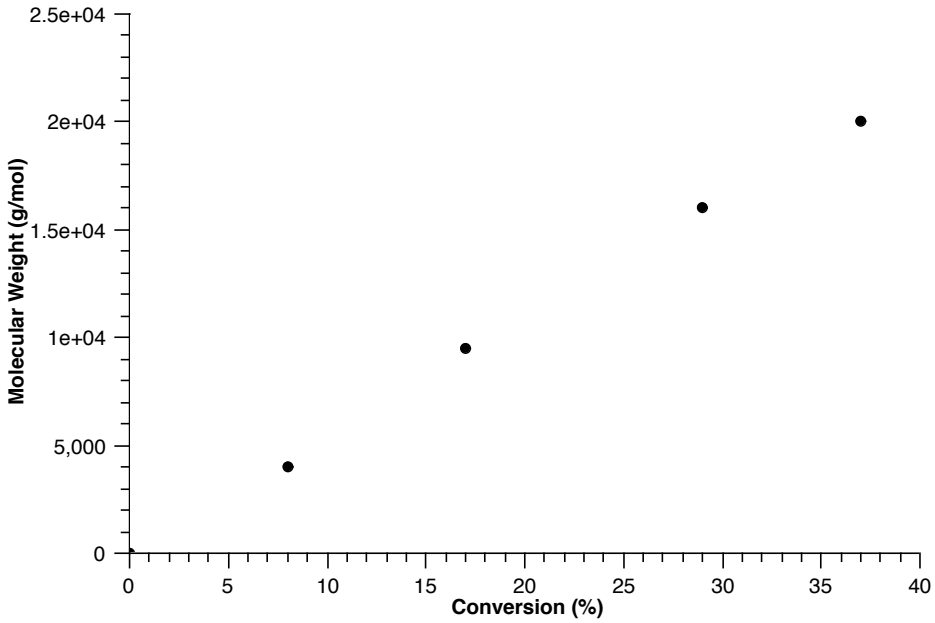

Figure 3.10 Relationship of conversion vs molecular weight for polymerization of HFBMA from the surface of silica NPs via RAFT.

surface layer. In order to test the presence of the fluorinated chains on the surface, ATR IR was performed on the treated surface. As can be seen in Figure 3.11 the carbonyl peak of the methacrylate at approximately 1700 cm^{-1} was still observed even on the surface of a PS sheet treated with 4k HFBMA/114k PS mixed bimodal nanoparticles.

To test the improvement in hydrophobic properties, a series of water contact angle measurements were performed. These results are illustrated in Figure 3.12. A film of pure NP-4 in THF was drop cast onto a glass slide. This is then compared with the untreated polystyrene sheet. The water contact angle of the treated glass slide (117°) is greater than that of the untreated glass slide (39°). Also, the water contact angle of the treated and annealed polystyrene sheet (104°) was greater than that of the untreated polystyrene sheet. This increase in water contact angle must be attributed to the presence of the fluorinated methacrylate NPs on the treated surfaces. Also in the case of the NP-4/PS surface, the presence of the flourinated short chains did

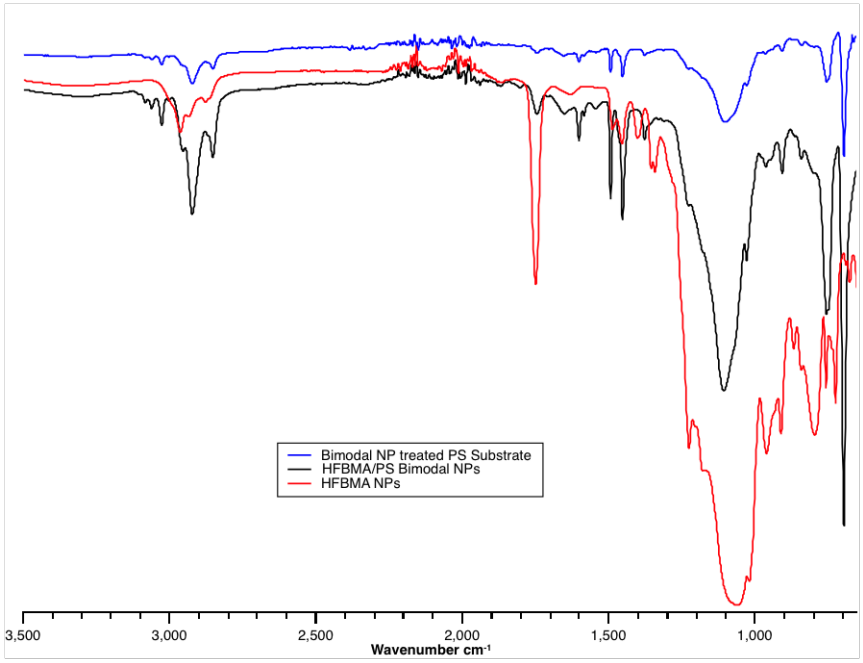

Figure 3.11 Comparison of IR specra from HFBMA NPs (red), HFBMA/PS bimodal NPs (black), and mixed bimodal treated PS surface (blue)

.

Table 3.2 Comparison of water contact angles of surfaces that are treated with NP-4 film and those left untreated.

Surface	**Water Contact Angle**
Glass	39°
PS	86°
NP-4/glass	117°
NP-4/PS	104°

not appear to affect the ability of the long, sparse brush of polystyrene to adhere to the polystyrene substrate. After annealing the film did not dewet or detach from the substrate surface, indicating chain entanglement between the grafted long brush and that of the substrate.

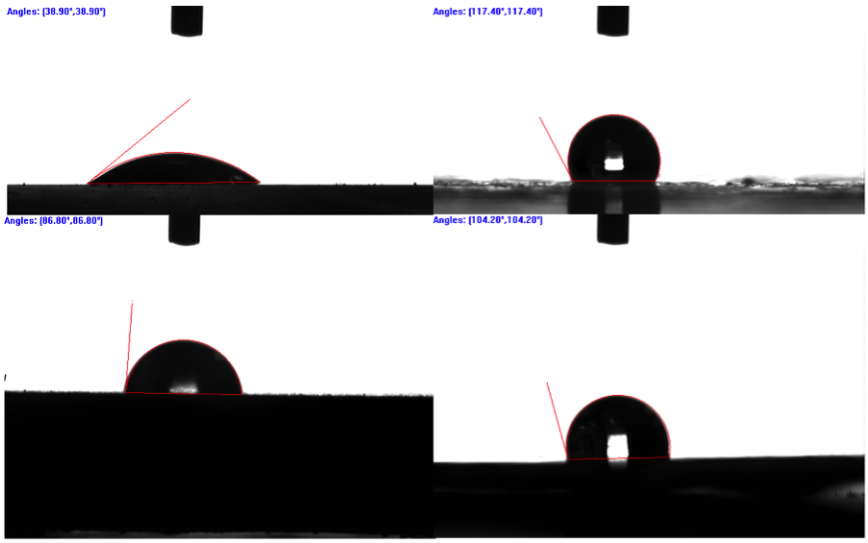

Figure 3.12 Water contact angle measurements for an untreated glass slide (top left), glass slide with drop cast NP-4 film (top right), untreated PS sheet (bottom left), and PS sheet with NP-4 film (bottom right)

.

3.4 Summary

In this chapter, the further development of a sequential RAFT polymerization technique was described for the synthesis of mixed bimodal brush grafted nanoparticles. TEM analysis of the brush grafted nanoparticles showed that the role of the short and long brush was truly decoupled. As long as the long brush chemistry remains matrix compatible, the short brush chemistry can be widely varied. Using this system, both good dispersion and good entanglement was observed even in a matrix incompatible with the short brush chemistry. These mixed bimodal samples also show an improvement in the mechanical properties within a long brush compatible matrix. In order to further test these roles and the ability for extremely incompatible chemistries to coexist on the same nanoparticle surface, a fluorocarbon/hydrocarbon mixed bimodal system was created and drop cast onto a hydrocarbon substrate. This system showed compatibility with the hydrocarbon substrate while also increasing the water contact angle of the surface. This further supports the possibility of allowing the short chain chemistry to be changed and also property enhancing while leaving the long chain chemistry compatible with the substrate or matrix of the application. These mixed binary/bimodal brush-grafted nanoparticles render themselves potentially useful as functional additives in a wide range of applications.

3.5 References

[1] Winey, K. I.; Vaia, R. A. *MRS Bulletin* **2007**, *32*, 314–319.

[2] Vaia, R. A.; Maguire, J. F. *Chemistry of Materials* **2007**, *19*, 2736–2751.

[3] Zou, H.; Wu, S.; Shen, J. *Chemical Reviews* **2008**, *108*, 3893–3957.

[4] Wang, M.-J. *Rubber Chemistry and Technology* **1998**, *71*, 520–589.

[5] Schadler, L. S.; Kumar, S. K.; Benicewicz, B. C.; Lewis, S. L.; Harton, S. E. *MRS Bulletin* **2007**, *32*, 335–340.

[6] Brown, J. M.; Anderson, D. P.; Justice, R. S.; Lafdi, K.; Belfor, M.; Strong, K. L.; Schaefer, D. W. *Polymer* **2005**, *46*, 10854 – 10865.

[7] Kumar, S. K.; Jouault, N.; Benicewicz, B.; Neely, T. *Macromolecules* **2013**, *46*, 3199–3214.

[8] Green, P. F. *Soft Matter* **2011**, *7*, 7914–7926.

[9] Green, P. F.; Oh, H.; Akcora, P.; Kumar, S. K. *Structure and Dynamics of Polymer Nanocomposites Involving Chain-Grafted Spherical Nanoparticles*; Dynamics of Soft Matter: Neutron Applications; 2012.

[10] Balazs, A. C.; Emrick, T.; Russell, T. P. *Science* **2006**, *314*, 1107–1110.

[11] Akcora, P.; Liu, H.; Kumar, S. K.; Moll, J.; Li, Y.; Benicewicz, B. C.; Schadler, L. S.; Acehan, D.; Panagiotopoulos, A. Z.; Pryamitsyn, V.; Ganesan, V.; Ilavsky, J.; Thiyagarajan, P.; Colby, R. H.; Douglas, J. F. *Nature Materials* **2009**, *8*, 354–U121.

[12] Ferreira, P. G.; Ajdari, A.; Leibler, L. *Macromolecules* **1998**, *31*, 3994–4003.

[13] Meli, L.; Arceo, A.; Green, P. F. *Soft Matter* **2009**, *5*, 533–537.

[14] Bansal, A.; Yang, H. C.; Li, C. Z.; Benicewicz, B. C.; Kumar, S. K.; Schadler, L. S. *Journal of Polymer Science Part B-Polymer Physics* **2006**, *44*, 2944–2950.

[15] Skvortsov, A. M.; Gorbunov, A. A.; Leermakers, F. A. M.; Fleer, G. J. *Macromolecules* **1999**, *32*, 2004–2015.

[16] Martin, T. B.; Jayaraman, A. *Soft Matter* **2013**,

[17] Ionov, L.; Houbenov, N.; Sidorenko, A.; Stamm, M.; Luzinov, I.; Minko, S. *Langmuir* **2004**, *20*, 9916–9919.

[18] Houbenov, N.; Minko, S.; Stamm, M. *Macromolecules* **2003**, *36*, 5897–5901.

[19] Kumar Vyas, M.; Schneider, K.; Nandan, B.; Stamm, M. *Soft Matter* **2008**, *4*, 1024–1032.

[20] Draper, J.; Luzinov, I.; Minko, S.; Tokarev, I.; Stamm, M. *Langmuir* **2004**, *20*, 4064–4075.

[21] Bao, C.; Tang, S.; Horton, J. M.; Jiang, X.; Tang, P.; Qiu, F.; Zhu, L.; Zhao, B. *Macromolecules* **2012**, *45*, 8027–8036.

[22] Jiang, X.; Zhong, G.; Horton, J. M.; Jin, N.; Zhu, L.; Zhao, B. *Macromolecules* **2010**, *43*, 5387–5395.

[23] Jiang, X.; Zhao, B.; Zhong, G.; Jin, N.; Horton, J. M.; Zhu, L.; Hafner, R. S.; Lodge, T. P. *Macromolecules* **2010**, *43*, 8209–8217.

[24] Zhao, B.; He, T. *Macromolecules* **2003**, *36*, 8599–8602.

[25] Ionov, L.; Minko, S. *ACS Applied Materials & Interfaces* **2012**, *4*, 483–489.

[26] Estillore, N. C.; Advincula, R. C. *Langmuir* **2011**, *27*, 5997–6008.

[27] Zhao, B.; Zhu, L. *Macromolecules* **2009**, *42*, 9369–9383.

[28] Stuart, M. A. C.; Huck, W. T. S.; Genzer, J.; Muller, M.; Ober, C.; Stamm, M.; Sukhorukov, G. B.; Szleifer, I.; Tsukruk, V. V.; Urban, M.; Winnik, F.; Zauscher, S.; Luzinov, I.; Minko, S. *Nature Materials* **2010**, *9*, 101–113.

[29] Rungta, A.; Natarajan, B.; Neely, T.; Dukes, D.; Schadler, L. S.; Benicewicz, B. C. *Macromolecules* **2012**, *45*, 9303–9311.

[30] Li, Y.; Tao, P.; Viswanath, A.; Benicewicz, B. C.; Schadler, L. S. *Langmuir* **2013**, *29*, 1211–1220.

[31] Natarajan, B.; Neely, T.; Rungta, A.; Benicewicz, B. C.; Schadler, L. S. *Macromolecules* **2013**, *46*, 4909–4918.

[32] Li, C.; Han, J.; Ryu, C. Y.; Benicewicz, B. C. *Macromolecules* **2006**, *39*, 3175–3183.

Chapter 4

One-Pot Synthesis of Bimodal Brush Grafted Nanoparticles via Thermally Initiated, Bulk RAFT Polymerization

4.1 Introduction

As a consequence of the larger surface area:mass ratio of nanoparticles when compared with conventional fillers, there is an immense interface between the polymer matrix and particles in polymer nanocomposites (PNCs). This large surface area can lead to enhanced optical, electrical, and thermomechanical properties of the resulting polymer nanocomposites, (PNCs)[1–14] when compared to conventional composites.[3] This large surface area also allows for a multitude of enhancements via modification of the interface. A commonly used modification is the grafting of polymer chains, with chemical composition the same as that of the matrix, onto the surface. It was originally shown on micrometer sized particles that with a high graft density of polymer chains, the particles are miscible within a matrix as long as the polymer chains of the matrix have a lower molecular weight than the grafted chains.[15] If the grafted polymer chains are of lower molecular weight than the matrix the chains become immiscible. Since the chemical composition of these chains are identical, this brush autophobicity is entropically driven.[4,16–20] These same ideas can be used for the incorporation of nanoparticles, controlling brush/matrix miscibility and as a result nanoparticle dispersion.[21] Recently this control has been used to create unique distributions of

nanoparticles within the polymer matrix while improving the physical properties of the nanocomposites.[21–26] However, these new structures are formed not by high graft density nanoparticles, but when low graft density nanoparticles are incorporated into the matrix.[20,21,23,27–33]

Two broad synthetic strategies exist for the attachment of a polymer chain to a surface: grafting-to and grafting-from. In the grafting-from method, the surface is functionalized with an appopriate initiator or chain transfer agent, and then the polymer chain is grown from the surface in a surface-initiated polymerization. Small molecules such as the initiator or monomers do not suffer from steric hindrance while migrating to the surface and/or a growing polymer chain. This allows for a high density brush to be grafted onto the surface of a nanoparticle. In contrast, the grafting-to method involves the attachment of a preformed and end-functionalized polymer chain. This attachment can occur through either physisorption (where the forces involved are intermolecular between the chain and the substrate surface) or chemisorption (where a covalent bond is formed between the chain end moiety and the surface). While not offering the availability of a high graft density polymer brush,[34] grafting-to has some unique advantages. Grafting-to offers a simple and modular method for the creation of polymer grafted nanoparticles. Monomers that traditionally cannot be polymerized via a surface initiated or controlled radical polymerization technique can be pre-made via the method of choice and then attached. Grafting-to can also enable a much easier scaling process as polymers can be made in bulk and then attached to a surface in a much smaller volume of solvent (without the need for such stringent controls over deoxygenating the solvents) when compared to grafting-from. This can lead to increased efficiency and decreased time and cost in an industrial setting.

Controlled or "living" polymerization techniques allow for control of the polymer composition, molecular weight, architecture, and polydispersity, however, controlled **radical** polymerizations (CRP) offer certain advantages over other methods such

as anionic, cationic, and ring-opening. Radical polymerizations are generally less restrictive in terms of reaction media, functional groups, and reaction conditions. For RAFT (reversible-addition fragmentation chain transfer) the versatility in compatible monomer functionality, lack of catalyst, and mild reaction conditions has made its continued growth of use in the last decade possible. Because of this, once a suitable RAFT agent has been chosen, adding it to a free radical polymerization elicits all of the described control while keeping all the other reaction conditions constant. The chosen RAFT agent contains a stabilizing Z group and a reactivating R group. Due to the RAFT mechanism these Z and R groups become the chain end functionality post polymerization. Therefore, through selection of RAFT agent chemistry the polymer chain end-group chemistry can be controlled as well. Through the use of RAFT and coupling agents, our group has shown control over graft density from 0.01 to 0.8 chains/nm^2 while growing polymer chains over 200 kg/mol with a polydispersity below 1.15.[35–37]

The control of the interface is accomplished through the previously described surface modifications, grafting methods, and controlled radical polymerization techniques. This control has been shown previously, along with the resulting control over nanocomposite morphology as well as properties dependent upon this morphology.[21,27,28,33,38] Using these techniques, heterogeniety can also be introduced into the interface. While adding complexity to the system, it affords the chemist with another parameter for the control and tunability of the resulting properties.[39] This heterogeneity is introduced by varying the architecture of the polymer chains and/or the interface directly. Two synthetic methods are the use of block and bimodal polymer chains. While we have previously used block copolymer brushes for the mechanical reinforcement in nanocomposites,[40,41] the use of bimodal brushes allows for the control of the polymer chain graft densities independently from each other.

A bimodal brush is defined as a homopolymer brush with two distinct monodis-

perse chains attached to a common surface.[42] If these polymer chains are chemically distinct, it is deemed a mixed bimodal brush. The general benefits of a bimodal system when compared to a block architecture is increased control over the different chains' independent graft density and a controlled increase in polydispersity of the brush system which has been suggested to control dispersion.[43] Few methods have been described for the synthesis of bimodal brush systems. Grafting-to approaches have been described by Luzinov, Minko, and Stamm[44–47] but these studies on micron-sized hairy particle colloidal systems are mostly focused on the response of the particles due to changes in the environment and not on the properties of nanocomposites made with grafted nanoparticles. Zhao has created a Y-shaped initiator that has been used with much success,[48–51] however, this does not allow for the chains to have an independent graft density. Previous work has suggested that the assembly of nanoparticles in the sparse brush regime is a competition between enthalpic core-core van der Waals attractions and entropic repulsion due to distortion of the attached brush.[21,52] Also, theoretical work done by Matsen has suggested the use of a bimodal brush could overcome autophobic dewetting between the chians of the polymer matrix and those grafted to the surface.[53] Simulation studies done by Jayaraman also support this theory.[39,43,54] In fact, this has been proven experimentally as well. As a new synthetic tactic for controlling nanoparticle aggregation/dispersion, we have synthesized bimodal brushes via grafting-to and grafting-from methods. For the controlled study of the contributing enthalpic and entropic factors of nanoparticle organization (separately and independently), a sequential RAFT polymerization technique was employed.[55]

Through the use of a modified RAFT agent attached via an aminosilane to a silica nanoparticle, the short chain can be grown from the surface. By varying the ratio of aminosilane to nanoparticles, the graft density can be controlled. In order to prevent the formation of block copolymers, the RAFT agent is cleaved from the

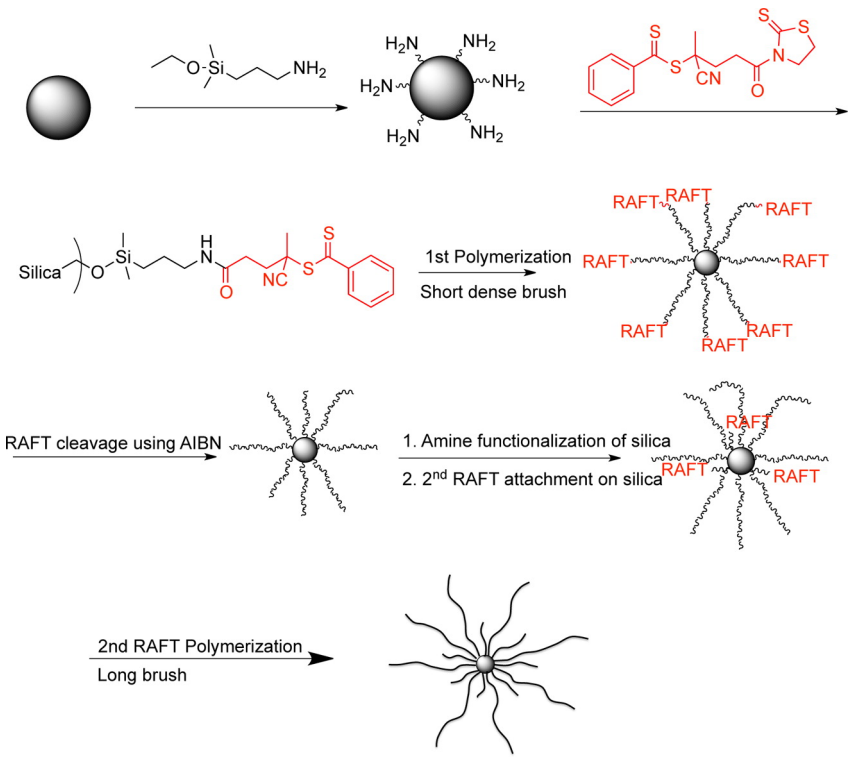

Figure 4.1 Sequential RAFT Polymerization for Synthesis of Bimodal Brushes

chain end, e.g. via a reaction with dilute AIBN. This exchanges the Z group of the RAFT agent that is present on the polymer chain end via a radical cross coupling mechanism. By keeping a relatively intermediate graft density, the core-core attractions are well screened by the short brush while leaving silica surface area available for secondary attachment. The long chains are produced via an identical procedure, however, at a lower graft density to enable entanglement with the polymer matrix. This method allows for the widest control of each chain's molecular weight, polydispersity, architecture, chemical identity, and graft density independently, however, it is a multi-step procedure. The bimodal nanocomposites showed increased dispersion, as well as increased storage and elastic modulus.[56] These nanoparticles also dispersed into a matrix of 180 kg/mol while the longest graft was only 118 kg/mol, contradicting the previous thought that matrix molecular weight must be lower than grafted molecular weight to allow for dispersion.

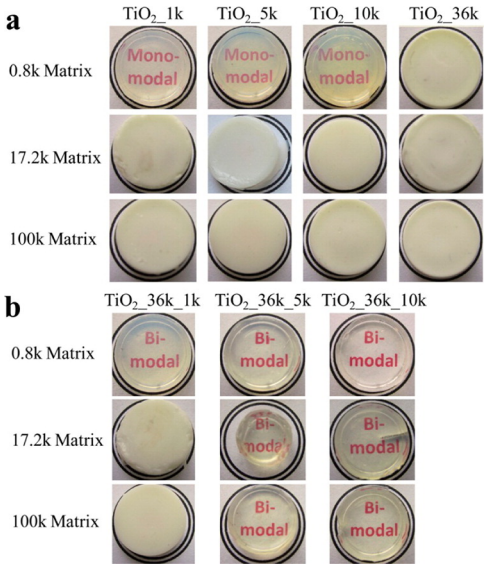

Figure 4.2 Silicone Composites of (a) Monomodal and (b) Bimodal Brushes via Sequential Grafting-to[57]

Because of the difficulty in using a surface initiated grafting-from approach for silicones, a grafting-to method was developed for the incorporation of TiO_2 nanoparticles into a silicone matrix.[57] Both monomodal and bimodal systems were grafted to titania nanoparticles with the greatest optical properties resulting from long brushes of 36 kg/mol and short brushes of 10 kg/mol. Compared to monomodal systems, the bimodal composites showed greater optical clarity even in a 100 kg/mol matrix, suggesting greater nanoparticle dispersion. More surprising was that this was accomplished via a grafting-to method with long chain densities of 0.01 chains/nm^2 and short chain denisities of 0.03 chains/nm^2. This would suggest that when compared to monomodal systems, higher graft densities aren't required for nanoparticle dispersion. However, this system is still a multi-step process.

In order to decrease complexity in the synthetic procedure and allow for easier scale-up, the development of a one-pot bimodal approach via a grafting-to method was investigated. Using aminosilanes and RAFT agents from our previous work on nanoparticle modification we elicit control over the end-group chemistry and therefore attachment. Two approaches are described for the incorporation of an acti-

vated R group onto a polymer chain end: post-polymerization modification and pre-polymerization modification. The polymerizations were done in bulk to decrease total solvent volume, increase kinetics, and decrease use of deoxygenated solvents. Silica nanoparticles are functionalized with an aminosilane, which is then reacted with the activated R group. Both short and long chains are allowed to react with the surface in a one-pot procedure. Demonstrated herein is that pre-polymerization modification and use of an infrequently utilized RAFT agent allows for higher graft density when compared to post-polymerization modification and that both chain populations attach creating a much simpler and more modular procedure for the synthesis of bimodal brushes on nanoparticles. Also, a method for labeling of one population for the ability to measure both populations' graft densities independently is discussed.

4.2 Experimental

Materials

Dicyclohexycarbodiimide (99%), (dimethylamino)-pyridine (99%), and 2-mercaptothiazoline (98%) were purchased from Acros. 2,2'-Azobis(isobutylnitrile) (AIBN) was used after recrystallization in methanol. 2,2-Dimethoxy-1,6-diaza-2-silacyclooctane was purchased form Gelest. 4-Cyanopentanoic acid dithiobenzoate (CPDB) was purchased from Strem. Styrene (99%, Acros) and methyl methacrylate (99%, Acros) were passed through basic alumina column to remove inhibitor before use. Colloidal silica nanoparticles (15 nm diamter) of 30 wt % dispersed in methyl ethyl ketone were provided by Nissan Chemical. Unless otherwise specified, all chemicals were used as received.

Instrumentation

Molecular weights and molecular weight distributions were determined by using a Polymer Laboratories PL-GPC 120 with refractive index detector; 3 PLgel 10 μm MIXED B columns in sequence with molecular weight range of 500 to 10,000,000 g/mol, THF as eluent at 30 °C and a flow rate of 1.0 mL/min. The GPC system was calibrated with both polystyrene and poly(methyl) methacrylate standards obtained from Polymer Laboratories. Thermogravimetric analysis was performed on a TA Instruments TGA-5000.

Activation of CPDB

CPDB (1.40 g, 5.00 mmol), 2-mercaptothiazoline (0.596 g, 5.00 mmol), and dicyclohexycarbodiimide (DCC) (1.24 g, 6.00 mmol) were dissolved in 30 mL of dichloromethane. (Dimethylamino)pyridine (DMAP) (61 mg, 0.50 mmol) was dissolved in 5 mL of dichloromethane and added dropwise to the solution. The reaction was allowed to stir overnight at room temperature. The solution was gravity filtered to remove the resulting salt. After removal of solvent via rotary evaporation, the crude red oil was purified via silica column chromatography (5:4 mixture of hexanes:ethyl acetate). The activated CPDB was obtained after removal of solvent as a red oil (1.41g, 74.5% yield). ^{1}H NMR (300 Mhz, $CDCl_3$): (ppm) 7.9 (d, 2H), 7.56 (t, 1H), 7.38 (t, 2H), 4.58 (t, 2H), 3.60-3.66 (m, 2H), 3.31 (t, 2H), 2.50-2.56 (m, 2H), 1.95 (s, 3H)

Preparation of Aminosilane Functionalized Silica Nanoparticles

A suspension (5 mL) of colloidal silica particles (30 wt% in methyl ethyl ketone) was diluted with 20 mL of tetrahydrofuran and added to a two-necked round bottom flask with 3-aminopropyldimethylethoxysilane (250 μL, 1 mmol) to ensure high coverage

and the mixture was heated at 70 °C overnight under nitrogen protection. The reaction was then cooled to room temperature and precipitated in 500 mL of hexanes. The particles were recovered via centrifugation, supernatant was decanted, and the particles were resuspended in THF. This process was repeated twice to ensure removal of unreacted silanes.

Thermal Initiation/Bulk Polymerization of Styrene via CPDB and Post Polymerization Modification

To a Schlenk tube was added 5 mL (0.044 mol) of styrene and 112 mg (0.0004 mol) of CPDB. The solution was subjected to 3 cycles of freeze-pump-thaw and then backfilled with nitrogen. The flask was heated at 102 °C for 48 hours to ensure high conversion and yield. The resulting polymer was precipitated into methanol, centrifuged, and dissolved in THF. This process was repeated twice more to ensure removal of excess monomer. GPC analysis indicates molecular weight of 10,000 g/mol and PDI of 1.09. Of the resulting polymer, 1g was used for post-polymerization modification of the end-group carboxylic acid.

Thermal Initiation/Bulk Polymerization of Styrene via Activated CPDB

To a Schlenk tube was added 5 mL (0.044 mol) of styrene and 150 mg (0.0004 mol) of activated CPDB. The solution was subjected to 3 cycles of freeze-pump-thaw and then backfilled with nitrogen. The flask was heated at 102 °C for 48 hours to ensure high conversion and yield. The resulting polymer was precipitated into methanol, centrifuged, and dissolved in THF. This process was repeated twice more to ensure removal of excess monomer. GPC analysis indicates molecular weight of 10,000 g/mol and PDI of 1.07. For the long chain populations, the exact procedure as above was

followed with variation of the styrene:activated CPDB ratio.

Grafting-to of Polystyrene on Silica Nanoparticles

To the solution of modified silica nanoparticles was added 1g of polystyrene with modified end-group (from either pre- or post- modification) for a total volume of 30 mL. The reaction was allowed to stir for 48 hrs at room temperature to ensure time for the polymer chain ends to react with the amino groups on the surface of the nanoparticle. This solution remained in THF and was centrifuged at 25,000 rpm for 1 hr. The nanoparticles act as an anchor in a good solvent, forming a pellet of nanoparticles at the bottom of the centrifuge tube while allowing unmodified polystyrene to remain in the supernatant. The supernatant is poured off, the pellet redispersed in THF and the cycle repeated to ensure removal of unattached polymer chains.

One-Pot Grafting-to of Bimodal Brushes on Silica Nanoparticles

To the solution of modified silica nanoparticles was both the short and long chains of polystyrene produced with activated CPDB. The ratios were varied for testing of control of graft density. The reaction was allowed to stir at room temperature for 48 hours. The particles were processed in the same manner as the monomodal samples.

Synthesis of Azo Bis Cyano Anthracene(ABCA)

4,4'-Aziobis(4-cyanovaleric acid) (2g, 7.1mmol) was dissolved into 30ml THF along with (9-anthracenemethanol (3.1g, 15mmol) and N,N'-dicyclohexylcarbodiimide (13g, 15 mmol). The solution was then cooled to 0 °C while stirring under nitrogen. A THF solution of 4-dimethylaminopyridine (0.17g, 1.4 mmol) was added dropwise

over 30 minutes. The solution was allowed to warm to room temperature and stir for 11 hours. The salts were then filtered and the solvent removed under reduced pressure. The resultant yellow solid was then recrystallized in ethanol. The product was recovered as a light yellow solid (4.5g) in 95% yield. Product was confirmed via ^{1}H NMR. (ppm) 8.40 (d, 2H), 8.22 (t, 4H), 7.94 (t, 4H), 7.52-7.38 (m, 8H), 6.06 (d, 4H), 2.39-2.30 (m, 8H), 1.51 (s, 6H).

Labeling of One Population with Modified Anthracene Initiator

A solution of polystyrene produced via activated CPDB in THF was transferred to a round bottom flask and 10-fold molar excess of the modified anthracene initiator was added to the solution. This is allowed to stir under nitrogen protection at 70 °C for 1 hour. The reaction was cooled to room temperature and the modified polystyrene was precipitated in methanol, centrifuged, and supernatant decanted. This was repeated twice more until the supernatant was colorless. After completion, the red/pink color of the Z-group from the CPDB RAFT agent disappeared and a yellowish tint from the anthracene was observed. This is also confirmed via UV-Vis at a wavelength range of 345-400 nm.

Attachment of Anthracene-Modified Polystyrene to Silica Nanoparticles

The attachment of the anthracene-modified polystyrene was conducted in a similar manner as the unmodified polystyrene.

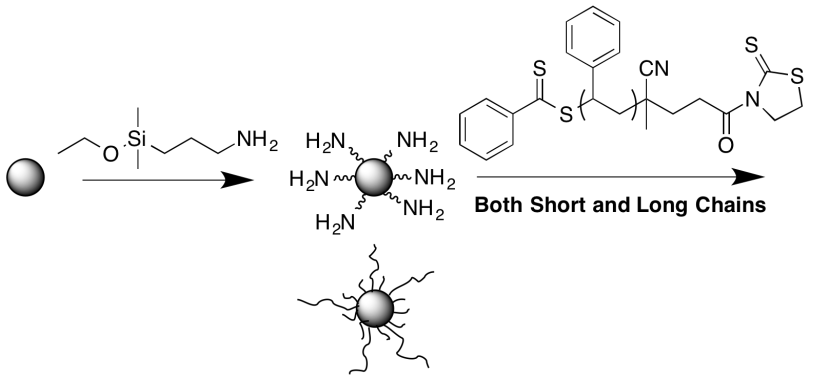

Figure 4.3 One Pot Synthesis of Bimodal Brushes via Grafting-to

4.3 Results and Discussion

To prepare a bimodal brush system, we previously developed a grafting-from approach using sequential RAFT polymerizations.[55] This method allows for the ultimate control over multiple variables such as chain molecular weight, chemistry, polydispersity, and graft density for both chains separately and independently. Yet, this method involves multiple steps including the deactivation of the first chains, attachment of a second population of aminosilane, and attachment of a second population of RAFT agent. Each of these steps also requires a workup process of precipitation, centrifugation, and redispersion. Once again this is necessary for the utmost control, however, there are times when a desired result doesn't require that level of control over the graft density. It was previously reported that unique structures/dispersions of nanoparticles in a composite were formed when lower graft densities are used.[21] We have also observed that even with lower graft density nanoparticles, a bimodal brush on the surface can improve dispersion.[57] Using this knowledge we have investigated the use of a one-pot grafting-to bimodal brush synthesis (Figure 4.3). These changes decrease solvent volume drastically which also allows for easier and more cost-efficient scale-up. Both solvent and monomer waste were also decreased by using a thermally initiated bulk polymerization at high percent conversions. Previous use by our group of a modified RAFT agent had shown that some sensitivity to solvents existed, occa-

sionally decomposing the RAFT agent during the polymerization process. With bulk polymerization this was eliminated.

One of the many benefits of RAFT polymerization is the control of polymer chain end-group chemistry. Because of the mechanism of RAFT, the chemistry of the RAFT agent used is incorporated as the chain ends. Once it was determined that thermal initiation and bulk polymerization were beneficial to the end-goal, it was decided to test two possible methods of activation of the R group: post-polymerization modification of the polymer end group and pre-polymerization modification of the RAFT agent R group (carboxylic acid shown in Figure 4.4). In the post-polymerization modification route, the RAFT agent was used in a thermally initiated bulk polymerization to yield the desired molecular weight of polystyrene. This polymer was then used in a DCC coupling reaction to modify the R group for attachment. Issues can arise with this method including efficiency of the end-group modification, which could become even more difficult with increased molecular weight. In a pre-polymerization modification of the RAFT agent's R group, CPDB was activated with the mercaptothiazoline group and then thermally initiated bulk polymerization was performed. While this method would ensure the desired group for attachment would be at the end of each chain, issues with decomposition of the RAFT agent and the desired control and stability at the required higher temperatures needed for thermal initiation were unknown.

The use of a thermally initiated, bulk polymerization for the production of these two chain-end modified polymers was first tested. As can be seen from Figures 4.5 and 4.6 both thermally initiated, bulk polymerizations are viable and afford polymer chains similar in molecular weight. Also, each polymerization method shows good control over the reaction with low PDIs.

First to test the efficiency of both the end group conversion and the attachment of the polymer chains in a grafting-to approach, polystyrene was made using both the

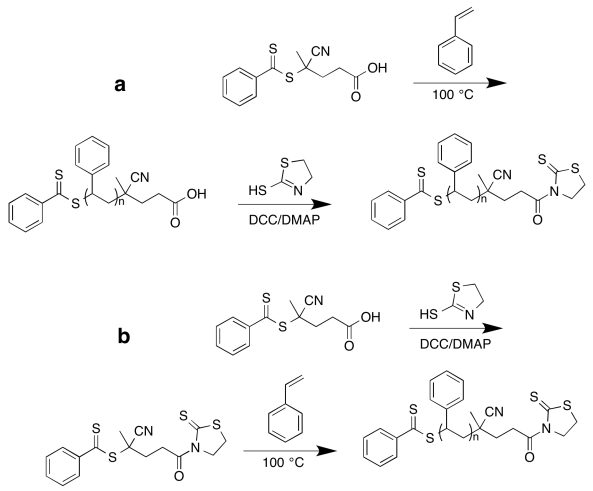

Figure 4.4 Comparison of Post-Polymerization Modification (a) and Pre-Polymerization Modification (b)

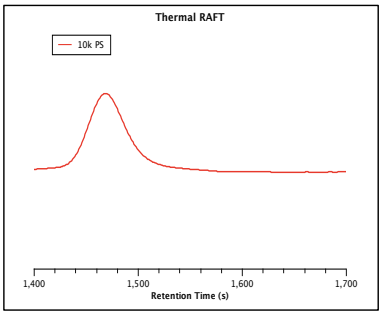

Figure 4.5 GPC of PS Using Thermally Initiated CPDB RAFT Agent (PDI of 1.09)

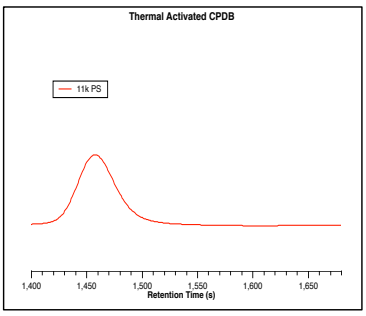

Figure 4.6 GPC of PS Using Thermally Initiated Activated CPDB (PDI of 1.07)

pre- and post-modification methods outlined above with similar molecular weights. Then in two separate reactions the chains were attached to silica nanoparticles modified with an aminosilane. The two reactions were processed as described in the experimental section and then thermogravimetric analysis was performed to determine the amount of polymer attached to the particle surface. As can be seen from the TGA traces (Figures 4.7 and 4.8), the pre-polymerization modification of CPDB afforded the attachment of more polymer chains and hence a higher graft density. This is believed to be due to the inefficiency that comes with the modification of the polymer end group in the post-polymerization modification route.

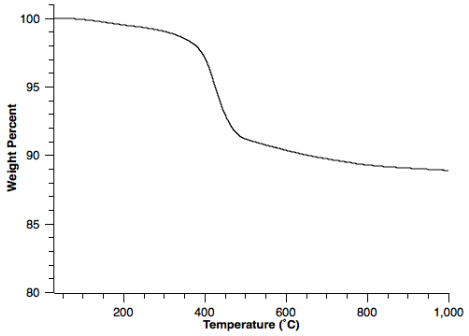

Figure 4.7 TGA of Monomodal Using Post-Polymerization Modification (0.04 chains/nm^2)

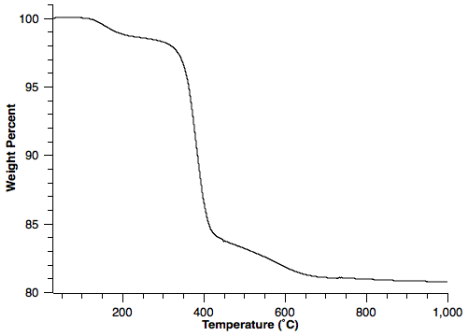

Figure 4.8 TGA of Monomodal Using Pre-Polymerization Modification (0.08 chains/nm^2)

Once the best modification method had been chosen and both long and short polymers made, the next step was to produce a bimodal brush nanoparticle using a one-pot grafting-to method. After the nanoparticles were modified with aminosilane, both short (11k PS) and long (90k PS) chains were allowed to react with the surface in one reaction. Based on our previous bimodal research we have observed that only a few long chain polymers are required for entanglement with the matrix. We have also observed that fewer long chains are actually better, as it allows for increased entanglement and therefore increased thermomechanical properties.[56] For the short chains, however, a higher graft density is needed to screen core-core attractions, which lead to agglomeration of the nanoparticles. To mimic this approach with a one-pot grafting-to method, a larger amount of short chains were used compared to long chains (3:1 ratio of short:long). The reaction was treated exactly as the monomodal samples and treated with HF for GPC analysis.

As seen in Figure 4.9 both chains were able to attach to the surface of the nanoparticle. The silica nanoparticles were easily separated from the free polymer in solution by centrifugation. Although the ability to attach two separate chain populations in a one-pot method for the creation of a bimodal brush had been demonstrated, it created another problem. Now that the brushes are attached in one step, the ability

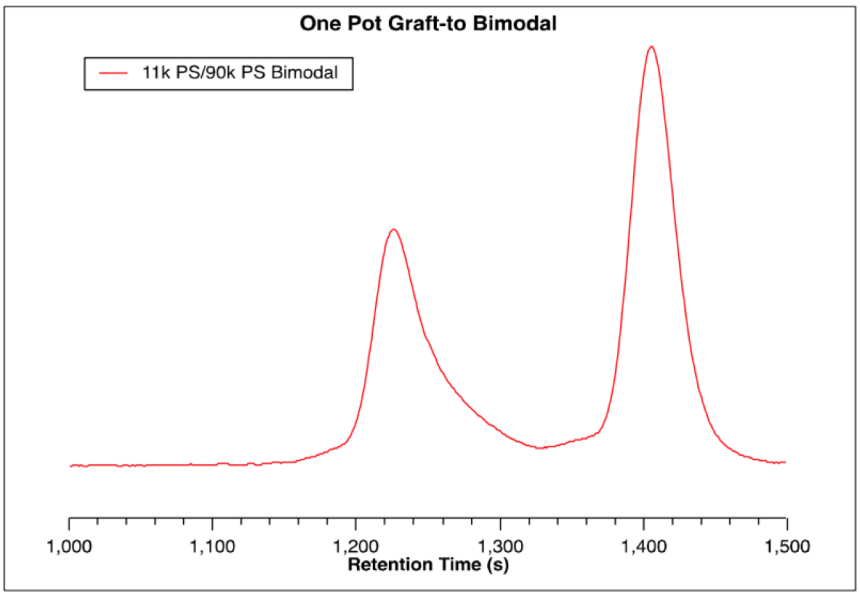

Figure 4.9 GPC of One Pot Modification of Silica NPs

to measure each chain population's graft density separately had been eliminated. In order to solve this problem, it was decided a method of labeling was needed.

As mentioned previously, one of the many benefits of RAFT polymerizations is the control of the end-group of the polymer chain. With the previously described methods of RAFT and polymer chain attachment, control over the R group chemistry was used for the grafting of polymer chains to the surface. The Z group was also previously controlled. Using a radical cross coupling mechanism, the Z group of the polymer chain was exchanged in order to keep the polymer chains from growing in a sequential RAFT polymerization technique.[55] Using this same radical cross coupling technique, the chain ends of one population can be labeled with a UV active moiety allowing for the analysis of each chain population independently (Figure 4.10). Because this new chain end must be UV active and also absorb in the spectrum away from CPDB that is present on the other chain population, it was decided that an anthracene containing initiator would be used. Using similar chemistry as previously described, the carboxylic acid of azobis(cyanovaleric acid) was converted into an anthracene group via DCC coupling (Figure 4.11).

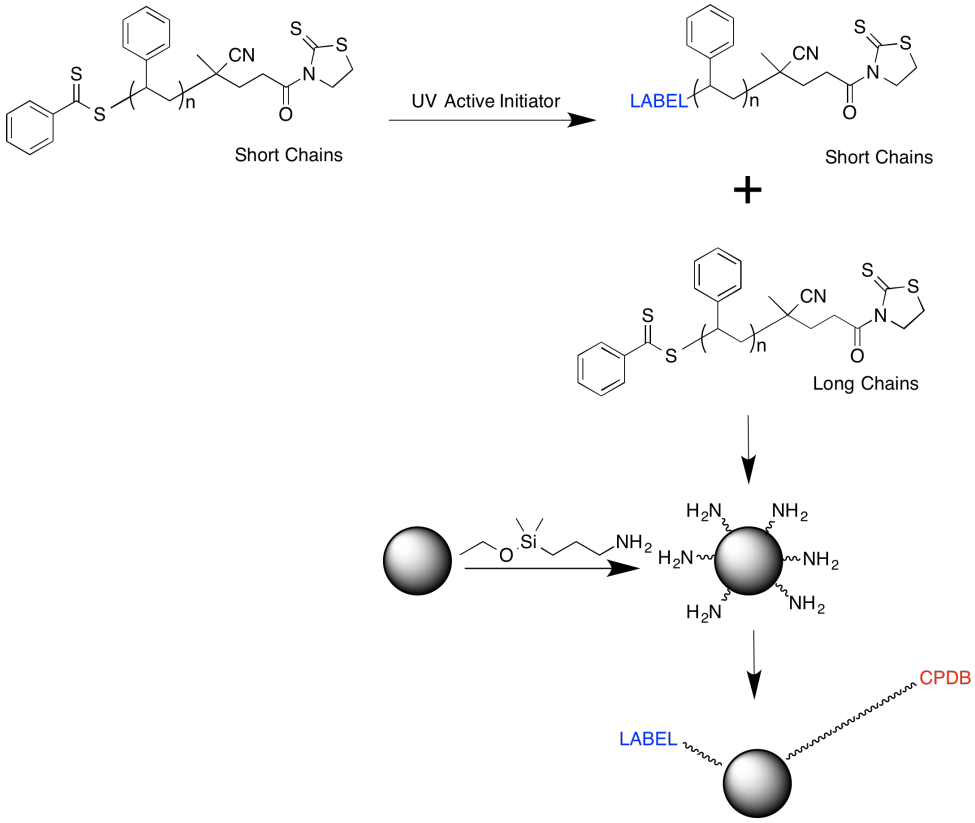

Figure 4.10 Method For Labeling One Population of Chains in a Bimodal Brush

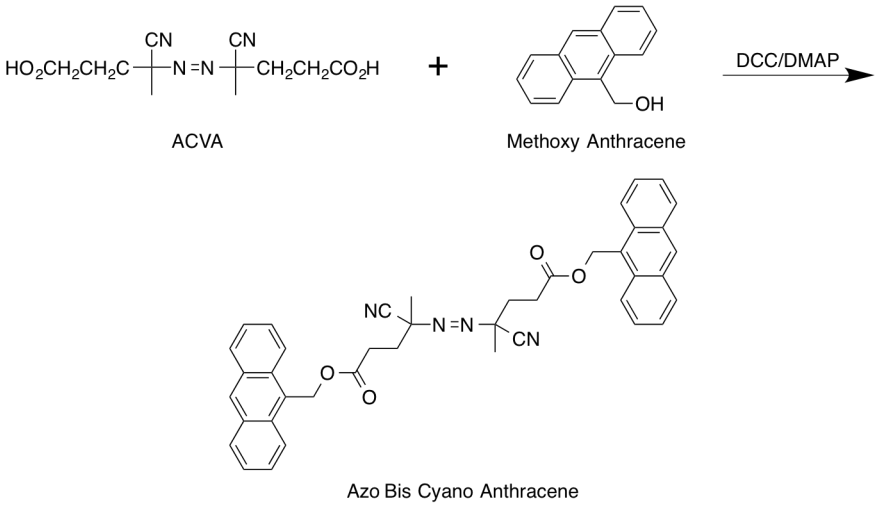

Figure 4.11 Synthesis of Anthracene Containing Initiator via DCC Coupling

After completion of the synthesis of the anthracene containing initiator, it was tested to see whether the chain ends could be completely exchanged and observed, even on a long polymer chain. Using a 10:1 excess of initiator, the end group of a 90k polystyrene polymer was exchanged. As can be seen in Figures 4.12 and 4.13, there is complete exchange of the polymer chain end. The peak at 303 nm that is indicative that the presence of CPDB's Z group is no longer present in Figure 4.13. Also in the range of 320-400 nm is a set of peaks indicative of the presence of anthracene that are not seen in Figure 4.12.

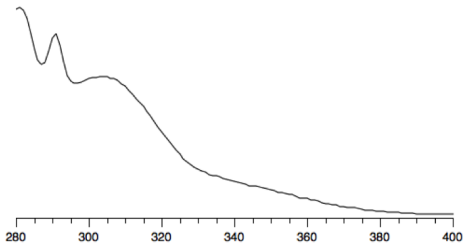

Figure 4.12 UV-Vis of 90k PS containing CPDB Chain End

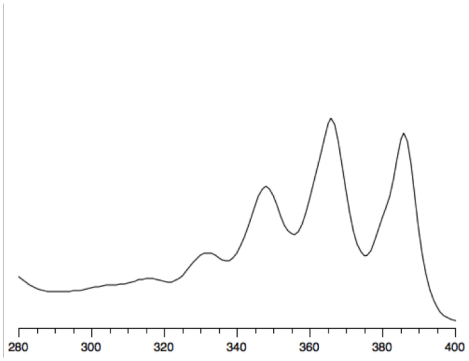

Figure 4.13 UV-Vis of 90k PS containing Anthracene Chain End

In order to test whether the anthracene chain end affects attachment, a bimodal brush was made using a short chain (11k) population of polystyrene whose Z group had been modified with the anthracene initiator and a long chain population (36k) of polystyrene with the Z group of CPDB left intact.

Figure 4.14 shows the UV-Vis spectrum of these bimodal chain grafted nanoparticles. As can be seen, both polymer chains were attached and confirmed via UV-Vis. Also, both chain ends absorb in separate regions of the spectrum allowing for their independent chain density analysis. In order to calculate chain density, a solution of bimodal nanoparticles was made and their absorption compared to calibration curves of free CPDB and anthracene in solution. The concentration of the solution must be corrected for polymer content via TGA in order to obtain accurate chain densities.

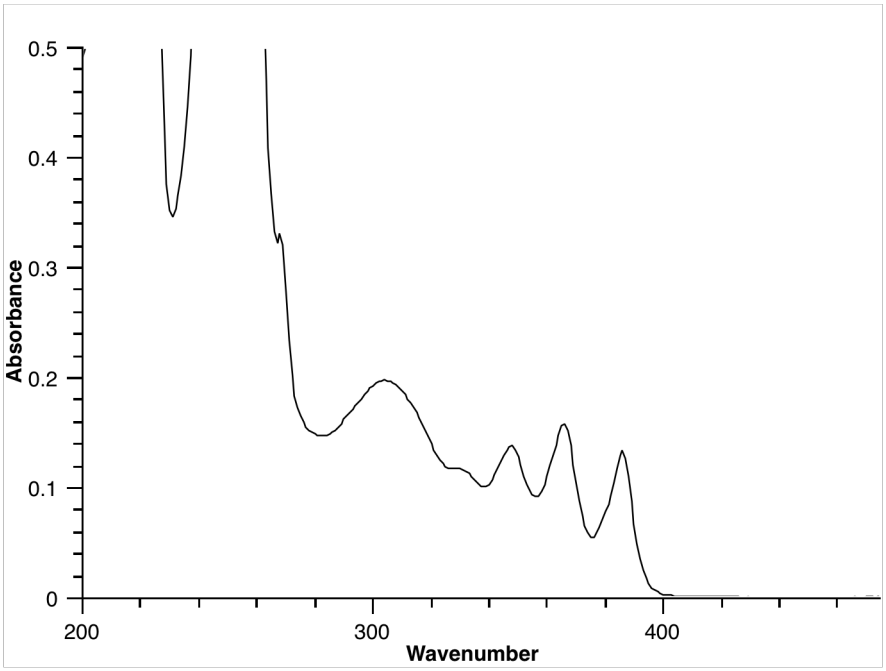

Figure 4.14 UV-Vis of Bimodal Brush With Anthracene-Containing PS Short Chains and 36k CPDB-Containing PS Long Chains

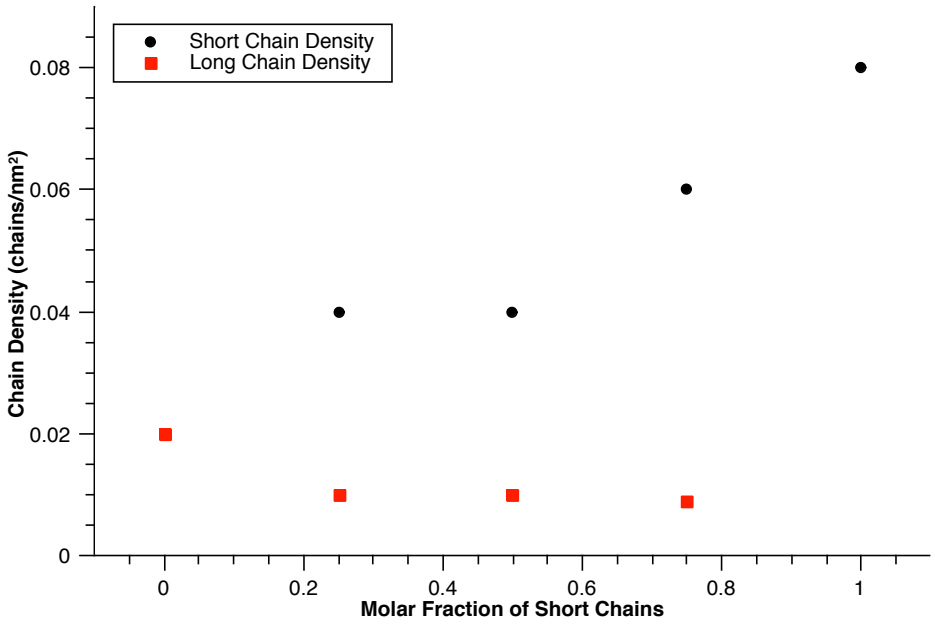

Figure 4.15 Bimodal Chain Densities With Variation in Short and Long Molar Fractions

Finally, a series of bimodal brushes were made via a one-pot grafting-to method. For testing control over graft density, the molar fraction of long (36k) and short (11k) chains was varied. These molecular weights were chosen in order to directly compare with the previously reported work using PDMS on titania. As seen in Figure 4.15, there was little variation in graft density with a variation in molar ratios. The highest graft density for the long chain population was 0.01 chains/nm^2 for the bimodal brushes. However, there was a slight increase seen in the graft density of the short chains by reacting the modified nanoparticles with a higher short:long ratio. This demonstrates that the graft density of the brushes is controlled via diffusion and molecular weight of the diffusing chain. Also, this demonstrates the ability to have similar results in total graft density using a one-pot approach as what was previously reported using a sequential grafting-to technique.

4.4 Summary

In this chapter a new method is described for the synthesis of bimodal brush grafted nanoparticles. By using a one-pot grafting-to approach, a less complicated and more modular synthetic route is available when compared to both sequential grafting-from and grafting-to modifications. Also by creating both short and long chains via thermally initiated bulk polymerizations with high percent conversions, there is a large decrease in wasted solvent and monomer. These characteristics show great opportunity for the industrially scaled production of bimodal brushes. Also described is the comparison of two synthetic techniques for the incorporation of an activated chain end for the attachment of polymer chains with an increase in graft density observed when using a pre-polymerization modification via an activated RAFT agent. Finally, a solution is given for the analysis of each chain population when both are attached in one step. By using a modified anthracene initiator, a single population is labeled before attachment allowing for each population's chain end to absorb in separate re-

gions of the UV-Vis spectrum. This versatile method could be used for introducing a host of other functionalities to polymer chains ends, not only labeling of polymer chains for analysis. These broad new synthetic techniques have the ability to be incorporated into a myriad of applications, especially those where scale-up is desired.

4.5 References

[1] Zhu, Z. Y.; Thompson, T.; Wang, S. Q.; von Meerwall, E. D.; Halasa, A. *Macromolecules* **2005**, *38*, 8816–8824.

[2] Winey, K. I.; Vaia, R. A. *MRS Bulletin* **2007**, *32*, 314–319.

[3] Vaia, R. A.; Maguire, J. F. *Chemistry of Materials* **2007**, *19*, 2736–2751.

[4] Schadler, L. S.; Kumar, S. K.; Benicewicz, B. C.; Lewis, S. L.; Harton, S. E. *MRS Bulletin* **2007**, *32*, 335–340.

[5] Payne, A. R. *Journal of Applied Polymer Science* **1965**, *9*, 2273–&.

[6] Oberdisse, J. *Soft Matter* **2006**, *2*, 29–36.

[7] Moniruzzaman, M.; Winey, K. I. *Macromolecules* **2006**, *39*, 5194–5205.

[8] Lin, Y.; Boker, A.; He, J. B.; Sill, K.; Xiang, H. Q.; Abetz, C.; Li, X. F.; Wang, J.; Emrick, T.; Long, S.; Wang, Q.; Balazs, A.; Russell, T. P. *Nature* **2005**, *434*, 55–59.

[9] LeBaron, P. C.; Wang, Z.; Pinnavaia, T. J. *Applied Clay Science* **1999**, *15*, 11–29.

[10] Krishnamoorti, R.; Vaia, R. A.; Giannelis, E. P. *Chemistry of Materials* **1996**, *8*, 1728–1734.

[11] Krishnamoorti, R. *MRS Bulletin* **2007**, *32*, 341–347.

[12] Kluppel, M. *Kautschuk Gummi Kunststoffe* **1997**, *50*, 282–291.

[13] Gilman, J. W.; Kashiwagi, T.; Lichtenhan, J. D. *SAMPE Journal* **1997**, *33*, 40–46.

[14] Bockstaller, M. R.; Mickiewicz, R. A.; Thomas, E. L. *Advanced Materials* **2005**, *17*, 1331–1349.

[15] Hasegawa, R.; Aoki, Y.; Doi, M. *Macromolecules* **1996**, *29*, 6656–6662.

[16] Zhao, L.; Li, Y. G.; Zhong, C. L. *Journal of Chemical Physics* **2007**, *127*, 154909.

[17] Xu, C.; Ohno, K.; Ladmiral, V.; Composto, R. J. *Polymer* **2008**, *49*, 3568–3577.

[18] Meli, L.; Arceo, A.; Green, P. F. *Soft Matter* **2009**, *5*, 533–537.

[19] Iacovella, C. R.; Horsch, M. A.; Glotzer, S. C. *Journal of Chemical Physics* **2008**, *129*, 044902.

[20] Harton, S. E.; Kumar, S. K. *Journal of Polymer Science Part B-Polymer Physics* **2008**, *46*, 351–358.

[21] Akcora, P.; Liu, H.; Kumar, S. K.; Moll, J.; Li, Y.; Benicewicz, B. C.; Schadler, L. S.; Acehan, D.; Panagiotopoulos, A. Z.; Pryamitsyn, V.; Ganesan, V.; Ilavsky, J.; Thiyagarajan, P.; Colby, R. H.; Douglas, J. F. *Nature Materials* **2009**, *8*, 354–U121.

[22] Putnam, S. A.; Cahill, D. G.; Ash, B. J.; Schadler, L. S. *Journal of Applied Physics* **2003**, *94*, 6785–6788.

[23] Nie, Z. H.; Fava, D.; Rubinstein, M.; Kumacheva, E. *Journal of the American Chemical Society* **2008**, *130*, 3683–3689.

[24] Nie, Z. H.; Fava, D.; Kumacheva, E.; Zou, S.; Walker, G. C.; Rubinstein, M. *Nature Materials* **2007**, *6*, 609–614.

[25] Nie, Z. H.; Petukhova, A.; Kumacheva, E. *Nature Nanotechnology* **2010**, *5*, 15–25.

[26] Merkel, T. C.; Freeman, B. D.; Spontak, R. J.; He, Z.; Pinnau, I.; Meakin, P.; Hill, A. J. *Science* **2002**, *296*, 519–522.

[27] Moll, J. F.; Akcora, P.; Rungta, A.; Gong, S. S.; Colby, R. H.; Benicewicz, B. C.; Kumar, S. K. *Macromolecules* **2011**, *44*, 7473–7477.

[28] Maillard, D.; Kumar, S. K.; Rungta, A.; Benicewicz, B. C.; Prud'homme, R. E. *Nano Letters* **2011**, *11*, 4569–4573.

[29] Liu, K.; Nie, Z. H.; Zhao, N. N.; Li, W.; Rubinstein, M.; Kumacheva, E. *Science* **2010**, *329*, 197–200.

[30] Lin, Y. L.; Chiou, C. S.; Kumar, S. K.; Lin, J. J.; Sheng, Y. J.; Tsao, H. K. *Journal of Physical Chemistry C* **2011**, *115*, 5566–5577.

[31] Fava, D.; Nie, Z.; Winnik, M. A.; Kumacheva, E. *Advanced Materials* **2008**, *20*, 4318–4322.

[32] Akcora, P.; Kumar, S. K.; Sakai, V. G.; Li, Y.; Benicewicz, B. C.; Schadler, L. S. *Macromolecules* **2010**, *43*, 8275–8281.

[33] Akcora, P.; Kumar, S. K.; Moll, J.; Lewis, S.; Schadler, L. S.; Li, Y.; Benicewicz, B. C.; Sandy, A.; Narayanan, S.; Illavsky, J.; Thiyagarajan, P.; Colby, R. H.; Douglas, J. F. *Macromolecules* **2010**, *43*, 1003–1010.

[34] Ligoure, C.; Leibler, L. *Journal De Physique* **1990**, *51*, 1313–1328.

[35] Li, C. Z.; Benicewicz, B. C. *Macromolecules* **2005**, *38*, 5929–5936.

[36] Li, C.; Han, J.; Ryu, C. Y.; Benicewicz, B. C. *Macromolecules* **2006**, *39*, 3175–3183.

[37] Wang, L.; Benicewicz, B. C. *ACS Macro Letters* **2013**, *2*, 173–176.

[38] Akcora, P.; Harton, S. E.; Kumar, S. K.; Sakai, V. G.; Li, Y.; Benicewicz, B. C.; Schadler, L. S. *Macromolecules* **2011**, *44*, 416–416.

[39] Jayaraman, A. *Journal of Polymer Science Part B: Polymer Physics* **2013**, *51*, 524–534.

[40] Gao, J.; Li, J.; Benicewicz, B. C.; Zhao, S.; Hillborg, H.; Schadler, L. S. *Polymers* **2012**, *4*, 187–210.

[41] Gao, J.; Li, J.; Zhao, S.; Benicewicz, B. C.; Hillborg, H.; Schadler, L. S. *Polymer* **2013**, *54*, 3961–3973.

[42] Skvortsov, A. M.; Gorbunov, A. A.; Leermakers, F. A. M.; Fleer, G. J. *Macromolecules* **1999**, *32*, 2004–2015.

[43] Martin, T. B.; Jayaraman, A. *Soft Matter* **2013**,

[44] Houbenov, N.; Minko, S.; Stamm, M. *Macromolecules* **2003**, *36*, 5897–5901.

[45] Ionov, L.; Houbenov, N.; Sidorenko, A.; Stamm, M.; Luzinov, I.; Minko, S. *Langmuir* **2004**, *20*, 9916–9919.

[46] Draper, J.; Luzinov, I.; Minko, S.; Tokarev, I.; Stamm, M. *Langmuir* **2004**, *20*, 4064–4075.

[47] Kumar Vyas, M.; Schneider, K.; Nandan, B.; Stamm, M. *Soft Matter* **2008**, *4*, 1024–1032.

[48] Zhao, B.; He, T. *Macromolecules* **2003**, *36*, 8599–8602.

[49] Jiang, X.; Zhong, G.; Horton, J. M.; Jin, N.; Zhu, L.; Zhao, B. *Macromolecules* **2010**, *43*, 5387–5395.

[50] Jiang, X.; Zhao, B.; Zhong, G.; Jin, N.; Horton, J. M.; Zhu, L.; Hafner, R. S.; Lodge, T. P. *Macromolecules* **2010**, *43*, 8209–8217.

[51] Bao, C.; Tang, S.; Horton, J. M.; Jiang, X.; Tang, P.; Qiu, F.; Zhu, L.; Zhao, B. *Macromolecules* **2012**, *45*, 8027–8036.

[52] Pryamtisyn, V.; Ganesan, V.; Panagiotopoulos, A. Z.; Liu, H. J.; Kumar, S. K. *Journal of Chemical Physics* **2009**, *131*, 221102.

[53] Edgecombe, S. R.; Gardiner, J. M.; Matsen, M. W. *Macromolecules* **2002**, *35*, 6475–6477.

[54] Jayaraman, A.; Nair, N. *Molecular Simulation* **2012**, *38*, 751–761.

[55] Rungta, A.; Natarajan, B.; Neely, T.; Dukes, D.; Schadler, L. S.; Benicewicz, B. C. *Macromolecules* **2012**, *45*, 9303–9311.

[56] Natarajan, B.; Neely, T.; Rungta, A.; Benicewicz, B. C.; Schadler, L. S. *Macromolecules* **2013**, *46*, 4909–4918.

[57] Li, Y.; Tao, P.; Viswanath, A.; Benicewicz, B. C.; Schadler, L. S. *Langmuir* **2013**, *29*, 1211–1220.

Chapter 5

Modification of Silica Nanoparticles via Cyclic Azasilanes: From Hours to Minutes

5.1 Introduction

Nano-sized inorganic oxides offer enhanced electrical, optical, and thermomechanical properties[1–14] when compared to conventional composite systems.[3] However, the high surface energy differences between nanoparticles and polymers[15,16] leads to nanoparticle agglomeration/phase separation.[17] The dispersion state of nanoparticles into a polymer matrix determines the amount of interface present and can be a major challenge due to the aforementioned incompatabilities. A common approach to overcome the agglomeration of nanoparticles is the grafting of polymer chains to the surface.[18] Among those techniques, reversible addition-fragmentation chain transfer (RAFT) polymerization has acquired attention as a facile method for the controlled polymerization of a wide range of monomers.[19]

Silica substrates, such as nanoparticles, silica gel, glass, and quartz, have been widely used to surface graft polymer chains. A general strategy to functionalize the silica substrates is using an organosilane to incorporate functional groups on nanoparticles using amine, carboxylic acid, and halogen functional groups. Further post-functionalization can introduce initiator or chain transfer agents (CTAs) to mediate surface-initiated controlled radical polymerizations. In this method, a condensation reaction between silanol groups (Si-OH) on silica surfaces and alkoxysilane or halogensilane molecules occurs resulting in the formation of Si-O-Si bonds.[20–24] A series

of mono- and tri-functional silanes have been widely employed, such as R-SiMe_2OMe, R-SiMe_2OEt, R-Si$(OMe)_3$, and R-Si$(OEt)_3$. The use of halogenated silanes for the modification of silica comes with the possibility of degrading the surface due to the release of strong acids as a byproduct of the reaction. Trifunctional organosilanes have been reported to polymerize with unreacted functional silane moieties in water, restricting the formation of a monolayer of surface functionlized groups and therefore potentially decreasing available graft density.[22] Other attachment methods have been employed towards increasing graft density. During a condensation reaction with an alkoxysilane, the alcohol byproduct could also condense onto the surface effectively decreasing the available graft density. Brittain et al. employed the use of an allyl silane whose byproduct would be volatile enough to escape the reaction flask without attaching to the surface.[25] Even though an increase in graft density was observed in some substrates, it was not observed in colloidal silica. As a different approach, silane-containing initiators or chain transfer agents have been employed to directly modify silica surfaces. Benicewicz et al. developed a silane-containing RAFT agent by multi-step synthesis to react with silanol groups on the surface of silica nanoparticles.[23] However, this silane-containing RAFT agent suffered from issues of low yield due to the silane's affinity for silica gel during column chromatography purification. Although modification of the silica surface was ultimately achieved via this method, the multistep synthesis and low yield was overcome by the use of a commercial available aminosilane and an activated RAFT agent.[24] This method allowed for the variation of the graft density by varying the feed ratio of aminosilane achieving graft densities from 0.05 to 0.7 chains/nm^2. The control over the graft density has proven to be of utmost importance in controlling the nanoparticle dispersion state and ultimately the thermomechanical properties of the composite.[20,26,27] This method was versatile enough to warrant its ubiquitous use for modification of silica nanoparticles via RAFT for monomodal,[20] block,[28] and bimodal[29] brush systems. While

this method has allowed for the synthesis and research of these systems, the modification time has yet to be improved. In order to guarantee high conversion of free hydroxyl surface groups to their silane reacted counterpart, reaction times up to 18 hours at high temperatures are required. In order to counteract these hurdles, herein is reported the use of a cyclic azasilane for the modification of silica nanoparticles. Cyclic azasilanes react with hydroxyl groups via a ring-opening reaction that is thermodynamically driven, without the formation of volatile byproducts. Because of this thermodynamic ring opening, the modification of these nanoparticles is completed at room temperature in less than 5 minutes compared to overnight reactions of acyclic organosilanes. The modification and therefore graft density can be varied via the feed ratio of silane in the exact manner as previously reported, allowing for attachment of an activated RAFT agent and the polymerization of both methyl methacrylate and styrene monomers while still maintaining control over the polymerization.

5.2 Experimental

Materials

Dicyclohexycarbodiimide (99%), (dimethylamino)-pyridine (99%), and 2-mercaptothiazoline (98%) were purchased from Acros. 2,2'-Azobis(isobutyronitrile) (AIBN) was used after recrystallization in methanol. 2,2-Dimethoxy-1,6-diaza-2-silacyclooctane was purchased form Gelest. 4-Cyanopentanoic acid dithiobenzoate (CPDB) was purchased from Strem. Styrene (99%, Acros) and methyl methacrylate (99%, Acros) were passed through basic alumina column to remove inhibitor before use. Colloidal silica nanoparticles (15 nm diamter) of 30 wt % dispersed in methyl ethyl ketone were provided by Nissan Chemical. Unless otherwise specified, all chemicals were used as received.

Instrumentation

Molecular weights and molecular weight distributions were determined by using a Polymer Laboratories PL-GPC 120 with refractive index detector; 3 PLgel 10 μm MIXED B columns in sequence with molecular weight range of 500 to 10,000,000 g/mol, THF as eluent at 30 °C and a flow rate of 1.0 mL/min. The GPC system was calibrated with both polystyrene and poly(methyl) methacrylate standards obtained from Polymer Laboratories. Thermogravimetric analysis was performed on a TA Instruments TGA-5000.

Activation of CPDB

CPDB (1.40 g, 5.00 mmol), 2-mercaptothiazoline (0.596 g, 5.00 mmol), and dicyclohexycarbodiimide (DCC) (1.24 g, 6.00 mmol) were dissolved in 30 mL of dichloromethane. (Dimethylamino)pyridine (DMAP) (61 mg, 0.50 mmol) was dissolved in 5 mL of dichloromethane and added dropwise to the solution. The reaction was allowed to stir overnight at room temperature. The solution was gravity filtered to remove the resulting salt. After removal of solvent via rotary evaporation, the crude red oil was purified via silica column chromatography (5:4 mixture of hexanes:ethyl acetate). The activated CPDB was obtained after remove of solvent as a red oil (1.41g, 74.5% yield). ^{1}H NMR (300 Mhz, $CDCl_3$): (ppm) 7.9 (d, 2H), 7.56 (t, 1H), 7.38 (t, 2H), 4.58 (t, 2H), 3.60-3.66 (m, 2H), 3.31 (t, 2H), 2.50-2.56 (m, 2H), 1.95 (s, 3H)

Preparation of Cyclic Azasilane Functionalized Silica Nanoparticles

A suspension of 30 wt % colloidal silica nanoparticles in methyl ethyl ketone was added to a round-bottom flask and diluted with an equal volume of tetrahydrofuran. This solution was placed under nitrogen and the cyclic azasilane added. The reac-

tion was allowed to stir for 5 minutes to ensure completion. The solution was used immediately afterwards for the attachment of RAFT agent.

Preparation of CPDB Anchored Silica Nanoparticles

To the solution of cyclic azasilane modified nanoparticles, excess activated CPDB was added (silane:RAFT ratio equal to 1:1.1). This solution was allowed to react overnight at room temperature to ensure the completion. This solution was then precipitated into hexanes, centrifuged, and then the supernatant decanted. This was repeated until the supernatant was free of unreacted RAFT agent.

Polymerization of Styrene from Cyclic Azasilane Modified, CPDB Anchored Silica Nanoparticles

To a Schlenk tube was added CPDB anchored silica nanoparticles (0.25 g of silica at a graft density of 0.31 chains/nm^2), styrene (5 mL), tetrahydrofuran (5 mL), and AIBN (180 μL of a 10 mM solution in THF). Once the nanoparticles were dispersed via stirring, the Schlenk tube was subjected to 3 cycles of freeze, pump, thaw and then backfilled with nitrogen. The reaction was allowed to stir at 65 °C for 14 hours. The polymerization was stopped by quenching the tubes in ice water and the polymerization mixture was precipitated in hexanes. The particles were recovered via centrifugation and the supernatant discarded.

Polymerization of Methyl Methacrylate from Cyclic Azasilane Modified, CPDB Anchored Silica Nanoparticles

To a Schlenk tube was added CPDB anchored silica nonoparticles (0.25 g of silica at a graft density of 0.16 chains/nm^2), methyl methacrylate (2.5 mL), tetrahydrofuran (2.5 mL), and AIBN (90 μL of a 10 mM solution in THF). Once the nanoparticles

were dispersed by stirring, the Schlenk tube was subjected to 3 cycles of freeze, pump, thaw and then backfilled with nitrogen. The reaction was allowed to stir at 60 °C for 6 hours. The polymerzation was stopped by quenching the tubes in ice water and the polymerization mixture was precipitated into hexanes. The particles were recovered via centrifugation and the supernatant discarded.

General Procedure for Measurement of Graft Density via UV-Vis

After precipitation into hexanes and centrifugation, the supernatant was decanted and particles were left to dry under vacuum. A solution of 50 mg of nanoparticles in THF for a total volume of 100 mL was prepared in a 100 mL volumetric flask. After a background scan of pure THF, the solution was used for UV-Vis analysis. The absorbance at 303 nm corresponding to the attached RAFT agent is compared to a standard absorption curve made from known amounts of free CDPB in THF to determine the concentration of RAFT agent attached to the nanoparticles.

General Procedure for Cleaving Grafted Polymer from Particles

In a typical experiment, 50 mg of PMMA or PSt grafted silica particles were dissolved in 3 mL of THF. Aqueous HF (49 %, 0.2 mL) was added and the solution was allowed to stir at room temperature overnight. The solution was poured into a PTFE Petri dish and allowed to stand in a fume hod to evaporate the volatile components. The recovered PMMA or PSt was then subjected to GPC analysis.

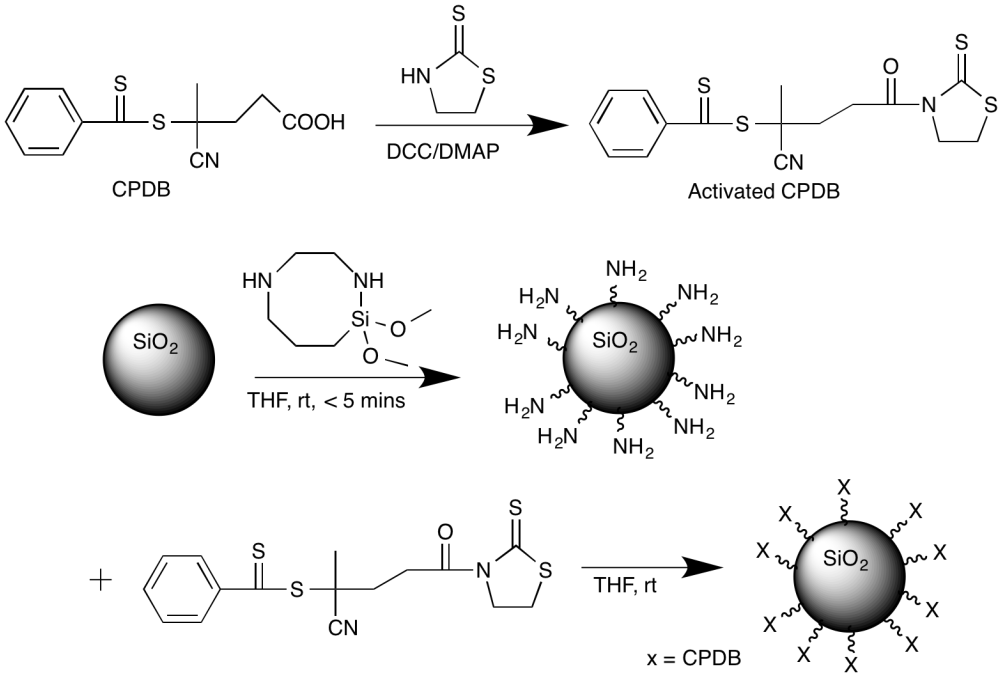

Figure 5.1 Synthesis and Attachment of Activated CPDB to Cyclic Azasilane Modified Silica Nanoparticles

5.3 Results and Discussion

In a previous publication, Benicewicz et al. reported the first preparation of a RAFT-silane agent and its use to prepare RAFT agent anchored silica nanoparticles.[23] The RAFT containing silane was prepared via a multistep synthetic route involving the use of column chromatography on intermediates containing methoxysilane groups. This led to an overall low yield due to the instability of the methoxysilane group and its affinity towards silica gel during purification via column chromatography. As an alternative, the Benicewicz group has previously separated the role of surface modification and RAFT agent attachment by using a commercially available aminosilane followed by reaction with an activated RAFT agent.[24] This method has allowed for the variation of graft densities from 0.05 to 0.7 chains/nm^2 for various polymer brush architectures including monomodal brushes, block copolymer brushes, and bimodal brushes on the surface of silica nanoparticles with control over parameters of the

polymer brush (molecular weight, polydispersity, etc.) that is inherent with RAFT polymerization. The graft density is a key parameter in determining nanoparticle dispersion in a polymer nanocomposite. With control over graft density and brush chain length, various nanoparticle dispersion states/nanocomposite morphologies can be achieved and controlled. Coupled to this improvement in dispersion is also an improvement in thermomechanical properties as has been shown in previous chapters using bimodal brushes created via this very same technique. However, the modification step using an acyclic aminosilane can take multiple hours for completion of the condensation reaction. In this work an alternative method is explored using the thermodynamically driven ring-opening reaction of a cyclic azasilane for the modification of silica surfaces. This reaction is conducted by simply stirring the cyclic azasilane with silica nanoparticles at room temperature in a suitable solvent and is completed in less than 5 minutes due to the thermodynamically driven ring opening reaction on the surface. (Figure 5.1)

Attachment of RAFT and Variation of Graft Density

Following the attachment of the cyclic azasilane is the addition of excess RAFT agent to ensure the conversion of the primary amino group produced from the ring opening to the desired RAFT agent. An advantage of this technique when compared to other grafting methods is the ease and accuracy in measuring the graft density prior to polymerization. The UV absorption at 303 nm of the $Si0_2$-*g*-CPDB nanoparticles is compared to a standard absorption curve made from known amounts of free CPDB to determine the concentration of RAFT agents attached onto the nanoparticles before polymerization. (Figure 5.2)

This concentration is then used to calculate a graft density using the surface area and density of the nanoparticle. Varying the feed ratio of cyclic azasilane to nanoparticles controls the final concentration of RAFT agent (Table 5.1). Previous

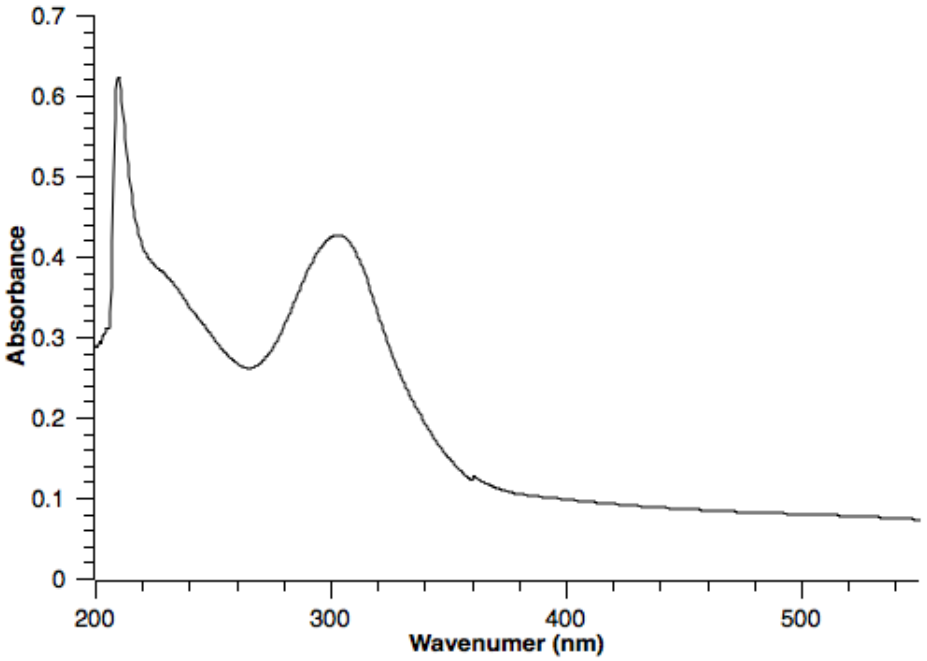

Figure 5.2 UV-Vis absorption spectrum of SiO_2-*g*-CPDB nanoparticles in THF

research has shown that polymer brushes of low graft density create interesting and controllable structures in nanocomposites and also that appropriate screening of agglomeration with 15 nm silica nanoparticles is achieved with only intermediate graft densities (approximately 0.20 chains/nm^2).

Table 5.1 Variation of Feed Ratio of Cyclic Azasilane and Control Over Graft Density

SiNPs (mL)	Cyclic Azasilane(mg)	Activated CPDB (mg)	Absorbance	RAFT Density (μmol/g silica)	Graft Density (c/nm^2)
2.5	12.5	25	0.1712	21.38	0.09
2.5	25	75	0.3319	40.87	0.16
2.5	32.5	100	0.4426	54.23	0.23
2.5	40	125	0.6293	76.95	0.32
2.5	50	150	0.8254	100.74	0.43

RAFT Polymerization of Styrene and Methyl Methacrylate

Following the attachment of the CPDB chain transfer agent on the surface of SiO_2-*g*-CPDB nanoparticles, the surface-initiated RAFT polymerization of both styrene and

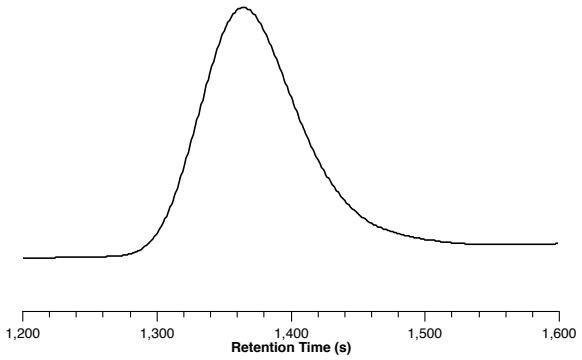

Figure 5.3 GPC trace of 18k PMMA from SI-RAFT via cyclic azasilane

methyl methacrylate was conducted to create polymer brushes of various lengths and graft densities. (Table 5.2) This ensures that not only can cyclic azasilanes modify silica nanoparticles in a fraction of the time of linear silanes, but also that the immobilized RAFT agent on the surface is still viable for polymerization. A representative GPC can be seen in Figure 5.3 for the polymerization of MMA mediated by a surface attached RAFT agent. As can be seen from 5.2, at each graft density a variety of molecular weights were achieved while still maintaning control over the polymerization as evidenced by the excellent agreement between measured and theoretical molecular weights and the narrow polydispersities of the polymers.

Table 5.2 Various Polymer Brushes Grafted From Silica Nanoparticles

Graft Density (c/nm^2)	**Monomer**	**Mn (Theor)**	**Mn (Actual)**	**PDI**
0.06	Styrene	3470	3280	1.13
0.06	Styrene	9900	10200	1.09
0.06	Styrene	57,450	58,900	1.10
0.20	MMA	4540	5000	1.14
0.20	MMA	18,100	17,400	1.11
0.20	MMA	77,500	75,000	1.13
0.42	Styrene	1600	1560	1.15
0.42	Styrene	34800	33700	1.15
0.42	Styrene	65000	65900	1.16

5.4 Summary

In this work, it was demonstrated that the attachment of a cyclic azasilane to the surface of silica nanoparticles is a viable alternative to the use of acyclic silane agents for the production of polymer brushes. This attachment is thermodynamically driven via a ring-opening reaction allowing for the completion of the modification of the surface in less than 5 minutes. The amino groups produced by the ring opening can then be used to immobilize a well-known and studied RAFT agent that has previously been used to make polymer brushes of various densities and architectures for the incorporation into polymer nanocomposites. The graft density can be controlled and varied via the feed ratio of cyclic azasilane just as previously done with acyclic aminosilanes. This graft density is measured via UV-Vis after RAFT agent attachment and compared to an absorption curve of known free RAFT agent in solution. After attachment to the surface, the RAFT agent was then used for surface initiated polymerization of both styrene and methyl methacrylate at various graft densities. At all graft densities, control over the polymerization was observed. This new attachment method allows for the creation of polymer brushes in a fraction of the time of previous methods while still maintaining control over the graft density and molecular weight which has been proven to be of utmost importance in polymer nanocomposites.

5.5 References

[1] Zhu, Z. Y.; Thompson, T.; Wang, S. Q.; von Meerwall, E. D.; Halasa, A. *Macromolecules* **2005**, *38*, 8816–8824.

[2] Winey, K. I.; Vaia, R. A. *MRS Bulletin* **2007**, *32*, 314–319.

[3] Vaia, R. A.; Maguire, J. F. *Chemistry of Materials* **2007**, *19*, 2736–2751.

[4] Schadler, L. S.; Kumar, S. K.; Benicewicz, B. C.; Lewis, S. L.; Harton, S. E. *MRS Bulletin* **2007**, *32*, 335–340.

[5] Payne, A. R. *Journal of Applied Polymer Science* **1965**, *9*, 2273–&.

[6] Oberdisse, J. *Soft Matter* **2006**, *2*, 29–36.

[7] Moniruzzaman, M.; Winey, K. I. *Macromolecules* **2006**, *39*, 5194–5205.

[8] Lin, Y.; Boker, A.; He, J. B.; Sill, K.; Xiang, H. Q.; Abetz, C.; Li, X. F.; Wang, J.; Emrick, T.; Long, S.; Wang, Q.; Balazs, A.; Russell, T. P. *Nature* **2005**, *434*, 55–59.

[9] LeBaron, P. C.; Wang, Z.; Pinnavaia, T. J. *Applied Clay Science* **1999**, *15*, 11–29.

[10] Krishnamoorti, R.; Vaia, R. A.; Giannelis, E. P. *Chemistry of Materials* **1996**, *8*, 1728–1734.

[11] Krishnamoorti, R. *MRS Bulletin* **2007**, *32*, 341–347.

[12] Kluppel, M. *Kautschuk Gummi Kunststoffe* **1997**, *50*, 282–291.

[13] Gilman, J. W.; Kashiwagi, T.; Lichtenhan, J. D. *SAMPE Journal* **1997**, *33*, 40–46.

[14] Bockstaller, M. R.; Mickiewicz, R. A.; Thomas, E. L. *Advanced Materials* **2005**, *17*, 1331–1349.

[15] Beecroft, L. L.; Ober, C. K. *Chemistry of Materials* **1997**, *9*, 1302–1317.

[16] Caseri, W. *Macromolecular Rapid Communications* **2000**, *21*, 705–722.

[17] Schaefer, D. W.; Justice, R. S. *Macromolecules* **2007**, *40*, 8501–8517.

[18] Barbey, R.; Lavanant, L.; Paripovic, D.; Schüwer, N.; Sugnaux, C.; Tugulu, S.; Klok, H.-A. *Chemical Reviews* **2009**, *109*, 5437–5527.

[19] Li, Y.; Schadler, L.; Benicewicz, B. In *Handbook of RAFT Polymerization*; Barner-Kowollik, C., Ed.; Wiley-VCH: Weinheim: Germany, 2008; pp 423–453.

[20] Akcora, P.; Liu, H.; Kumar, S. K.; Moll, J.; Li, Y.; Benicewicz, B. C.; Schadler, L. S.; Acehan, D.; Panagiotopoulos, A. Z.; Pryamitsyn, V.; Ganesan, V.; Ilavsky, J.; Thiyagarajan, P.; Colby, R. H.; Douglas, J. F. *Nature Materials* **2009**, *8*, 354–U121.

[21] Cash, B. M.; Wang, L.; Benicewicz, B. C. *Journal of Polymer Science Part A: Polymer Chemistry* **2012**, *50*, 2533–2540.

[22] Fadeev, A. Y.; McCarthy, T. J. *Langmuir* **2000**, *16*, 7268–7274.

[23] Li, C. Z.; Benicewicz, B. C. *Macromolecules* **2005**, *38*, 5929–5936.

[24] Li, C.; Han, J.; Ryu, C. Y.; Benicewicz, B. C. *Macromolecules* **2006**, *39*, 3175–3183.

[25] Wang, Y.; Hu, S.; Brittain, W. J. *Macromolecules* **2006**, *39*, 5675–5678.

[26] Kumar, S. K.; Jouault, N.; Benicewicz, B.; Neely, T. *Macromolecules* **2013**, *46*, 3199–3214.

[27] Natarajan, B.; Neely, T.; Rungta, A.; Benicewicz, B. C.; Schadler, L. S. *Macromolecules* **2013**, *46*, 4909–4918.

[28] Gao, J.; Li, J.; Zhao, S.; Benicewicz, B. C.; Hillborg, H.; Schadler, L. S. *Polymer* **2013**, *54*, 3961–3973.

[29] Rungta, A.; Natarajan, B.; Neely, T.; Dukes, D.; Schadler, L. S.; Benicewicz, B. C. *Macromolecules* **2012**, *45*, 9303–9311.

Summary and Conclusions

The modification of silica surfaces for controlling and designing interfaces was investigated via the development of new synthetic techniques for grafting polymer chains on surfaces. The use of inorganic oxides as fillers in nanocomposites is widely used, however, the surface of the filler and therefore interface between the filler and matrix is of the utmost importance for the end property enhancement of the nanocomposite. The grafting of polymer brushes is a well-known technique for the compatibalization of nanoparticles and matrix. However, variation of polymer brush parameters such as graft density and molecular weight have a drastic effect on the nanoparticle dispersion, entanglement, and thermomechanical properties. In order to allow for complete control over nanoparticle dispersion, grafted brush entanglement, brush graft density, brush molecular weight, etc. a sequential, surface-initiated RAFT polymerization technique was used for the creation of bimodal brushes on the surface of nanoparticles. An aminosilane was used for the attachment of an activated RAFT agent. The graft density was controlled via the feed ratio of aminosilane. A short, dense brush was created for the screening of core-core attraction between nanoparticles allowing for increased dispersion. In order to prevent the short brush from growing further, a radical cross coupling mechanism with excess AIBN was performed exchanging the Z group of the RAFT agent from the polymer chain end in effect "killing" the RAFT agent. In the subsequent step, a second population of aminosilane and RAFT agent was attached at a lower graft density and then a second population of a long, sparse brush was created to allow for entanglement with the matrix. A kinetic study was performed to show that the controlled RAFT polymerization of the second popula-

tion wasn't impeded by the presence of a short brush on the same surface. Using this method, various polystyrene bimodal brushes were created and incorporated into polystyrene matrices for the testing of dispersion, entanglement, and resulting thermomechanical properties. The long brush graft density was varied in order to determine the preferred graft density for entanglement of the long brush with the chains of the matrix. TEM micrographs showed that bimodal brushes allowed for the dispersion in and entanglement with matrix chains of higher molecular weight than the grafted brush. In a monomodal brush system, this has classically caused dewetting of the grafted brush from the matrix. The testing of the thermomechanical properties showed that bimodal brushes resulted in an increase in both modulus and T_g over monomodal brushes. Also, a lower graft density of long chains was preferred for increased entanglement and therefore T_g.

Using the knowledge gained from the initial synthesis and testing of bimodal brushes, mixed bimodal brushes were created using the same sequential surface-initated RAFT polymerization technique. Poly(methyl) methacrylate short, dense brushes with long, sparse brushes of polystyrene were created as well as the inverse of PS short, PMMA long brushes. These mixed bimodal brush samples were mixed with both PS and PMMA matrices of varying molecular weights. TEMs proved that the roles of the short and long brushes were truly decoupled. In systems where the long brush chemistry matched that of the matrix, the particles are well dispersed despite the fact that there were short brushes of incompatible chemistry. In systems where the matrix chemistry matched that of the short brush and not of the long brush, the long brush dewets from the matrix chains. The mechanical properties of these systems were tested as well showing an increase over the neat matrix. Therefore, this study proves that the role of the short brush is that of core-core screening, while the role of the long brush is that of chain entanglement. With this knowledge, it was proposed that the short chemistry could be changed to not only be incompatible with

the matrix but also property enhancing similar to work that has been done previously with block copolymers. A mixed bimodal brush of 1H,1H-heptafluorobutyl methacrylate short chains and polystyrene long chains was created. A film of this brush was drop casted onto glass and styrene substrates. The water contact angle measurement of both treated substrates was higher than that of the untreated. Also, the treated styrene substrate was annealed above the T_g while still maintaining entanglement of the film with the substrate. The presence of fluorinated chains at the film's surface was confirmed via ATR-IR.

While the sequential surface-initiated RAFT polymerization technique allows for the increased control over a large number of the molecular variables of the polymer brush and nanoparticle surface, it is a multi-step procedure with multiple work-up steps and polymerizations of low conversion. Some remaining problems include longer reaction times and waste of solvent and monomer needed for the production of bimodal brushes. To address these problems, a one-pot grafting-to method was used to create bimodal brushes. The same chemistry for modification of the surface and chain attachment was used. However, the incorporation of the mercaptothiazoline moiety onto the polymer chain-end can be accomplished via either post-polymerization modification or pre-polymerization modification i.e. the use of the activated RAFT agent for the creation of free chains. The use of an activated RAFT agent allowed for a higher graft-density and was used for the creation of both short and long chains via a bulk, thermal-initiated polymerization for the decrease in solvent and monomer waste. Both short and long chains were attached to an aminosilane modified silica nanoparticle and their presence confirmed via GPC. While total graft densities were low in a grafting-to strategy, previous work has shown that high graft densities aren't required for dispersion or entanglement with bimodal brush systems. For the characterization of each brush population's chain density, an anthracene-containing initiator was created and used for the exchange of the Z group of one population. Since each

population then absorbs in a different region of the UV-Vis, the graft densities can be calculated independently.

While the modification of silica surfaces with linear aminosilanes is a facile and common method, the attachment reaction can take 12-24 hours. In order to increase the efficiency of this modification, a cyclic azasilane was employed for the modification of silica nanoparticles. This amine-containing cyclic azasilane allows for attachment in under 5 minutes due to the thermodynamically driven ring-opening reaction. This new cyclic aminosilane still allows for the control of the graft density via controlling the feed ratio of aminosilane. RAFT polymerizations of poly(methyl) methacrylate and polystyrene at various graft densities were performed proving that the attached RAFT agent retained its viability after attachment.

Future Work

Based on the results of this work, two major concepts are shown to be significant. They are: (a) bimodal brushes offer the ability to introduce heterogeneity onto the surface while overcoming issues with dispersion and entanglement. However, there exists a much greater potential as to the types of polymer brushes that can be created and coexist as well as their applications and (b) the creation of these brushes on the surface should be tested and applied in industrial settings and quantities. As a result, this section addresses potential avenues for future work in developing bimodal brushes and optimizations for their creation.

Bimodal brushes were shown to improve dispersion and entanglement within a nanocomposite. Their production via a sequential surface-initiated RAFT polymerization allows for the variation of all molecular variables of the brushes including the heterogeniety and architecture. While bimodal and mixed bimodal brushes have been studied previously, no other method has allowed for this level of control. Also, most other research into bimodal brushes are for the study of smart surfaces. The ability to produce nanoparticles with various chemistries of short chains while allowing the long chains to remain static and matrix compatible cannot be overstated in its importance towards the ability to create a brand new class of materials. Analogous to block copolymers, the properties of a range of polymers can be introduced into composites with incompatible chemistry via the short polymer chains of a bimodal brush. While the work described in this dissertation describes the methodology for the creation of these materials along with their property enhancement, one only needs to look at the wide range of block copolymer materials and their applications for inspiration and

direction for these systems.

While control over all molecular variables is achieved in a sequential RAFT approach, it is still prohibitive towards their large scale production. The methodologies described for the attachment of bimodal brushes in a one-pot procedure sets the groundwork for the ability to produce bimodal brushes on a much larger scale and with much less waste. This is imperative for their production in an industrial setting. The approach of polymer chain modification used is also quite versatile and modular i.e. the modification of the polymer chain end for both attachment and labeling could be extrapolated for use in a variety of surfaces and polymers. Varying the chemistry of the RAFT agent to match the desired chemistry for the modified surface of choice is a more efficient process than post polymerization modification thus allowing for higher graft densities. Also, the use of a radical cross coupling mechanism for the exchange of Z groups on the polymer chain end can be used not only for labeling but for the incorporation of a host of other functional groups. These can be matched to a desired property enhancement such as dielectric enhancement, bacteria or cell targeting/recognition for drug delivery, etc. This approach also has the potential for the creation of block copolymers both as grafted chains on nanoparticles and as free chains. As a general example, a hydroxy terminated poly(ethylene oxide) chain could be modified via a DCC coupling reaction to azobiscyanovaleric acid for the creation of a PEGylated initiator. The same radical cross coupling mechanism used for labeling could potentially generate block copolymers.

Finally, the use of alkoxy silanes has been the classic way of modifying silica surfaces. This has evolved into single alkoxy groups for prevention of multilayered depositon of the silane onto surfaces. However, even this reaction is still relatively slow. The use of a more thermodynamically driven reaction such as the opening of a cyclic azasilane allows for the reaction to be complete in minutes. However, the use of this silane in literature is extremely limited. The work presented herein is solely

the initial investigation into its use. The creation of a multitude of architectures such as block and bimodal brushes as well as its use for the attachment of other small molecules has yet to be investigated.

Bibliography

[1] Li, Y.; Tao, P.; Viswanath, A.; Benicewicz, B. C.; Schadler, L. S. *Langmuir* **2013**, *29*, 1211–1220.

[2] Zhu, Z. Y.; Thompson, T.; Wang, S. Q.; von Meerwall, E. D.; Halasa, A. *Macromolecules* **2005**, *38*, 8816–8824.

[3] Winey, K. I.; Vaia, R. A. *MRS Bulletin* **2007**, *32*, 314–319.

[4] Vaia, R. A.; Maguire, J. F. *Chemistry of Materials* **2007**, *19*, 2736–2751.

[5] Schadler, L. S.; Kumar, S. K.; Benicewicz, B. C.; Lewis, S. L.; Harton, S. E. *MRS Bulletin* **2007**, *32*, 335–340.

[6] Payne, A. R. *Journal of Applied Polymer Science* **1965**, *9*, 2273–&.

[7] Oberdisse, J. *Soft Matter* **2006**, *2*, 29–36.

[8] Moniruzzaman, M.; Winey, K. I. *Macromolecules* **2006**, *39*, 5194–5205.

[9] Lin, Y.; Boker, A.; He, J. B.; Sill, K.; Xiang, H. Q.; Abetz, C.; Li, X. F.; Wang, J.; Emrick, T.; Long, S.; Wang, Q.; Balazs, A.; Russell, T. P. *Nature* **2005**, *434*, 55–59.

[10] LeBaron, P. C.; Wang, Z.; Pinnavaia, T. J. *Applied Clay Science* **1999**, *15*, 11–29.

[11] Krishnamoorti, R.; Vaia, R. A.; Giannelis, E. P. *Chemistry of Materials* **1996**, *8*, 1728–1734.

[12] Krishnamoorti, R. *MRS Bulletin* **2007**, *32*, 341–347.

[13] Kluppel, M. *Kautschuk Gummi Kunststoffe* **1997**, *50*, 282–291.

[14] Gilman, J. W.; Kashiwagi, T.; Lichtenhan, J. D. *SAMPE Journal* **1997**, *33*, 40–46.

[15] Bockstaller, M. R.; Mickiewicz, R. A.; Thomas, E. L. *Advanced Materials* **2005**, *17*, 1331–1349.

[16] Kumar, S. K.; Jouault, N.; Benicewicz, B.; Neely, T. *Macromolecules* **2013**, *46*, 3199–3214.

[17] Hasegawa, R.; Aoki, Y.; Doi, M. *Macromolecules* **1996**, *29*, 6656–6662.

[18] Zhao, L.; Li, Y. G.; Zhong, C. L. *Journal of Chemical Physics* **2007**, *127*, 154909.

[19] Xu, C.; Ohno, K.; Ladmiral, V.; Composto, R. J. *Polymer* **2008**, *49*, 3568–3577.

[20] Meli, L.; Arceo, A.; Green, P. F. *Soft Matter* **2009**, *5*, 533–537.

[21] Iacovella, C. R.; Horsch, M. A.; Glotzer, S. C. *Journal of Chemical Physics* **2008**, *129*, 044902.

[22] Harton, S. E.; Kumar, S. K. *Journal of Polymer Science Part B-Polymer Physics* **2008**, *46*, 351–358.

[23] Yezek, L.; Schartl, W.; Chen, Y. M.; Gohr, K.; Schmidt, M. *Macromolecules* **2003**, *36*, 4226–4235.

[24] Wang, X. R.; Foltz, V. J.; Rackaitis, M.; Bohm, G. G. A. *Polymer* **2008**, *49*, 5683–5691.

[25] Voudouris, P.; Choi, J.; Gomopoulos, N.; Sainidou, R.; Dong, H. C.; Matyjaszewski, K.; Bockstaller, M. R.; Fytas, G. *ACS Nano* **2011**, *5*, 5746–5754.

[26] Sunday, D.; Ilavsky, J.; Green, D. L. *Macromolecules* **2012**, *45*, 4007–4011.

[27] Sunday, D.; Curras-Medina, S.; Green, D. L. *Macromolecules* **2010**, *43*, 4871–4878.

[28] Shull, K. R. *Macromolecules* **1996**, *29*, 2659–2666.

[29] Reiter, G.; Auroy, P.; Auvray, L. *Macromolecules* **1996**, *29*, 2150–2157.

[30] Ojha, S.; Beppler, B.; Dong, H. C.; Matyjaszewski, K.; Garoff, S.; Bockstaller, M. R. *Langmuir* **2010**, *26*, 13210–13215.

[31] McEwan, M. E.; Egorov, S. A.; Ilavsky, J.; Green, D. L.; Yang, Y. *Soft Matter* **2011**, *7*, 2725–2733.

[32] Lindenblatt, G.; Schartl, W.; Pakula, T.; Schmidt, M. *Macromolecules* **2001**, *34*, 1730–1736.

[33] Lindenblatt, G.; Schartl, W.; Pakula, T.; Schmidt, M. *Macromolecules* **2000**, *33*, 9340–9347.

[34] Jia, X. L.; Listak, J.; Witherspoon, V.; Kalu, E. E.; Yang, X. P.; Bockstaller, M. R. *Langmuir* **2010**, *26*, 12190–12197.

[35] Huang, C. L.; Tassone, T.; Woodberry, K.; Sunday, D.; Green, D. L. *Langmuir* **2009**, *25*, 13351–13360.

[36] Green, D. L.; Mewis, J. *Langmuir* **2006**, *22*, 9546–9553.

[37] Ferreira, P. G.; Ajdari, A.; Leibler, L. *Macromolecules* **1998**, *31*, 3994–4003.

[38] Clarke, C. J.; Jones, R. A. L.; Edwards, J. L.; Shull, K. R.; Penfold, J. *Macromolecules* **1995**, *28*, 2042–2049.

[39] Choi, J.; Hui, C. M.; Pietrasik, J.; Dong, H. C.; Matyjaszewski, K.; Bockstaller, M. R. *Soft Matter* **2012**, *8*, 4072–4082.

[40] Borukhov, I.; Leibler, L. *Macromolecules* **2002**, *35*, 5171–5182.

[41] Borukhov, I.; Leibler, L. *Physical Review E* **2000**, *62*, R41–R44.

[42] Putnam, S. A.; Cahill, D. G.; Ash, B. J.; Schadler, L. S. *Journal of Applied Physics* **2003**, *94*, 6785–6788.

[43] Nie, Z. H.; Fava, D.; Rubinstein, M.; Kumacheva, E. *Journal of the American Chemical Society* **2008**, *130*, 3683–3689.

[44] Nie, Z. H.; Fava, D.; Kumacheva, E.; Zou, S.; Walker, G. C.; Rubinstein, M. *Nature Materials* **2007**, *6*, 609–614.

[45] Nie, Z. H.; Petukhova, A.; Kumacheva, E. *Nature Nanotechnology* **2010**, *5*, 15–25.

[46] Merkel, T. C.; Freeman, B. D.; Spontak, R. J.; He, Z.; Pinnau, I.; Meakin, P.; Hill, A. J. *Science* **2002**, *296*, 519–522.

[47] Akcora, P.; Liu, H.; Kumar, S. K.; Moll, J.; Li, Y.; Benicewicz, B. C.; Schadler, L. S.; Acehan, D.; Panagiotopoulos, A. Z.; Pryamitsyn, V.; Ganesan, V.; Ilavsky, J.; Thiyagarajan, P.; Colby, R. H.; Douglas, J. F. *Nature Materials* **2009**, *8*, 354–U121.

[48] Moll, J. F.; Akcora, P.; Rungta, A.; Gong, S. S.; Colby, R. H.; Benicewicz, B. C.; Kumar, S. K. *Macromolecules* **2011**, *44*, 7473–7477.

[49] Maillard, D.; Kumar, S. K.; Rungta, A.; Benicewicz, B. C.; Prud'homme, R. E. *Nano Letters* **2011**, *11*, 4569–4573.

[50] Liu, K.; Nie, Z. H.; Zhao, N. N.; Li, W.; Rubinstein, M.; Kumacheva, E. *Science* **2010**, *329*, 197–200.

[51] Lin, Y. L.; Chiou, C. S.; Kumar, S. K.; Lin, J. J.; Sheng, Y. J.; Tsao, H. K. *Journal of Physical Chemistry C* **2011**, *115*, 5566–5577.

[52] Fava, D.; Nie, Z.; Winnik, M. A.; Kumacheva, E. *Advanced Materials* **2008**, *20*, 4318–4322.

[53] Akcora, P.; Kumar, S. K.; Sakai, V. G.; Li, Y.; Benicewicz, B. C.; Schadler, L. S. *Macromolecules* **2010**, *43*, 8275–8281.

[54] Akcora, P.; Kumar, S. K.; Moll, J.; Lewis, S.; Schadler, L. S.; Li, Y.; Benicewicz, B. C.; Sandy, A.; Narayanan, S.; Illavsky, J.; Thiyagarajan, P.; Colby, R. H.; Douglas, J. F. *Macromolecules* **2010**, *43*, 1003–1010.

[55] Zhao, B.; Brittain, W. J. *Progress in Polymer Science* **2000**, *25*, 677–710.

[56] Barbey, R.; Lavanant, L.; Paripovic, D.; Schüwer, N.; Sugnaux, C.; Tugulu, S.; Klok, H.-A. *Chemical Reviews* **2009**, *109*, 5437–5527.

[57] Zou, H.; Wu, S.; Shen, J. *Chemical Reviews* **2008**, *108*, 3893–3957.

[58] Ligoure, C.; Leibler, L. *Journal De Physique* **1990**, *51*, 1313–1328.

[59] Li, C. Z.; Benicewicz, B. C. *Macromolecules* **2005**, *38*, 5929–5936.

[60] Li, C.; Han, J.; Ryu, C. Y.; Benicewicz, B. C. *Macromolecules* **2006**, *39*, 3175–3183.

[61] Fadeev, A. Y.; McCarthy, T. J. *Langmuir* **2000**, *16*, 7268–7274.

[62] Cash, B. M.; Wang, L.; Benicewicz, B. C. *Journal of Polymer Science Part A: Polymer Chemistry* **2012**, *50*, 2533–2540.

[63] Wang, Y.; Hu, S.; Brittain, W. J. *Macromolecules* **2006**, *39*, 5675–5678.

[64] Larsen, E. K. U.; Nielsen, T.; Wittenborn, T.; Birkedal, H.; Vorup-Jensen, T.; Jakobsen, M. H.; Ostergaard, L.; Horsman, M. R.; Besenbacher, F.; Howard, K. A.; Kjems, J. *ACS nano* **2009**, *3*, 1947–1951.

[65] White, M. A.; Johnson, J. A.; Koberstein, J. T.; Turro, N. J. *Journal of the American Chemical Society* **2006**, *128*, 11356–7.

[66] Hojjati, B.; Charpentier, P. A. *Journal of Polymer Science Part aPolymer Chemistry* **2008**, *46*, 3926–3937.

[67] Hojjati, B.; Sui, R.; Charpentier, P. A. *Polymer* **2007**, *48*, 5850–5858.

[68] Truong, L. T.; Larsen, Å.; Holme, B.; Diplas, S.; Hansen, F. K.; Roots, J.; Jørgensen, S. *Surface and Interface Analysis* **2010**, *42*, 1046–1049.

[69] Gupta, S.; Ramamurthy, P. C.; Madras, G. *Polymer Chemistry* **2011**, *2*, 221.

[70] Xiong, L.; Liang, H.; Wang, R.; Chen, L. *Journal of Polymer Research* **2010**, *18*, 1017–1021.

[71] Liu, X.; Ye, Q.; Yu, B.; Liang, Y.; Liu, W.; Zhou, F. *Langmuir : The ACS Journal of Surfaces and Colloids* **2010**, *26*, 12377–82.

[72] Robbes, A.-S.; Cousin, F.; Meneau, F.; Chevigny, C.; Gigmes, D.; Fresnais, J.; Schweins, R.; Jestin, J. *Soft Matter* **2012**, *8*, 3407.

[73] Ngo, V. G.; Bressy, C.; Leroux, C.; Margaillan, A. *Polymer* **2009**, *50*, 3095–3102.

[74] Demmer, C. S.; Krogsgaard-Larsen, N.; Bunch, L. *Chemical Reviews* **2011**, *111*, 7981–8006.

[75] Mutin, P. H.; Guerrero, G.; Vioux, A. *Journal of Materials Chemistry* **2005**, *15*, 3761.

[76] Queffélec, C.; Petit, M.; Janvier, P.; Knight, D. A.; Bujoli, B. *Chemical reviews* **2012**, *112*, 3777–807.

[77] Tchoul, M. N.; Fillery, S. P.; Koerner, H.; Drummy, L. F.; Oyerokun, F. T.; Mirau, P. A.; Durstock, M. F.; Vaia, R. A. *Chemistry of Materials* **2010**, *22*, 1749–1759.

[78] Tao, P.; Li, Y.; Rungta, A.; Viswanath, A.; Gao, J. N.; Benicewicz, B. C.; Siegel, R. W.; Schadler, L. S. *Journal of Materials Chemistry* **2011**, *21*, 18623–18629.

[79] Tao, P.; Viswanath, A.; Schadler, L. S.; Benicewicz, B. C.; Siegel, R. W. *ACS Applied Materials & Interfaces* **2011**, *3*, 3638–3645.

[80] Boyer, C.; Bulmus, V.; Priyanto, P.; Teoh, W. Y.; Amal, R.; Davis, T. P. *Journal of Materials Chemistry* **2009**, *19*, 111.

[81] Dong, H.; Huang, J.; Koepsel, R. R.; Ye, P.; Russell, A. J.; Matyjaszewski, K. *Biomacromolecules* **2011**, *12*, 1305–11.

[82] Lowe, A. B.; Sumerlin, B. S.; Donovan, M. S.; McCormick, C. L. *Journal of the American Chemical Society* **2002**, *124*, 11562–11563.

[83] Ohno, K.; Koh, K.-m.; Tsujii, Y.; Fukuda, T. *Macromolecules* **2002**, *35*, 8989–8993.

[84] Duwez, A.-S.; Guillet, P.; Colard, C.; Gohy, J.-F.; Fustin, C.-A. *Macromolecules* **2006**, *39*, 2729–2731.

[85] Qin, S.; Qin, D.; Ford, W. T.; Resasco, D. E.; Herrera, J. E. *Journal of the American Chemical Society* **2003**, *126*, 170–176.

[86] Yang, Q.; Wang, L.; Xiang, W.-d.; Zhou, J.-f.; Tan, Q.-h. *Journal of Polymer Science Part A: Polymer Chemistry* **2007**, *45*, 3451–3459.

[87] Li, J.; Benicewicz, B. C. *Journal of Polymer Science Part A: Polymer Chemistry* **2013**, 3572–3582.

[88] Carlmark, A.; Malmström, E. *Journal of the American Chemical Society* **2002**, *124*, 900–901.

[89] Liu, Y.; Klep, V.; Zdyrko, B.; Luzinov, I. *Langmuir* **2005**, *21*, 11806–11813.

[90] Yao, F.; Fu, G.-D.; Zhao, J.; Kang, E.-T.; Neoh, K. G. *Journal of Membrane Science* **2008**, *319*, 149–157.

[91] Coiai, S.; Passaglia, E.; Ciardelli, F. *Macromolecular Chemistry and Physics* **2006**, *207*, 2289–2298.

[92] Yu, W. H.; Kang, E. T.; Neoh, K. G. *Langmuir* **2004**, *21*, 450–456.

[93] Chen, Y.; Deng, Q.; Xiao, J.; Nie, H.; Wu, L.; Zhou, W.; Huang, B. *Polymer* **2007**, *48*, 7604–7613.

[94] Barner, L.; Zwaneveld, N.; Perera, S.; Pham, Y.; Davis, T. P. *Journal of Polymer Science Part A: Polymer Chemistry* **2002**, *40*, 4180–4192.

[95] Rizzardo, E.; Serelis, A.; Solomon, D. *Australian Journal of Chemistry* **1982**, *35*, 2013–2024.

[96] Moad, G.; Rizzardo, E. *Macromolecules* **1995**, *28*, 8722–8728.

[97] Husseman, M.; Malmström, E. E.; McNamara, M.; Mate, M.; Mecerreyes, D.; Benoit, D. G.; Hedrick, J. L.; Mansky, P.; Huang, E.; Russell, T. P.; Hawker, C. J. *Macromolecules* **1999**, *32*, 1424–1431.

[98] Chevigny, C.; Gigmes, D.; Bertin, D.; Jestin, J.; Boue, F. *Soft Matter* **2009**, *5*, 3741–3753.

[99] Wang, J.-S.; Matyjaszewski, K. *Journal of the American Chemical Society* **1995**, *117*, 5614–5615.

[100] Kato, M.; Kamigaito, M.; Sawamoto, M.; Higashimura, T. *Macromolecules* **1995**, *28*, 1721–1723.

[101] Matyjaszewski, K. *Macromolecules* **2012**, *45*, 4015–4039.

[102] Huang, X.; Wirth, M. J. *Analytical Chemistry* **1997**, *69*, 4577–4580.

[103] Wang, Y.-P.; Pei, X.-W.; He, X.-Y.; Yuan, K. *European Polymer Journal* **2005**, *41*, 1326–1332.

[104] Matyjaszewski, K.; Dong, H.; Jakubowski, W.; Pietrasik, J.; Kusumo, A. *Langmuir* **2007**, *23*, 4528–4531.

[105] Chiefari, J.; Chong, Y. K.; Ercole, F.; Krstina, J.; Jeffery, J.; Le, T. P. T.; Mayadunne, R. T. A.; Meijs, G. F.; Moad, C. L.; Moad, G.; Rizzardo, E.; Thang, S. H. *Macromolecules* **1998**, *31*, 5559–5562.

[106] Li, Y.; Schadler, L.; Benicewicz, B. In *Handbook of RAFT Polymerization*; Barner-Kowollik, C., Ed.; Wiley-VCH: Weinheim: Germany, 2008; pp 423–453.

[107] Tsujii, Y.; Ejaz, M.; Sato, K.; Goto, A.; Fukuda, T. *Macromolecules* **2001**, *34*, 8872–8878.

[108] Wang, L.; Benicewicz, B. C. *ACS Macro Letters* **2013**, *2*, 173–176.

[109] Takafuji, M.; Ide, S.; Ihara, H.; Xu, Z. *Chemistry of Materials* **2004**, *16*, 1977–1983.

[110] Stuart, M. A. C.; Huck, W. T. S.; Genzer, J.; Muller, M.; Ober, C.; Stamm, M.; Sukhorukov, G. B.; Szleifer, I.; Tsukruk, V. V.; Urban, M.; Winnik, F.; Zauscher, S.; Luzinov, I.; Minko, S. *Nature Materials* **2010**, *9*, 101–113.

[111] Roy, M.; Nelson, J. K.; MacCrone, R. K.; Schadler, L. S.; Reed, C. W.; Keefe, R. *Dielectrics and Electrical Insulation, IEEE Transactions on* **2005**, *12*, 629–643.

[112] Lu, A.-H.; Salabas, E. L.; Schüth, F. *Angewandte Chemie International Edition* **2007**, *46*, 1222–1244.

[113] Green, P. F.; Oh, H.; Akcora, P.; Kumar, S. K. *Structure and Dynamics of Polymer Nanocomposites Involving Chain-Grafted Spherical Nanoparticles*; Dynamics of Soft Matter: Neutron Applications; 2012.

[114] Green, P. F. *Soft Matter* **2011**, *7*, 7914–7926.

[115] Rungta, A.; Natarajan, B.; Neely, T.; Dukes, D.; Schadler, L. S.; Benicewicz, B. C. *Macromolecules* **2012**, *45*, 9303–9311.

[116] Natarajan, B.; Neely, T.; Rungta, A.; Benicewicz, B. C.; Schadler, L. S. *Macromolecules* **2013**, *46*, 4909–4918.

[117] Maillard, D.; Kumar, S. K.; Fragneaud, B.; Kysar, J. W.; Rungta, A.; Benicewicz, B. C.; Deng, H.; Brinson, L. C.; Douglas, J. F. *Nano Letters* **2012**, *12*, 3909–3914.

[118] Liang, J.; Huang, Y.; Zhang, L.; Wang, Y.; Ma, Y.; Guo, T.; Chen, Y. *Advanced Functional Materials* **2009**, *19*, 2297–2302.

[119] Coleman, J. N.; Khan, U.; Blau, W. J.; Gun'ko, Y. K. *Carbon* **2006**, *44*, 1624–1652.

[120] Coleman, J. N.; Khan, U.; Gun'ko, Y. K. *Advanced Materials* **2006**, *18*, 689–706.

[121] Fang, M.; Wang, K.; Lu, H.; Yang, Y.; Nutt, S. *Journal of Materials Chemistry* **2009**, *19*, 7098–7105.

[122] McEwan, M.; Green, D. *Soft Matter* **2009**, *5*, 1705–1716.

[123] Pryamtisyn, V.; Ganesan, V.; Panagiotopoulos, A. Z.; Liu, H. J.; Kumar, S. K. *Journal of Chemical Physics* **2009**, *131*, 221102.

[124] Sternstein, S. S.; Zhu, A. J. *Macromolecules* **2002**, *35*, 7262–7273.

[125] Jouault, N.; Vallat, P.; Dalmas, F.; Said, S.; Jestin, J.; Boue, F. *Macromolecules* **2009**, *42*, 2031–2040.

[126] Montes, H.; Chaussée, T.; Papon, A.; Lequeux, F.; Guy, L. *The European Physical Journal E* **2010**, *31*, 263–268.

[127] Tao, P.; Viswanath, A.; Li, Y.; Siegel, R. W.; Benicewicz, B. C.; Schadler, L. S. *Polymer* **2013**, *54*, 1639–1646.

[128] Tao, P.; Li, Y.; Siegel, R. W.; Schadler, L. S. *Journal of Applied Polymer Science* **2013**, *130*, 3785–3793.

[129] Akcora, P.; Harton, S. E.; Kumar, S. K.; Sakai, V. G.; Li, Y.; Benicewicz, B. C.; Schadler, L. S. *Macromolecules* **2011**, *44*, 416–416.

[130] Jayaraman, A. *Journal of Polymer Science Part B: Polymer Physics* **2013**, *51*, 524–534.

[131] Martin, T. B.; McKinney, C.; Jayaraman, A. *Soft Matter* **2013**, *9*, 155–169.

[132] Singh, C.; Balazs, A. C. *Macromolecules* **1996**, *29*, 8904–8911.

[133] Zhao, B.; Brittain, W. J. *Journal of the American Chemical Society* **1999**, *121*, 3557–3558.

[134] Zhao,; Perrier, S. *Macromolecules* **2006**, *39*, 8603–8608.

[135] Estillore, N. C.; Advincula, R. C. *Macromolecular Chemistry and Physics* **2011**, *212*, 1552–1566.

[136] Motornov, M.; Malynych, S. Z.; Pippalla, D. S.; Zdyrko, B.; Royter, H.; Roiter, Y.; Kahabka, M.; Tokarev, A.; Tokarev, I.; Zhulina, E.; Kornev, K. G.; Luzinov, I.; Minko, S. *Nano Letters* **2012**, *12*, 3814–3820.

[137] Gao, J.; Li, J.; Zhao, S.; Benicewicz, B. C.; Hillborg, H.; Schadler, L. S. *Polymer* **2013**, *54*, 3961–3973.

[138] Skvortsov, A. M.; Gorbunov, A. A.; Leermakers, F. A. M.; Fleer, G. J. *Macromolecules* **1999**, *32*, 2004–2015.

[139] Martin, T. B.; Jayaraman, A. *Soft Matter* **2013**,

[140] Ionov, L.; Houbenov, N.; Sidorenko, A.; Stamm, M.; Luzinov, I.; Minko, S. *Langmuir* **2004**, *20*, 9916–9919.

[141] Houbenov, N.; Minko, S.; Stamm, M. *Macromolecules* **2003**, *36*, 5897–5901.

[142] Kumar Vyas, M.; Schneider, K.; Nandan, B.; Stamm, M. *Soft Matter* **2008**, *4*, 1024–1032.

[143] Draper, J.; Luzinov, I.; Minko, S.; Tokarev, I.; Stamm, M. *Langmuir* **2004**, *20*, 4064–4075.

[144] Bao, C.; Tang, S.; Horton, J. M.; Jiang, X.; Tang, P.; Qiu, F.; Zhu, L.; Zhao, B. *Macromolecules* **2012**, *45*, 8027–8036.

[145] Jiang, X.; Zhong, G.; Horton, J. M.; Jin, N.; Zhu, L.; Zhao, B. *Macromolecules* **2010**, *43*, 5387–5395.

[146] Jiang, X.; Zhao, B.; Zhong, G.; Jin, N.; Horton, J. M.; Zhu, L.; Hafner, R. S.; Lodge, T. P. *Macromolecules* **2010**, *43*, 8209–8217.

[147] Zhao, B.; He, T. *Macromolecules* **2003**, *36*, 8599–8602.

[148] Ionov, L.; Minko, S. *ACS Applied Materials & Interfaces* **2012**, *4*, 483–489.

[149] Estillore, N. C.; Advincula, R. C. *Langmuir* **2011**, *27*, 5997–6008.

[150] Zhao, B.; Zhu, L. *Macromolecules* **2009**, *42*, 9369–9383.

[151] Edgecombe, S. R.; Gardiner, J. M.; Matsen, M. W. *Macromolecules* **2002**, *35*, 6475–6477.

[152] Jayaraman, A.; Nair, N. *Molecular Simulation* **2012**, *38*, 751–761.

[153] Perrier, S.; Takolpuckdee, P.; Mars, C. A. *Macromolecules* **2005**, *38*, 2033–2036.

[154] Trombly, D. M.; Ganesan, V. *Journal of Chemical Physics* **2010**, *133*.

[155] Chevigny, C.; Dalmas, F.; Di Cola, E.; Gigmes, D.; Bertin, D.; Boue, F.; Jestin, J. *Macromolecules* **2011**, *44*, 122–133.

[156] Dodd, P. M.; Jayaraman, A. *Journal of Polymer Science Part B-Polymer Physics* **2012**, *50*, 694–705.

[157] Bansal, A.; Yang, H. C.; Li, C. Z.; Benicewicz, B. C.; Kumar, S. K.; Schadler, L. S. *Journal of Polymer Science Part B-Polymer Physics* **2006**, *44*, 2944–2950.

[158] Oh, H.; Green, P. F. *Nature Materials* **2009**, *8*, 139–143.

[159] Dukes, D.; Li, Y.; Lewis, S.; Benicewicz, B.; Schadler, L.; Kumar, S. K. *Macromolecules* **2010**, *43*, 1564–1570.

[160] Wang, M.-J. *Rubber Chemistry and Technology* **1998**, *71*, 520–589.

[161] Brown, J. M.; Anderson, D. P.; Justice, R. S.; Lafdi, K.; Belfor, M.; Strong, K. L.; Schaefer, D. W. *Polymer* **2005**, *46*, 10854 – 10865.

[162] Balazs, A. C.; Emrick, T.; Russell, T. P. *Science* **2006**, *314*, 1107–1110.

[163] Gao, J.; Li, J.; Benicewicz, B. C.; Zhao, S.; Hillborg, H.; Schadler, L. S. *Polymers* **2012**, *4*, 187–210.

[164] Beecroft, L. L.; Ober, C. K. *Chemistry of Materials* **1997**, *9*, 1302–1317.

[165] Caseri, W. *Macromolecular Rapid Communications* **2000**, *21*, 705–722.

[166] Schaefer, D. W.; Justice, R. S. *Macromolecules* **2007**, *40*, 8501–8517.